THE ELUCIDATION AND QUANTIFICATION OF THE DECOMPOSITION PRODUCTS OF SODIUM DITHIONITE AND THE DETECTION OF PEROXIDE VAPORS WITH THIN FILMS

By

TRAVIS HOUSTON JAMES

Bachelor of Science in Chemistry
Hillsdale College
Hillsdale, MI
2009

Submitted to the Faculty of the
Graduate College of the
Oklahoma State University
in partial fulfillment of
the requirements for
the Degree of
DOCTOR OF PHILOSOPHY
July, 2014

THE ELUCIDATION AND QUANTIFICATION OF THE DECOMPOSOTION PRODUCTS OF SODIUM DITHIONITE AND THE DETECTION OF PEROXIDE VAPORS WITH THIN FILMS

Dissertation Approved:

Dr. Nicholas F. Materer

Dissertation Advisor

Dr. Allen Apblett

Dr. Frank Blum

Dr. Richard Bunce

Dr. Ziad El-Rassi

Dr. Tyler Ley

ACKNOWLEDGEMENTS

I would like to thank anyone who, whether I am aware of his or her actions or not, has contributed meaningfully to my life and my efforts.

Name: TRAVIS HOUSTON JAMES

Date of Degree: JULY, 2014

Title of Study: THE ELUCIDATION AND QUANTIFICATION OF THE DECOMPOSOTION PRODUCTS OF SODIUM DITHIONITE AND THE DETECTION OF PEROXIDE VAPORS WITH THIN FILMS

Major Field: CHEMISTRY

Abstract:

Sodium dithionite ($Na_2S_2O_4$) is an oxidizable sulfur oxyanion often employed as a reducing agent in environmental and synthetic chemistry. When exposed to the atmosphere, dithionite degrades through a series of decomposition reactions to form a number of compounds, with the primary two being bisulfite (HSO_3^{2-}) and thiosulfate ($S_2O_3^{2-}$). Ten samples of sodium dithionite ranging from brand new to nearly fifty years old were analyzed using ion chromatography; from this, a new quantification method for dithionite and thiosulfate was achieved and statistically validated against the current three iodometric titration method used industrially. Additional sample analysis with Raman spectroscopy of solid and dissolved samples identified unique compounds in the oldest samples, including dithionate ($S_2O_6^{2-}$) and tetrathionate ($S_4O_6^{2-}$).

Additionally, titania nanoparticles in a hydroxypropyl cellulose matrix were used to prepare films on polycarbonate slides and coatings on cellulose papers. The exposure of these materials to hydrogen peroxide gas led to the development of an intense yellow color. Using an inexpensive web camera and a tungsten lamp to measure the reflected light, first-order behavior in the color change was observed when exposed to peroxide vapor of less than 50 ppm. For 50 mass percent titania nanoparticles in hydroxypropyl cellulose films on polycarbonate, the detection limit was estimated to be 90 ppm after a 1-minute measurement and 1.5 ppm after a 1-hour integration. The coatings on the filter paper had a threefold higher sensitivity compared to the films, with a detection limit of 5.4 ppm peroxide for a 1-minute measurement and 0.09 ppm peroxide for a 1-hour integration period. Further experimentation with the effects of acid loading on the filter paper coatings identified these as possible sensors for organic peroxides. With the addition of sulfuric acid, the support was changed from cellulose to glass microfiber or silica. This coatings showing increased sensitivity when compared to coatings with hydrochloric acid. Finally, coatings containing an ionic liquid solvent and trifluoromethanesulfonic acid were produced and found to have increased longevity. These coatings have potential as peroxide vapor sensors for both industrial and security applications.

TABLE OF CONTENTS

Chapter Page

Chapter Page

LIST OF TABLES

LIST OF FIGURES

Figure Page

CHAPTER I

INTRODUCTION

This introduction, as with the following dissertation, is broken into two parts.

The first part of the dissertation (Chapters II – III) details my research with sodium dithionite. Topics of discussion include an instrumental approach for dithionite and thiosulfate quantification (Chapter II) and a study of the long-term decomposition products of sodium dithionite in the solid phase (Chapter III). The second part of the dissertation (Chapters IV and V) describes research accomplished with titania-cellulose thin films produced through a sol-gel method. These films show sensitivity to both hydrogen peroxide (Chapter IV) and organic peroxides (Chapter V); as such, the sensitivities and limits of quantification of the films will be discussed. As such, there is great potential for these films to be used as sensors for industrial and security purposes.

Given the two unique projects presented in this dissertation, this introductory chapter will present a brief history about the important compounds, the unique characteristics that make them of interest, and methods in which they are used.

A. Sodium Dithionite

Sodium dithionite, i.e. sodium hydrosulfite, ($Na_2S_2O_4$) is a complex sulfur oxyanion of great importance in the industrial, textile, and environmental fields.[1] In these sectors, the primary role of sodium dithionite is generally as a reducing agent due to its extremely strong oxidizing potential. Dithionite's role as a reducing agent is well exemplified by its use for the bleaching of cellulose in wood pulping and fixation of indigo and indanthrene dyes in fabrics in the textile industries,[2-9] which together have consumed nearly 80% of the annually-produced U.S. supply over the last twenty-five years.[10-13] It is also used as a reducing agent in chemical syntheses[14-16] and, with iron(III), for treatment and remediation of water supplies containing heavy metal, complex organic, and chlorinated pollutants.[17-20]

As a strong reducing agent, sodium dithionite is particularly unstable, both in solutions and in the solid crystalline form. In solutions, the reaction pathway for the oxidation of sodium dithionite is highly dependent upon the pH of the environment, the oxygen content, and the temperature at which compound breakdown occurs. Additionally, the inevitable presence of additional sulfur oxyanions gives rise to numerous competing side reactions and unknown complex equilibria.[21-26] With this in mind, there have been a great number of decomposition studies at varied pH levels and solution compositions, resulting in numerous proposed and sometimes contradictory intermediates and overall decomposition mechanisms.[27] While the complete picture describing dithionite decomposition in extremely complicated solutions has yet to be resolved, there have been notable advances in the understanding of the overall trends in these systems.

The initial decomposition products of dithionite as a function of pH have been elucidated. When in an acidic solution (pH < 5.5), sodium dithionite rapidly decomposes to form sodium thiosulfate ($Na_2S_2O_3$) and sodium metabisulfite ($Na_2S_2O_5$) [Equation I-1].[1,28]

$$2\ Na_2S_2O_4 + H^+ (excess) \rightarrow Na_2S_2O_3 + Na_2S_2O_5 \qquad \text{[Equation I-1]}$$

In neutral solutions, sodium dithionite reacts with water to produce a 2:1 ratio of sodium bisulfite ($NaHSO_3$) and sodium thiosulfate ($Na_2S_2O_3$) [Equation I-2].[21,27-29]

$$2\ Na_2S_2O_4 + H_2O \rightarrow 2\ NaHSO_3 + Na_2S_2O_3 \qquad \text{[Equation I-2]}$$

It has been reported that any dithionite remaining in solution can react with the thiosulfate produced to generate hydrogen sulfide gas (H_2S) and sodium bisulfite, which can further react to form elemental sulfur (S^0) [Equations I-3 and I-4].[30]

$$2\ Na_2S_2O_4 + Na_2S_2O_3 + 2\ H_2O + H^+ \rightarrow H_2S + 3\ NaHSO_3 \qquad \text{[Equation I-3]}$$

$$2\ H_2S + NaHSO_3 \rightarrow 3\ S^0 + 3\ H_2O \qquad \text{[Equation I-4]}$$

Weakly alkaline (pH ~ 8) solutions with no dissolved oxygen have a stabilizing effect on dithionite solutions, which can be stored in a cold environment for an extended but unspecified period of time.[1] If the alkalinity of the solution is further increased to near pH = 13 or nearly any amount of oxygen is present in the solution, dithionite has been reported to decompose through various pathways, producing a number of sulfur anions including thiosulfate, sulfite (SO_3^{2-}), and sulfide (S^{2-}) [Equations I-5 - I-7].[1,5,31]

$$2\ Na_2S_2O_4 + 2\ NaOH \rightarrow Na_2S_2O_3 + 2\ Na_2SO_3 + H_2O \qquad \text{[Equation I-5]}$$

$$Na_2S_2O_4 + 4\ NaOH \rightarrow 2\ Na_2SO_3 + 2\ H_2O \qquad \text{[Equation I-6]}$$

$$3\ Na_2S_2O_4 + 6\ NaOH \rightarrow Na_2S + 5\ Na_2SO_3 + 3\ H_2O \qquad \text{[Equation I-7]}$$

As can be imagined, given the sheer number of possible reactions that can occur in any solution of dithionite, complete characterization and quantification of every species present is extremely difficult.

There are several proposed mechanisms for the decomposition pathway of dithionite in solution. In 1941, Kolthoff and Miller suggested that dithionite decomposition occurred through the creation of two SO_2 anions, with the -1 charged radical in slightly acidic solutions and the -2 anion produced if pH < 5.5.[32] These possibilities were in agreement with later research by Rinker and coworkers, who studied the decomposition of dithionite in solutions of varied temperature, pH and oxygen content.[24,33] In the first study, it was found that the rate of dithionite decomposition in alkaline solutions with high oxygen content was first order with respect to oxygen and half order with respect to dithionite, a result of the SO_2^- ion as an intermediate in the reactions [Equations I-8 and I-9].

$$S_2O_4^{2-} \rightleftharpoons 2\ SO_2^- \qquad \text{[Equation I-8]}$$

$$SO_2^- + O_2 \rightarrow \text{Products} \qquad \text{[Equation I-9]}$$

Further work performed in slightly acidic solutions (pH between 4.8 – 7.0) and elevated temperatures (60 – 80 °C) revealed that decomposition under certain conditions occurred via a two-step process: an initial induction period followed by a rapid autocatalytic process. During the induction period, the rate of decomposition of dithionite was inversely proportional to the amount present in the solution. It was also determined that induction time decreased with increasing H^+ concentration, with the induction time going to zero when solution pH < 4.5. Immediately following the induction period, there was a rapid decrease in the dithionite concentration. It was found that the reaction rate was

three-halves order in dithionite and one-half order in H^+. The rate controlling reaction was suggested to be

$$HS_2O_4^- + HSO_2^{\bullet} \rightarrow HSO_3^{\bullet} + HS_2O_3^- \qquad \text{[Equation I-10]}$$

with the HSO_2 radical being a product of the proton-mediated dissociation of dithionite. These findings were echoed by Wayman and Lem, who focused on the effects that possible decomposition products had on the decomposition rate.[34] It was also observed by Wayman and Lem as well as Rinker *et al.* that immediately prior to the onset of the rapid autocatalytic decomposition of dithionite, the solutions became turbid and cloudy, possibly due to the formation of colloidal sulfur in solution. It is possible that the turbidity could be due to the production of elemental sulfur, which could act as a catalyst for dithionite decomposition; however, no direct analysis of the turbid solution was performed to confirm the identity of the colloidal species. Additional testing of the dithionite decomposition in the presence of possible side products showed that other sulfur oxyanions had no effect on the rate of decomposition; however, in the presence of small amounts of sulfide, the induction period was removed and decomposition progressed at an extremely accelerated rate.

The molecular explanation for the ready decomposition of dithionite and its strength as a reducing agent comes from two characteristics: dithionite's abnormally long S-S bond and the low oxidation state of the sulfur atoms. The structure of dithionite as a solid is that of an eclipsed dimer of two SO_2 units, connected by an S-S bond of 2.39 angstroms in length (see Figure I-1).[35]

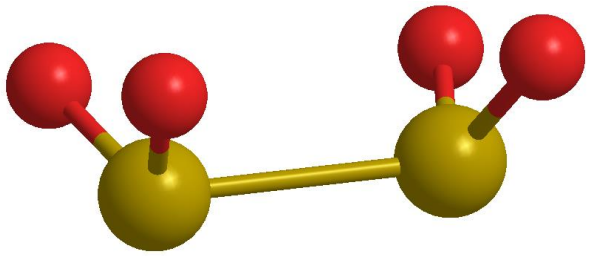

Figure I-1. Structure of the dithionite anion, with the -2 charge spread over the four oxygen atoms. The unmarked OSO and SSO bonding angles are 108.2° and 98.7°, respectively.

For comparison, the lengths of the S-S bonds in the most prevalent form of elemental sulfur, α-octasulfur, and in dithionate ($S_2O_6^{2-}$), another sulfur oxyanion, have been measured to be 2.04 and 2.15 angstroms, respectively.[36,37] As a result of this much longer disulfide bond, dithionite is more reactive than many other compounds containing shorter disulfide bonds, a direct result of the weakened bond. For this reason, dithionite may easily dissociated into two SO_2^- subunits or undergo protonated decomposition to $HSO_2^{\bullet}$. One electron spin resonance study was able to confirm the formation of the $SO_2^{\bullet}$ radical at elevated temperatures.[38]

The other (and arguably primary) contribution to dithionite's instability comes from the ascribed 3+ oxidation state of the sulfur atoms. In separate studies of ocean water by Sillén and Kumar, the stabilities of the different oxidation states of sulfur were evaluated through analysis of normalized reduction potentials of various sulfur oxyanions in acidic and alkaline solutions containing little to no dissolved oxygen (anoxic) or abundant oxygen (oxic), and reported in the form of Frost diagrams (see Figure I-2).[39,40] To interpret a Frost diagram correctly, a few pieces of information are required.[41] First, the more negative the volt – equivalent is for each species (i.e. the lower it lies on the y-axis),

the more thermodynamically stable the compound. Conversely, the more positive, the less stable and more reactive the compound is (though the kinetics of the reaction may be slow). Second, deviation from the overall trend in the element's behavior (the slope gradient and direction) is indicative of singular compound reactivity; that is, convex and concave points in the lines are significant. Compounds that lie near the apex of a convex curve will tend to disproportionate to the species proximate to it and those in a concavity will result from comproportionation of the two proximate species.

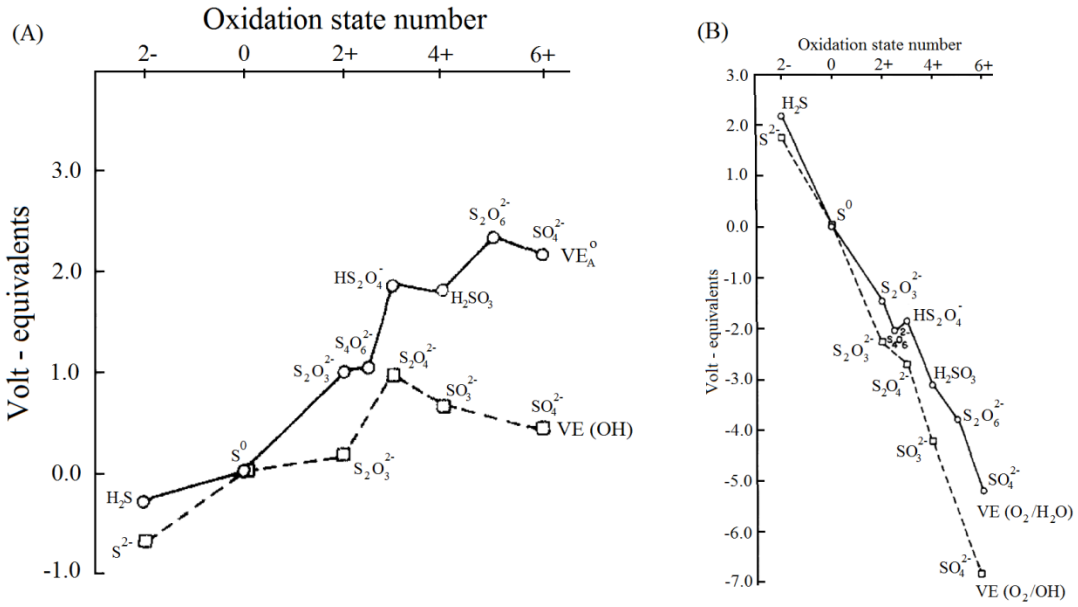

Figure I-2. Frost diagrams (oxidation state vs. standard potential) for sulfur in (A) anoxic and (B) oxic solutions. The solid line signifies a solution pH = 0, while the dashed line represents a solution pH = 14.[41,42] Adapted from Reference 39.

In anoxic solutions, it can be seen that the higher oxidation states of sulfur lie at higher standard potentials with stability increasing as the oxidation number is decreased, with S^{2-} under these conditions the most stable ion in both acidic and alkaline solutions. In oxygen-rich solutions, however, the trend reverses and stability decreases with decreasing oxidation state, resulting in the sulfate ion (with the 6+ sulfur oxidation state) being the

most stable. Given the more negative reduction potentials present in both oxic and anoxic solutions, the alkaline solution provided a better stabilizing environment for sulfur compounds compared to the acidic solution. Interestingly, it is apparent that in each of the four solutions described, dithionite lies at the apex of a small convex part of the curve, indicating the tendency of dithionite to decompose into sulfite and thiosulfate, the neighboring sulfur oxyanions. While in anoxic environments, the eventual end product of dithionite decomposition would likely be of a lower oxidation state (sulfur or sulfide). However, given the ubiquity of molecular oxygen in both the atmosphere and in untreated water, it is much more likely that any dithionite sample will dissociate and eventually decompose to sulfate (Figure I-2B).

B. History of Synthesis and Quantification

Dithionite was reportedly first produced by Georg Stahl in 1718 upon reduction of aqueous sulfur dioxide with iron, although the original work detailing this could not be located and verification of this comes from secondary sources.[1,43] While work describing the use of dithionite as a reducing agent and the elemental composition was completed in the 19th century,[44-46] it was not until 1907 that a method for producing crystalline anhydrous sodium dithionite from sulfur dioxide using zinc dust with sodium hydroxide was accomplished by Bazlen.[47] Once this production method was reported and anhydrous, high purity dithionite was made widely available, there was a surge of dithionite research, including some initial studies on the mechanisms and kinetics of the decomposition of dithionite. Even at this early date, one of the primary focuses was in

determining a method for direct quantification of dithionite in a solution containing other reducible sulfur oxyanion species.

The primary and most quantitative method for dithionite determination in the early 20th century was a colorimetric titration using a known solution of indigo dye i.e. 2,2'-Bis(2,3-dihydro-3-oxoindolyliden) which, when reacted with a solution of dithionite in an air-free environment, produced a direct measure of dithionite content.[48] Unfortunately, this method required an advanced workup and a complex setup to maintain an inert atmosphere for the titration. Additionally, considering the kilogram or more scale of the product, it was required to be both economically and temporally justified. This titration method was useful in situations where numerous or constant measurements of dithionite were required, though not ideal for situations when a simple, individual measurement was required.[49]

In 1923, Merriman described a simple, two-step titration procedure to quantify dithionite which required no inert atmosphere or complex setup. The first part of this method involves the reaction of a solid sample of dithionite with formaldehyde, producing two sodium formaldehyde adducts.

$$Na_2S_2O_4 + 2\ CH_2O + H_2O \rightarrow HOCH_2SO_2Na + HOCH_2SO_3Na \qquad \text{[Equation I-11]}$$

The first listed product, sodium hydroxymethanesulfinate (industrially known as Rongalite), is produced. This adduct is titratable with iodine.

$$HOCH_2SO_2^- + 2\ I_3^- + 2\ H_2O \rightarrow SO_4^{2-} + 6\ I^- + 5\ H^+ + CH_2O \qquad \text{[Equation I-12]}$$

The other product, sodium hydroxymethanesulfonate (HMS), does not react with iodine and thus there is no direct interference with the titration of Rongalite. This procedure was found to be highly accurate for relatively pure samples of dithionite and was recommended for industrial use. However, in older samples, the impurities present from dithionite decomposition could also be reduced by iodine, resulting in measurement errors by the single titration.

This issue was resolved by Robert Wollak in 1930.[50] In his seminal paper, Wollak detailed a series of three iodometric titrations which eliminated the interferences from additional reducible species and measured the amounts of dithionite, thiosulfate, and sulfite (i.e. bisulfite) present in the samples. This approach became the standard method for dithionite quantification and analysis in the textile and paper-making industries for the next fifty years.[51] Following its publication, the Wollak method was reviewed by numerous authors, many of whom found the methodology unsatisfactory due to potential errors in measurement resulting from the presence of additional unreduced species (mainly thiosulfate and bisulfite) in high concentration and pH effects. Zocher and Saechtling reported that the thiosulfate measurement was prone to error, while Danehy and Zubritsky considered the Wollak procedure "unexceptional" and cited concern over potential errors resulting from high bisulfite concentrations.[52,53] In response to these concerns, William P. Kilroy highlighted the possible errors associated with the Wollak procedure, and published a revised Wollak method for dithionite analysis in a series of papers.[54-56] This revised method is currently used for dithionite quantification in industry and analytical laboratories.

Kilroy's revised method follows the same three iodometric titration structure.[56] In the first titration, a sample is reacted with an excess of iodine to convert all reducible ions to non-reactive species [Equations I-13 – I-15].

$$S_2O_4^{2-} + 3\ I_2 + 4\ H_2O \rightarrow 2\ HSO_4^- + 6\ HI \qquad \text{[Equation I-13]}$$

$$2\ S_2O_3^{2-} + I_2 \rightarrow S_4O_6^{2-} + 2\ I^- \qquad \text{[Equation I-14]}$$

$$HSO_3^- + I_2 + H_2O \rightarrow HSO_4^- + 2\ HI \qquad \text{[Equation I-15]}$$

Following this, sodium hydroxide is added to adjust the final pH to 8 - 10, which causes the reaction of sulfite with dithionate [Equation I-16].

$$S_4O_6^{2-} + SO_3^{2-} \rightarrow S_2O_3^{2-} + S_3O_6^{2-} \qquad \text{[Equation I-16]}$$

The thiosulfate can then be directly titrated with iodine, as seen in Equation I-14. The number of moles of iodine used to titrate the thiosulfate, be it equal to A, are proportional to the amount of thiosulfate originally present in the sample, equal to 4A. In the second titration, a basic solution of formaldehyde is added to a sample of dithionite, forming the Rongalite adduct, which is titratable (see Equation I-11 and I-12). The moles of iodine used in this titration (B) react with both Rongalite and thiosulfate, meaning the difference of (B – 2A)/2 yields the amount of dithionite initially present. The last titration is a direct titration of the sample and quantifies all reducible species present (Equations I-13 – I-15). If the moles of iodine in this titration used are equal to C, then the amount of sulfite present in the solution is equal to (2C + 2A – 3B)/2 moles. Of note, Kilroy went one step further and has described a four-step titration in which sulfide is also quantified, but it requires a substantial amount of specialized glassware and an inert atmosphere, complicating an already challenging titration scheme.[57]

Considering the expense and difficulties in repeatedly preparing the iodine and thiosulfate standards used in the titrations as well as the extensive glassware setup and the need for high accuracy and precision when performing these titrations, alternate methods for dithionite composition analysis using existing instrumentation has been the major research focus for dithionite recently. The use of analytical instrumentation has a major advantage over the titration approach – namely, each species can be directly quantified and is not dependent on the accurate quantification of another species (i.e. subtracting thiosulfate to determine the dithionite composition in the first and second titration). Direct quantification has the added benefit of decreasing the propagated error of the measurement. Reported methods for dithionite quantification include capillary electrophoresis,[23] chromatography,[58] cyclic voltammetry,[21] differential pulse polarography,[59] ion-pair chromatography,[60] and isotachophoresis.[22] Of the chromatographic studies, the capillary electrophoresis work of de Carvalho and Schwedt was the most quantitative, determining dithionite, thiosulfate, sulfite and sulfate.[23] However, in each of these studies, no direct statistical comparison of the equivalency of the instrumental method to the accepted titration methodology was presented, underscoring the need for mathematical validation of the proposed instrumental equivalent to the accepted iodometric titration. An instrumental quantification approach yields an additional benefit – if additional sulfur oxyanion impurities are present, these compounds may be directly detectable and identifiable. In the accepted titration procedure, the identities of the additional decomposition products cannot be elucidated beyond the fact that they may be reducible through the iodometric titration, which would result in measurement errors. Direct detection by an instrument is preferable in that these

additional decomposition products could be identified. With the use of ion chromatography (IC), such an approach is described in Chapter II.

C. A Brief Review of Thin Film Production

From the first published description[61] by Paul Drude in 1889 to the current deposition methods used industrially for integrated circuit technologies, thin films and coatings have grown into a broad research area of both industrial and academic significance. Historically, the term 'thin film' describes a layer or coating nanometers to micrometers in thickness, deposited onto some other, generally flat material (substrate).[62] With the wide range of materials to use as either the film or substrate along with numerous deposition methods possible, there are almost a limitless number of permutations for the integration of thin films into a desired application.

Historically, the unique traits imparted by thin films have been known since before their description by Drude. Well known examples of the early use of thin films include glass mirrors backed by a thin layer of metal (first described by the Roman scholar Pliny the Elder in the year 77 CE[63]) and the application of thin gold films (i.e. gold leaf) to cover statues and other items of significance, both for beauty as well as protection of the underlying surface (seen in numerous cultures, from ancient Egypt to modern day).[64] For most purposes, the early use of thin films and coatings was primarily for imparting or enhancing a particular quality of the substrate (e.g. reflectance, durability, impression of opulence) and not for a self-contained characteristic the film possessed. As both research and technology in this field has matured, the focus of thin films has shifted from this

substrate-centric view to one in which the film plays an equal if not superior role compared to the substrate. This shift in thin film philosophy has undoubtedly come from the increased amount of control in film creation resulting from the numerous deposition methods which have been described. While the application of gold leaf (generally 0.3 – 2 μm thick) was accomplished by hand, current thin film production methods do not require direct contact and instead can be accomplished through the production method itself.

Broadly, thin film production methods can be separated into two categories: physical and chemical depositions.[65] Physical deposition methods generally use a solid starting material and, through a physical method such as vaporization, evaporation, or sputtering of a sample, transfer atoms of the compound through a vacuum environment to a substrate on which it is deposited. In this process, the starting material and the thin film material at the end can be the same chemically, although the structure may be altered (i.e. amorphous to polycrystalline or a well-defined crystalline lattice structure), or there may be a reaction which produces the film. Choice examples of this method include sputter and RF-coil depositions, thermal evaporation, and molecular beam epitaxy. Conversely, chemical deposition methods widely employ a chemical reaction occurring in the solution or vapor phase, or at the gas-solid interface to produce the film. The deposited material is usually some stoichiometric mixture of the reacting compounds or film built of alternating layers of the reactants, in some situations having produced a layer which is only one atom thick. Given the number of possible starting materials and subsequent reactions, chemical deposition is more versatile and offers a wider range of possible reactants and products. Well known deposition methods include chemical vapor

deposition, atomic layer deposition, electroplating, and the sol-gel method. While many of the vapor phase deposition methods offer more control in terms of layer thickness and crystalline homogeneity, the sol-gel approach is attractive due to the low temperatures at which it occurs, lower operating cost as it does not require a vacuum environment, and good particle size control to ensure a homogenous film.[66] Due to these characteristics, the sol-gel method plays a key role in the preparation and development of new materials or as a proof-of-concept step in film productions.

In the traditional sol-gel process, a metal alkoxide is mixed with an alcohol or water-based solution.[41,65-68] When mixed, the alkoxide group is hydrolyzed and forms a colloidal solution of metal oxides or hydroxides and an alcohol. Over time, the colloidal particles will aggregate through polycondensation, producing an alcohol or water, while this product and the remaining solvent is removed. This can occur either through evaporation or by directed heating of the solution (a process called sintering). If the sol is applied to a substrate during the polycondensation and sintering steps, the final product is a gel film composed of colloidal particles of the ceramic metal oxide. The classic sol-gel reaction is the production of silicon dioxide (silica) from tetramethyl orthosilicate [Equations I-17 and I-18].[66,68]

$$Si(OMe)_4 + 4\ H_2O \rightarrow Si(OH)_4 + 4\ MeOH \qquad \text{[Equation I-17]}$$

$$Si(OH)_4 \rightarrow SiO_2 + 2\ H_2O \qquad \text{[Equation I-18]}$$

This sol-gel route is similar to the first reported sol-gel method by Jacques-Joseph Ebelman in 1845, who hydrolyzed a silicic acid ester to obtain a transparent ceramic material.[67,69] However, it was not until 1939 that Geffcken and Berger detailed and patented the use of the sol-gel method for the building of layered films.[70] Since then,

numerous other metal and mixed metal oxides have been produced using the sol-gel method.

D. Applications of Titania

One metal oxide which has garnered much attention recently is titania (i.e. titanium dioxide, TiO_2). Titania is the most prominent and important titanium compounds, and represents the bulk of the geologically extractable form of titanium.[71] Titania has found widespread use in the 20th century, as an ingredient in cosmetics, sunscreen, paints, and toothpaste.[66,72] However, it was not until its use for the photolysis of water by Fujishima and Honda in 1972[73] and its incorporation into the first dye-sensitized solar cell by O'Regan and Grätzel in 1988[74] that a renewed focus on titania research was initiated. The following decades contained a dramatic rise in the amount of published research using TiO_2.[72] Over the next two decades, many new applications for titania were described. As it possesses interesting optical properties (i.e. band gap) and strong UV absorbance, titania has been reported as a strong candidate for thin film coatings on glass for the creation of self-cleaning windows, which are able to repel dirt and decompose organic materials when they come in contact with the windows surface.[66,75-77] It has also been found to be a good photocatalyst, useful in the oxidation and treatment of organic and pharmaceutical environmental pollutants.[78,79]

One of the most dynamic applications has been the use of titania as a sensing material for gases. Generally, a titania surface is positioned as to allow some gas of interest to be directed over the surface. During this time, the electrical properties (usually surface

resistance) of the material are monitored, where a change in the monitored property is indicative of the gas of interest being present in the sample.[80-84] However, sensors based on these titania films and powders generally suffer from detection ranges that are highly dependent on the particle size and surface structure of the TiO_2 (i.e. rutile, anatase, amorphous) or require an elevated operating temperature and complicated operating parameters for accurate measurements.[81] New preparation methods for less complex sensors using these materials are desired to alleviate these shortcomings. Of note, titania powders and films have been used for detection of ethanol,[81] hydrogen sulfide,[85] carbon monoxide[83,84] and many other gaseous compounds.[80]

E. Detection of Gaseous Peroxides

Peroxides (O_2^{2-}) are extremely strong oxidizing agents of great importance in many industrial and biological fields. Arguably the most prominent of these oxidants, hydrogen peroxide (H_2O_2), finds use as a bleaching agent in the paper and textile industries, which together consume over half of the annually produced supply,[5,86] and as a reagent for treatment of organic and other pollutants in water supplies.[87,88] Gaseous hydrogen peroxide is often used in the food and medicinal fields as a cleaning technique in situations where a sterile environment with no bacterial or microbial growth is essential.[89-95] Due to its strong oxidizing potential, the Occupational Safety and Health Administration (OSHA) has set a permissible average exposure limit of 1 ppm over an eight hour day.[96] This limit requires users to be constantly monitored. The primary OSHA-approved method for quantification of gaseous peroxide include drawing the

atmosphere in question through an acidified solution of titanium oxide sulfate,[97] where an optical measurement of the solution at approximately 410 nm can determine the peroxide concentration. This method is still the preferred laboratory standard technique for gaseous peroxide quantification. Another less quantitative method is the use of Dräger tubes specific to hydrogen peroxide, where a color change over a measured length of a stationary phase indicates peroxide concentration.[98] Additional methods for peroxide detection and quantification include fluorometric,[99-102] amperometric,[103-106] spectroscopic analysis,[107-110] and electrochemical sensing.[111] Many of these methods cannot be easily automated as they require pre-concentration of the atmosphere in solution and some amount of wet chemistry, or require constant attention by a technician to ensure instrumental stability.

Another motivation for the interest in peroxide detection comes from the fact that many improvised explosive devices (IEDs) utilize a peroxide-based compound as the main charge. Examples of these compounds include triacetone triperoxide (TATP) and hexamethylene triperoxide diamine (HMTD), both of which have been used in terror-related incidents in the last two decades (see Figure I-3 below).[112-115]

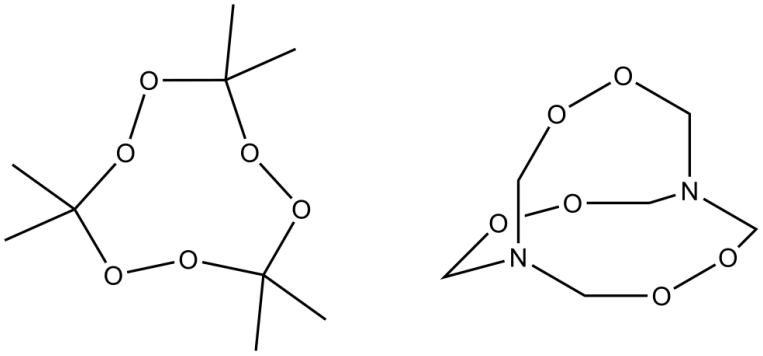

Figure I-3. Molecular structures of (left) triacetone triperoxide and (right) hexamethylene triperoxide diamine.

Because these compounds do not contain a nitro group or metal atoms and are instead comprised of carbon, hydrogen, oxygen and nitrogen, the detection of these compounds through spectroscopic means is difficult in air given the inevitable presence of species possessing similar spectroscopic shifts.[116,117] These compounds also possess low vapor pressures, making sampling from the atmosphere difficult.[118] Reported methods for the detection of these compounds include ion mobility spectroscopy (IMS),[119-122] laser-induced breakdown spectroscopy (LIBS),[123-125] gas exposure over mixed metal and metal oxide materials,[126-128] surface enhanced Raman spectroscopy (SERS),[125,129] and mass spectrometry.[130-133] While useful, these approaches are hampered by an inability to miniaturize instrumentation for field use, a required pre-concentration of the sample for analysis, necessary wet chemistry, and a lack of real-time measurement capability.

A simple approach to detection would be one where a simple yes-no system can indicate the presence of peroxides through an event such as a change in color. This can possibly be addressed through the creation of titanium peroxo complexes. It has been well known that titanium peroxo complexes form in acidic solutions, resulting in an intense yellow or orange-red color. This behavior was originally reported by Sehönn in 1870, who remarked on the intense color formed.[134] Many studies attempted to elucidate the molecular formula for the colored product, with a number of crystalline compounds being isolated but found to be amorphous and structurally unresolvable.[135-137] It was not until 1970 that Schwarzenbach, Müehlebach, and Müeller successfully characterized some of these compounds crystallized with organic acids and EDTA using X-Ray diffraction.[138] It was concluded that the colored titanium peroxo complex exists in two

forms, the formation of which was dependent on the pH on the environment. (see Figure I-4).[139]

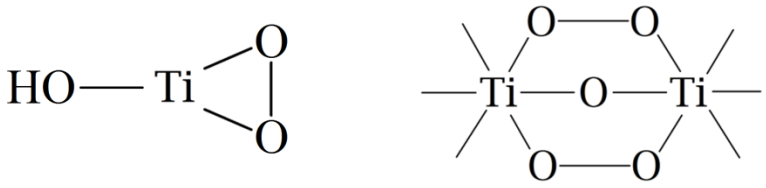

Figure I-4. The (left) mononuclear and (right) dinuclear titanium(IV) peroxo complexes. Adapted from Reference 139.

First, in extremely acidic solutions (pH < 1), the titanium peroxo complex exists in the form of $[Ti(O_2)OH]^+$, which exhibits an intense orange color. In less acidic solutions (pH between 1 and 3), a dinuclear unit is formed where the peroxide groups acts bridging ligand between two Ti^{4+} centers, characterized by a yellow coloration. It can be seen that the pH of the solutions used to detect peroxides play an important role in the observed color of the solutions. Vogel described a detection method for titanium(IV) detection using acidic peroxide solutions.[140] However, reversing this method is possible, where titanium(IV) compounds could be used to detect peroxide through forming the titanium(IV) peroxo complexes and undergoing a color change.

Succinctly, it is extremely important that a simple, inexpensive and direct method for detection and, if possible, quantification be developed. With the knowledge that Ti(IV) compounds in acidic solutions can formed colored charge-transfer complexes with peroxides (seen by the OSHA and Dräger tube quantification methods as well as Sehönn and Vogel), it was of interest to attempt the creation of a sol-gel film of titania containing a high acid content which could provide a visual indication of the presence of peroxide vapors. To this end, films containing titanium(IV) isoproproxide in a hydroxypropyl cellulose matrix were formed on polycarbonate slides and cellulose filter papers

according to a method previously described by Kozuka and coworkers,[141] without calcination after the initial drying period. When exposed to peroxide vapors, the films change from colorless to yellow, with the final coloration dependent on the amount of titania present. It is anticipated that these films can be integrated into a low-cost sensor to monitor peroxide concentrations in industrial workplaces.

CHAPTER II

A METHOD FOR RAPID QUANTIFICATION OF SODIUM DITHIONITE AND ITS DECOMPOSITION PRODUCTS BY ION CHROMATOGRAPHY

A. Introduction

As was extensively discussed in the introductory Chapter, sodium dithionite ($Na_2S_2O_4$) is an oxidizable sulfur oxyanion often employed as a reducing agent in the textile and paper industries, environmental remediation treatments and synthetic chemistry. [2-20] This industrially important reagent slowly decomposes in both the solid and solution phases into a variety of sulfur oxyanions. For this reason, a method for the rapid assessment of purity of a given sample is crucial for its continued use. Despite the importance of this material to the wood pulping and textile industries, a rapid, reliable method to quantify dithionite and its decomposition products remains a challenge. Currently, a three-step iodometric titration formulated by Wollak and revised by Kilroy is used for routine sample analysis.[50,56] However, this method requires extensive bench-top chemistry and a high level of precision for accurate measurements of dithionite and its decomposition products. Ion chromatography can provide a simple one-step method that can easily be automated to rapidly and accurately determine the concentration of dithionite and its decomposition product, thiosulfate. The results are statistically non-different with those obtained using a multi-step iodometric titration, validating the proposed instrumental approach.

B. Experimental Details

B.1 . Sodium Dithionite Samples

A total of five samples were analyzed (see Table II-1). Sample 1 was unopened while Samples 2 and 3 have been used as regents in our laboratories. The lot analysis for these three samples was performed less than one year before the analysis discussed here. The other two samples were purchased more than five years ago and have been in sporadic use until the study. These samples represent a range from unopened and relatively new to older samples that one may find in a typical analytical or inorganic laboratory. Lot analyses are assumed to use a single iodometric titration, which is acceptable for pure materials.

Table II-1. Sodium dithionite samples, suppliers, production date and lot analyses.

Sample	Chemical Grade	Supplier	Production Date	Lot Analysis
1	Purified	J. T. Baker	December 2010	88%
2	Technical (85%+)	Alfa Aesar	September 2010	90.3%
3	Technical (85%)	Sigma-Aldrich	May 2010	83.6%
4	Purified	GFS Chemicals	August 2003	84%
5	Technical (~85%)	Aldrich Chemical Co.	March 1998	82.5%

The newer samples were expected to be relativity pure, while the older samples were expected to have significant decomposition. The use of these older samples allowed the assessment of the effects of decomposition products on the precision and accuracy of this method. With older samples, the early titration methodology produced inaccurate results[52,53] due to the high concentration of decomposition products, such as thiosulfate.

B.2. Solution Preparation

Potassium iodate (Mallinckrodt), dried at 95 °C for 24 hours prior to use, was used as a primary standard. Iodate was used to reduce potassium iodide to triiodide and standardize a 0.10 M sodium thiosulfate pentahydrate (Fisher, Certified ACS) solution. A 0.050 M solution of triiodide was made by mixing iodine (Spectrum) and a 2:1 excess of potassium iodide (Fisher, Certified ACS) in 2 L water. Using the standardized thiosulfate solution, this solution was standardized by titration with thiosulfate to four significant digits.[142] The 0.10 and 5.0 x 10^{-3} M triiodide solutions were prepared and standardized in a similar manner. The 37% (w/w) formaldehyde solution was obtained from Fisher (Certified ACS) and used as supplied. Sodium hydroxymethanesulfinate hydrate (Aldrich) was used for calibration of the ion chromatograph. Iodometric titration was used to determine hydration of the Rongalite sample. All solutions were prepared using ultrapure water (18 MΩ-cm).

B.3. Ion Chromatography Setup

A Metrohm Advanced IC-2 System was utilized for sample analysis. For thiosulfate and Rongalite quantification, the apparatus was equipped with a Metrosep A Supp 7-250 column and a Metrosep RP Guard column, both heated to 35 °C. A 3.60 mM sodium carbonate (EMD, Anhydrous ACS Grade) mobile phase was used with a flow rate of 0.7 mL/min. An 853 suppressor module was fed with a 0.10 M H_2SO_4 (Pharmco-Aaper, ACS Reagent) solution and deionized water. A CO_2 and an H_2O absorber cartridge preceded the air inlet.

IC samples were prepared by adding an accurately weighed 1.0000 g sample of dithionite to 75 mL of a basic formaldehyde solution. As discussed in Chapter I, the reaction of formaldehyde with dithionite quantitatively forms Rongalite (i.e. sodium hydroxymethanesulfinate, $HOCH_2SO_2Na$) and HMS (i.e. sodium hydroxymethanesulfonate, $HOCH_2SO_3Na$).

$$Na_2S_2O_4 + 2\ CH_2O + H_2O \rightarrow HOCH_2SO_2Na + HOCH_2SO_3Na \qquad \text{[Equation II-1]}$$

The formaldehyde solution contained 37.5 mL of the stock 37% formaldehyde solution which was diluted with 37.5 mL water and made basic with 7 or 8 drops of 10 M sodium hydroxide. After allowing reaction of the dithionite for approximately 20 minutes, the solution was diluted to 250 mL. From this solution, 50 mL aliquots were removed and further diluted to 2 L for IC analysis. At least three injections were analyzed per sample.

B.4. Titration Methodology

While a brief survey of the iodometric titration method for dithionite analysis was discussed in Chapter I, a more thorough exploration of the topic is presented here. The titration results are labeled X, Y and Z as in the original publication.[56] When a dithionite sample is added to a solution of iodine under acidic conditions, Equations II-2 - II-4 can occur depending on the species present.

$$S_2O_4^{2-} + 3\ I_2 + 4\ H_2O \rightarrow 2\ HSO_4^- + 6\ HI \qquad \text{[Equation II-2]}$$

$$2\ S_2O_3^{2-} + I_2 \rightarrow S_4O_6^{2-} + 2\ I^- \qquad \text{[Equation II-3]}$$

$$HSO_3^- + I_2 + H_2O \rightarrow HSO_4^- + 2\ HI \qquad \text{[Equation II-4]}$$

For these reactions, triiodide (I_3^-) and not iodine was used due to the presence of excess iodide and the insolubility of elemental iodine due to the large equilibrium constant for

the complex ion formation.[143] In addition, under acidic conditions sulfite (SO_3^{2-}) is typically protonated and is present as bisulfite (HSO_3^-).

The thiosulfate ($S_2O_3^{2-}$) concentration in the sample was determined by first reacting a dithionite solution with excess triiodide. Typically, approximately 1.0000 g of the dithionite sample was accurately weighed and dissolved in 75 mL 0.2500 M of triiodide solution containing 10 g of sodium acetate trihydrate. This was a scale-up from the original method which used 0.4000 g of dithionite for analysis. The rationale for this action was to obtain five significant digits in the analyses for statistical purposes. For older samples suspected to contain little sodium dithionite by weight (< 40%), 12.5 mL of a 3.5 M equivalent molar acetic acid-acetate buffer was used, as recommended by Kilroy.[56] Once all reducible sulfur species were reacted, excess sulfite was added in the form of a 10% sulfite solution until all the triiodide was removed and the solution became clear. Next, an additional 8 mL of the sulfite solution was added to regenerate the thiosulfate ion from the tetrathionate ($S_4O_6^{2-}$) ion (II-Equation 5).

$$S_4O_6^{2-} + SO_3^{2-} \rightarrow S_2O_3^{2-} + S_3O_6^{2-} \qquad \text{[Equation II-5]}$$

After these steps, the solution became acidic and was neutralized with 10 M sodium hydroxide using phenolphthalein as an indicator. Following neutralization, 10 mL of 37% formaldehyde followed by 25 mL of 20% acetic acid was added. This process removed the unreacted sulfite by reacting it with formaldehyde under acidic conditions to produce HMS.

$$SO_3^{2-} + CH_2O \rightarrow HOCH_2SO_3^- \qquad \text{[Equation II-6]}$$

A 50 mL aliquot was taken from the sample and acidified with 20% acetic acid to a pH of 3.5 to 4 as indicated by pH paper. Finally, the thiosulfate concentration was determined through titration of the pH-adjusted aliquot with the 5.00 x 10^{-3} M triiodide solution (Equation II-2). At least three aliquots were titrated per sample. If the amount of triiodide required to titrate the thiosulfate was **A**, the total amount of thiosulfate present in the sample was deemed to be 4**A**, as seen in Equations II-2 and II-4 (two $S_2O_3^{2-}$ ions are required to form one $S_4O_6^{2-}$ ion, which is then converted back to one $S_2O_3^{2-}$ ion) and the titration (Equation II-2) stoichiometry.

Once the thiosulfate is determined, the dithionite concentration can be quantified by reaction with formaldehyde to form Rongalite and HMS. Similar to the IC samples, 1.0000 g of the dithionite sample was weighed precisely and then added to 75 mL of basic formaldehyde solution described in the IC experimental. After 20 minutes, a 10 mL aliquot was removed. The aliquot was diluted with 150 mL of water and made acidic using 7.5 mL of an acetic acid-acetate buffer (3.5 M acetic acid and 3.5 M sodium acetate). The resulting solution was titrated with the 0.050 M triiodide solution. Again, at least three aliquots were titrated. In an idealized pure dithionite sample, an iodometric titration will provide the concentration of Rongalite and, in turn, the original concentration of dithionite.

$$HOCH_2SO_2^- + 2I_3^- + 2H_2O \rightarrow SO_4^{2-} + 6I^- + 5H^+ + CH_2O \quad \text{[Equation II-7]}$$

However, any thiosulfate present in the original sample will also react with the triiodide (Equation II-3). Thus, if the amount of triiodide required to titrate the Rongalite solution is **B**, the dithionite concentration was equal to (**B** - 2**A**)/2.

The final titration quantifies the amount of all reducible species present, namely thiosulfate, dithionite, and sulfite. Again, the reaction was scaled up for more accurate measurements. In this titration, 50 mL of 0.15 M triiodide and either 13 mL of the 3.5 M acetic acid-acetate buffer solution or 10 g sodium acetate trihydrate were mixed in a 250 mL volumetric flask, to which 1.0000 g of sample was added slowly. Once diluted, a 25 mL aliquot was removed and titrated with a 0.1000 M thiosulfate solution using starch as the indicator. This titration measures the amount of reducible species present as a whole, and the back titration with thiosulfate quantifies how much iodine was initially consumed. The amount of thiosulfate required to titrate is subtracted from the initial amount of iodine present; the difference, which would be the moles of iodine consumed when the sample is added to the iodine solution is labeled **C**. When combined with Equations II-2 - II-4, the amount of sulfite present in the original sample is equal to (2**C** + 2**A** – 3**B**)/2.

C. Results and Discussion

For dithionite analysis, the five samples were reacted with formaldehyde and analyzed by ion chromatography and the three-step titration method.

C.1. Ion Chromatography Results

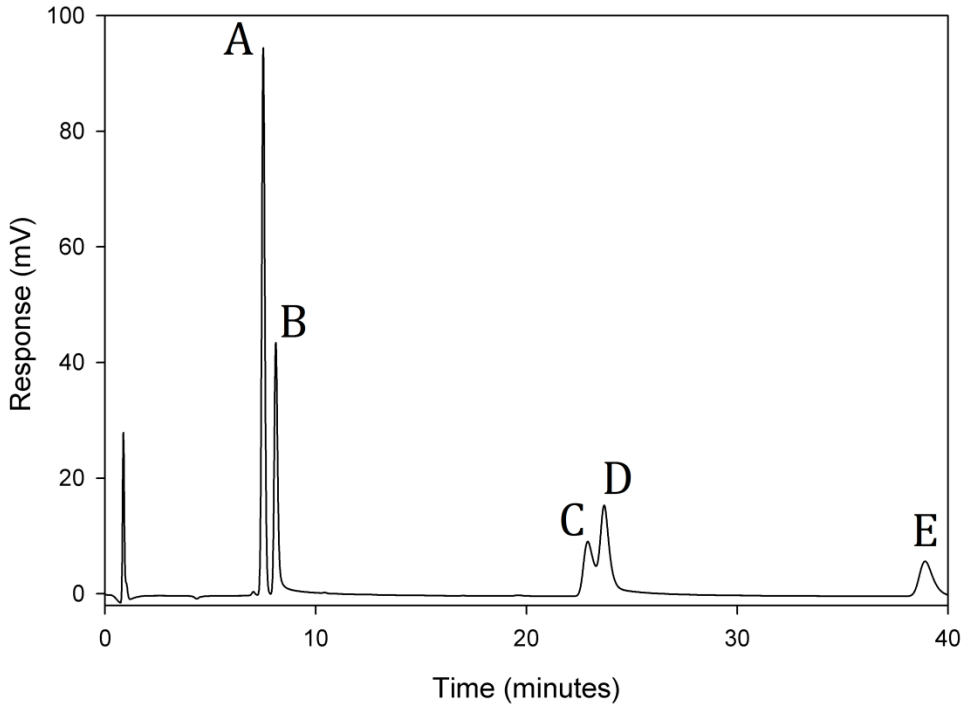

Figure II-1. Ion chromatogram showing Rongalite (Peak A), formate (Peak B), sulfite/sulfate (Peak C), HMS (Peak D), and thiosulfate (Peak E).

A typical ion chromatogram is shown in Figure II-1. As discussed in the Experimental section, the dithionite sample was first reacted with formaldehyde under basic conditions before injection into the IC. The disproportionation of dithionite in aqueous solutions[144] hindered accurate quantification of its concentration. Transforming the dithionite to a stable Rongalite product and the HMS adduct results in a solution that can be reproducibly quantified. In Figure II-1, Rongalite (Peak A) eluted between 7.6 and 7.8 minutes after injection. Peak B is due to formate, an impurity in the formaldehyde solution. This species eluted immediately following the Rongalite peak and is a potential interference. If a large excess of formaldehyde was used to react with the dithionite, as suggested in the titration study by Danehy *et al.*,[53] the two peaks

coeluted and made quantification impossible. Thus, the method of Kilroy,[56] which employed a much lower concentration of formaldehyde, was used. Given that Rongalite is quantitatively produced from the initial dithionite present (Equation II-1), measurement of this peak allows dithionite and thus the purity of the sample to be quantified.

In addition to Rongalite, HMS is also formed (Peak D). Equation II-1 implies that HMS is also quantitatively produced from the initial dithionite. Since HMS can also be formed from a reaction with sulfite and formaldehyde under acidic conditions (Equation II-6), it was initially hoped that both dithionite and sulfite could be quantified by measurement of both the Rongalite and HMS peaks. However, analysis showed that the resulting HMS peak area, calibrated using HMS standards, was inconsistent with this assumption. This signifies that HMS is either not quantitatively produced or decomposes in the alkaline mobile phase during the one-hour time scale of the experiment. Furthermore, the HMS species is partially coeluted with the Peak C. Standard solutions of both sulfite and sulfate produced peaks at approximately the same retention time as Peak Cs. These species are probably due to impurities in the initial material, due to the decomposition of dithionite, or generated from the reaction of formaldehyde with dithionite. This coelution prevents the quantification of this HMS, sulfite and sulfate. It is possible that an IC injection of an unfunctionalized (i.e. no formaldehyde) sample of dithionite solution could potentially prevent the coelution and allow for sulfite and sulfate quantification. However, since these coelutions do not affect the measurement of Rongalite and the determination of the dithionite, no further steps were taken. Finally, the thiosulfate (Peak E) was well separated from all other species with a retention time of 38.4 minutes and was easily quantified.

The Rongalite concentrations were determined by the peak areas of Peak A. For the calibration plot (R^2 = 1.00), four different Rongalite solutions were prepared. The concentrations of the dithionite anion were determined from the Rongalite concentration using Equation II-1 and are tabulated in Table II-2. The thiosulfate anion is an expected decomposition product of dithionite[144] and was quantified by measuring the peak area (for Peak E). A calibration curve (R^2 = 1.00) was also generated using four different sodium thiosulfate pentahydrate solutions. The standard deviations for the IC results are also reported in Table II-2 and were determined using multiple injections (at least three), and from the slope in the calibration plot and the dilution steps required to prepare the samples. Both the Rongalite and thiosulfate calibration curves can be found in Appendix A.

Both the dithionite and thiosulfate calibrations plots were analyzed to determine the limits of quantification using the methodology developed by Hubaux and Vos.[145] For the used calibration curve, the limit of quantification for sodium dithionite is 0.3% by mass. All samples are significantly above this limit. For the thiosulfate anion, the peak area in the newer samples (1 through 3) is relatively small. Although two samples with different dilution factors could have been utilized, the conditions used to optimize the determination of dithionite results in a limit of quantification at the 95% confidence level of 5% thiosulfate by mass. Thus, the thiosulfate concentration determined by IC in Table II-2 is at or under this limit and the error bars are not reported.

C.2. Titration Results

Table II-2 also reports the titration results for the dithionite and thiosulfate oxyanions of interest. The thiosulfate composition is directly measured. The standard deviations reported in Table II-2 are determined by multiple measurements (at least three). As discussed in the experimental, the dithionite titration results must be first corrected for the thiosulfate initially present in the sample. The standard deviations for dithionite included the uncertainty of both titration steps. Thus, the standard deviations for dithionite are consistently larger than those reported for thiosulfate.

C.3. Comparison of IC and Titration Methods

The IC and titration methods gave extremely similar results for dithionite and thiosulfate (Table II-2), with differences of less than 2% and 1%, respectively.

Table II-2. Sample anion concentrations and their associated standard deviations as mass percent determined by IC and titration. The error bars are the propagated error of the measurements, solution concentrations, and titration volume deviations.

Sample	**IC**		**Titration**		
	Dithionite	*Thiosulfate*	*Dithionite*	*Thiosulfate*	*Sulfite*
1	62.9 ± 0.7%	0.25%*	61.4 ± 1.2%	0.84 ± 0.07%	2.12 ± 1.73%
2	51.2 ± 0.8%	3.3%*	49.9 ± 1.0%	4.0 ± 0.1%	3.98 ± 1.73%
3	36.7 ± 0.4%	5.0%*	35.8 ± 0.7%	5.9 ± 0.1%	18.08 ± 1.35%
4	15.8 ± 0.1%	16.1 ± 0.2%	16.2 ± 0.4%	15.8 ± 0.2%	28.61 ± 1.00%
5	14.8 ± 0.2%	16.5 ± 0.3%	14.9 ± 0.4%	16.4 ± 0.2%	31.43 ± 1.23%

*These samples have concentration under the limit of quantification.

The IC measurements require only one straightforward derivation step before measurement. Assuming that dithionite is present solely as sodium dithionite, the purity of the sample can be computed and compared to the lot analysis provided by the supplier (Table II-3).

Table II-3. Compositions in mass percent for neutral sodium dithionite determined by IC and titration methods.

Sample	Date	Sodium Dithionite		Lot Purity
		IC	*Titration*	
1	December 2010	85.4 ± 1.0%	83.4 ± 1.6%	88%
2	September 2010	69.6 ± 1.0%	67.8 ± 1.3%	90.3%
3	May 2010	49.9 ± 0.6%	48.6 ± 0.9%	83.6%
4	August 2003	21.5 ± 0.2%	22.0 ± 0.6%	84%
5	March 1998	20.0 ± 0.2%	20.3 ± 0.6%	82.5%

Sample 1 was received and immediately tested upon opening. For this sample, both methods find that the purity is only slightly lower than the reported lot analysis, for which the uncertainly is not known. However, the two other samples, which were only half a year old or less, had lost 20% or more of the reported sodium dithionite content. This large decrease clearly illustrates the need for a quick and accurate determination of the concentration of dithionite before its use in an industrial process. The older samples are considerably different than the lot analyses and have significant decomposition. The similarities between the values determined by both methods for the highly decomposed samples show that the IC method is accurate, even in the presence of impurities. Finally, the difference between the measured dithionite and the lot analysis (Table II-3) is correlated with an increasing thiosulfate concentration (Table II-2).

Of note, while the measured quantities for dithionite and thiosulfate were extremely similar between the two methods, the sulfite was not quantifiable through IC, meaning the only quantification came from the titration method. While the sulfite was detectable in the IC, it was present in the chromatogram as a coelution, as seen in Figure II-1. This may be resulting from a pH effect or an equilibrium existing between the anion and its formaldehyde adduct, HMS. Additional work is needed to elucidate the reason for this

issue. In situations where quantification of the sulfite is required, the titration method should be used.

To confirm the similarities between the two analytical methods, a mean t-test analysis was performed. The calculated dithionite t-values are all less than 2.0 with an average of 1.6 and a minimum of 0.7. All values are below the critical t-value of 2.78 for a 95% confidence level and four degrees of freedom (i.e. N – 2, where N is the six observations made). Thus, the differences between the measured means for both these methods are not statistically significant. For thiosulfate, the t-values for sample 4 and 5 were 1.56 and 0.35, respectively, again implying that these methods produce results that are not statistically different. Since the first three samples are under the quantification limit for the given IC procedure, the calculated t-values were not calculated.

D. Conclusions

Five sodium dithionite samples were analyzed for dithionite composition using the established multi-step iodometric titration method and an ion chromatography (IC) approach. The IC method provided a simple one-step protocol to rapidly and accurately determine the concentration of dithionite. For the method presented, the limit of detection for sodium dithionite was 0.3% percent by mass, more than sufficient to determine the purity of the sample. The IC results were in excellent agreement with those obtained by titration, even for samples with significant decomposition. Once the IC calibration curves were generated, only one injection was required for determination the purity of a dithionite sample. The process, including the generation of the calibration curve, could be automated. In contrast, the titration method required multiple standard

solutions of triiodide, complex bench-top chemistry and, because the thiosulfate was required to determine dithionite concentration, significant skill is required. Compared to the titration method, the IC approach required less solution preparation and sample analysis and the results could be rapidly obtained. However, analysis for sulfite was only possible using the titration method, as the IC approach could not quantify sulfite.

CHAPTER III

SODIUM DITHIONITE PURITY AND DECOMPOSITION PRODUCTS IN SOLID SAMPLES SPANNING 50 YEARS

A. Introduction

Having previously validated the use of ion chromatography for analysis of sodium dithionite (Chapter II), ten samples of solid sodium dithionite ($Na_2S_2O_4$) at various stages of decomposition were analyzed using iodometric titration, ion chromatography, and Raman spectroscopy. Raman analysis of the soluted samples was also performed. Sample ages at the time of analysis ranged from within a month of being produced to 1963, nearly half a century old. As the sample age increased, there was a significant decrease in the measured dithionite and sodium compositions with a corresponding increase in the decomposition products of sulfite, thiosulfate, and sulfate. Significant decrease in purity occurs over first month for samples used as laboratory chemical regents. This decomposition is likely a result of the adsorption and reaction of water when the sample was exposed to atmosphere as well as redox reactions between oxygen and sulfur oxide species present in the samples.

For the oldest solid sample, Raman peaks characteristic of sulfate and tetrathionate were also present, signifying additional decomposition pathways had occurred. The presence of these decomposition species appears to affect the established iodometric titration results for quantification of sodium dithionite.

B. Experimental Details

B.1. Sodium Dithionite Samples

Ten samples of sodium dithionite were analyzed. Sample 1 was obtained specifically for this study and kept sealed while the other samples were in use in departmental labs at the time of this study. Of note, Sample 8 was located in a storeroom, unused for an extended but unknown amount of time. Lot analyses were acquired for the newest five samples while the remaining analyses could not be located. It is assumed that the analyses were completed using a single iodometric titration, which is acceptable given the high initial purities. The ages of the samples range from less than half a year to almost 50 years at the time of analysis (see Table III-1).

Table III-1. Sodium dithionite sample information, including the production dates and lot analyses.

Sample	Chemical Grade	Supplier	Production Date	Lot Analysis
1	*Purified*	J. T. Baker	Dec-2010	88%
2	*Technical (85%+)*	Alfa Aesar	Sep-2010	90.3%
3	*Technical (85%)*	Sigma-Aldrich	May-2010	83.6%
4	*Purified*	GFS Chemicals	Aug-2003	84%
5	*Technical (~85%)*	Aldrich Chemical Co.	Mar-1998	82.5%
6 , 7	*Laboratory*	Fisher Scientific	Feb-1985	-
8	*Purified*	J. T. Baker	Sep-1978	-
9	*Purified*	J. T. Baker	Aug-1978	-
10	*Purified*	J. T. Baker	Sep-1963	-

This span provides a wide range of samples with various degrees of decomposition in which to examine the decomposition products and assess the success of the different analytical techniques utilized. To ensure accurate sampling, all samples were homogenized through grinding and shaking of the powder before analysis.

B.2. Materials and Synthesis of Polythionates

Solid samples and solutions of sodium sulfite anhydrous (Fisher, Certified ACS), sodium sulfate (EMD, ACS), sodium thiosulfate pentahydrate (Fisher, Certified ACS), sodium metabisulfite (Mallinckrodt, Analytical Reagent), and sodium persulfate (Aldrich, ACS) were used as standards for Raman spectrum peak identification.

Sodium dithionate ($Na_2S_2O_6$) was synthesized and purified as previously reported.[146] In this approach, sodium sulfite and silver nitrate are reacted to prepare silver sulfite, which is then reduced to give sodium dithionate [Equations III-1 and III-2].

$$Na_2SO_3 + 2\ AgNO_3 \rightarrow Ag_2SO_3 + 2\ NaNO_3 \qquad \text{[Equation III-1]}$$

$$Ag_2SO_3 + Na_2SO_3 \rightarrow Na_2S_2O_6 + 2\ Ag \qquad \text{[Equation III-2]}$$

To save on the cost of production (namely, the amount of silver nitrate used), the described synthetic route was scaled down by a factor of 20. To begin, 5 g (0.04 moles) of sodium sulfite was added to 50 mL of H_2O while stirring. Once dissolved, a solution of 6.5 g (0.038 moles) of silver nitrate (GFS Chemicals, $\geq$ 99.9%) in 10 mL of H_2O was slowly added. The stirring solution was heated to boiling point, until the silver sulfite precipitate dissolved and was replaced by a precipitation of pure silver. The solution was vacuum filtered, and the removed silver precipitate was washed with two quantities of 5 mL of boiling H_2O. The filtrate was heated until the solution volume was approximately

15 mL, at which time the solution was cooled to room temperature and placed into an ice bath to effect crystallization. The crystals were filtered out and kept unwashed while the filtrate was further heated, mixed with 15 mL of boiling ethanol (Pharmco-Aaper, ACS/USP Grade), cooled and allowed to crystallize. The crystalline product was added to the first quantity of precipitate left on the filter and then pressed, washed with 5 mL of ethanol and 3 mL of acetone, and air dried for one hour. Recrystallization of the sodium dithionate product was performed with 5 mL of a 1:1 ethanol:water mixture heated to 80 ºC. The crystals were placed into a 50 mL round-bottom flask and stored at 4 ºC.

Anhydrous sodium trithionate ($Na_2S_3O_6$) was produced as a nonhydrated crystal as previously reported,[147] although it was scaled down by a factor of 10. In brief, 15 g (0.060 moles) of sodium thiosulfate pentahydrate was dissolved in 9 mL of H_2O and stirred into an ice bath. Over a period of forty minutes, 14 mL of 30% hydrogen peroxide (BDH) was added dropwise. Following this, more ice was added to the bath and the temperature was kept below 5 ºC for two hours. Following the precipitation, filtration and washing of sodium sulfate crystals with 25 mL of chilled (0 ºC) ethanol, the filtrate was removed. After mixing with 25 mL of chilled ethanol and filtering, an additional 120 mL of chilled ethanol was added, the solution stirred, and cooled in an ice bath for two hours. The produced trithionate crystals were filtered, washed with 5 mL portions of ethanol and acetone, and dried overnight in a vacuum desiccator. As with dithionate, the trithionate crystals were placed into a 50 mL round-bottom flask and stored at 4 ºC.

Sodium tetrathionate dihydrate ($Na_2S_4O_6 \bullet 2H_2O$) was the last compound synthesized for this study, using the method reported by Blitz and Blitz.[148] Again, the scale of the synthesis was reduced by an order of magnitude. Succinctly, 5 g (0.02 moles) of sodium

thiosulfate pentahydrate was mixed with 2.6 g (0.010 moles) of iodine and 2 mL of H_2O in a mortar and ground to a fine paste. The paste was transferred with 25 mL of ethanol to an Erlenmeyer flask and left to sit for three hours. Over this time, the sodium tetrathionate product was precipitated; this product was washed with an additional 25 mL ethanol to remove any residual iodine. Purification of the sodium tetrathionate was accomplished with its dissolution in 2.5 mL of H_2O, addition of 5 x 1 mL ethanol portions to the solution at five minute intervals, and letting sit undisturbed in a vacuum desiccator for ten hours. The formed crystals were then vacuum filtered, washed with 5 mL of chilled ethanol, and transferred into a beaker stored in a desiccator. After drying overnight, the sodium tetrathionate crystals were placed into a 50 mL round-bottomed flask and stored at 4 ºC.

B.3. Raman Spectroscopy

A Nicolet NXR 9610 FT-Raman spectrometer was used for the Raman analysis. The commercially-obtained and synthesized reference samples were utilized for characteristic peak identification. Samples were analyzed in both their solid and solution phases (0.10 g in 8 mL of H_2O) from 200 to 2000 cm^{-1} with a 4 cm^{-1} resolution and a minimum of 800 scans per compound to minimize noise. The laser power was reduced to 0.20 Watts to prevent compound degradation or destruction of either the solid samples or the Mylar sheet covering the cell window in which the solutions were contained. An InGaAs detector was used. The recorded Raman spectra can be found in Appendix B.

B.4. Titration and Ion Chromatograph Methodology

Samples were iodometrically titrated using the Wollak method as adapted by Kilroy and described in Chapter II.[50,56] As discussed by Kilroy, dithionite, thiosulfate and sulfite are determined from the results of three titrations of the samples under different conditions. [56] For ion chromatography, a Metrohm Advanced IC-2 System was utilized for sample analysis. Briefly, 1.0000 g of a dithionite sample was reacted with 70 mL of a 1:1 formaldehyde/water solution made slightly basic (pH = 10) with 10 M NaOH. After mixing for 20 minutes, the solution was diluted to a volume of 250 mL of H_2O. From this, a 50 mL aliquot was removed with a 50 mL Class A transfer pipette and diluted with RO-grade H_2O to 2 L, which was used for IC analysis. A minimum of three aliquots were analyzed per sample.

Solutions of sodium hydroxymethanesulfinate *x*•hydrate i.e. Rongalite (Aldrich) and sodium thiosulfate pentahydrate were used to construct calibration curves for the ion chromatograph. An iodometric titration was used to determine the extent of hydration of the Rongalite sample, which was found to be 77.15% Ronaglite ion mass per sample mass. These curves were constructed with four points each measured three times (R^2 = 1). These calibrations allowed the concentrations of thiosulfate and dithionite, determined from the Rongalite concentration, to be quantified. A detailed description of the ion chromatograph methodology and the three-part titration can be found in Chapter II and the measured calibration curves can be found in Appendix A.

In cation detection mode, the system was run with no chemical suppression. The column was switched to a Metrohm C2 150 cation exchange column set to 35 °C. The mobile phase was comprised of a 1.70 mM HNO_3 and 0.70 mM dipicolinic acid solution

and was run at 0.7 mL/min. For sodium sample analysis, approximately 0.10 g sample was dissolved in 1 L of RO-grade H_2O and injected into the IC, with four injections made per sample. For sodium quantification, a calibration curve was constructed with five sodium chloride solutions (ranging from 0.50 to 1.80 mM) and showed excellent linearity ($R^2 = 1$). The obtained sodium calibration curve can be found in Appendix A.

C. Results and Discussion

C.1. Raman Analysis of Sodium Dithionite Samples

Raman analyses of the samples as solids and aqueous solutions were performed. Raman spectroscopy provides qualitative information on the species present in each sample. As the dithionite decomposed, there were noticeable changes in the associated Raman spectra. To qualitatively determine composition of the samples, Table III-2 lists the characteristic vibrations for possible species both as solids and in solution, compiled from published sources.[149,150] When possible, standards were prepared and measured to confirm the assignments. In addition, the intensities and primary peaks were not the same for solid and solution samples, and relative intensity differences were not interpreted as concentration differences.

Table III-2. Characteristic vibrational frequencies for both the solid material and solutions compiled from published sources.[149,150]

	Solid / (cm^{-1})	Solution / (cm^{-1})
Bisulfite/Metabisulfite	273	1023
HSO_3^- / $S_2O_5^{2-}$	660	1051
	1064	
Sulfite	948	470
SO_3^{2-}	987	964
Bisulfate	1002	981
HSO_4^-	1026	1052
Sulfate	993	981
SO_4^{2-}		
Thiosulfate	433	447
$S_2O_3^{2-}$	452	997
Dithionite	250	229
$S_2O_4^{2-}$	1061	457
Dithionate	310	279
$S_2O_6^{2-}$	723	709
	1099	1091
Persulfate	834	835
$S_2O_8^{2-}$	852	1075
	1087	
Trithionate	262	419
$S_3O_6^{2-}$	441	1052
	1068	
Tetrathionate	395	387
$S_4O_6^{2-}$	1052	1039
Sulfur	154	Not
S	219	Soluble
	472	

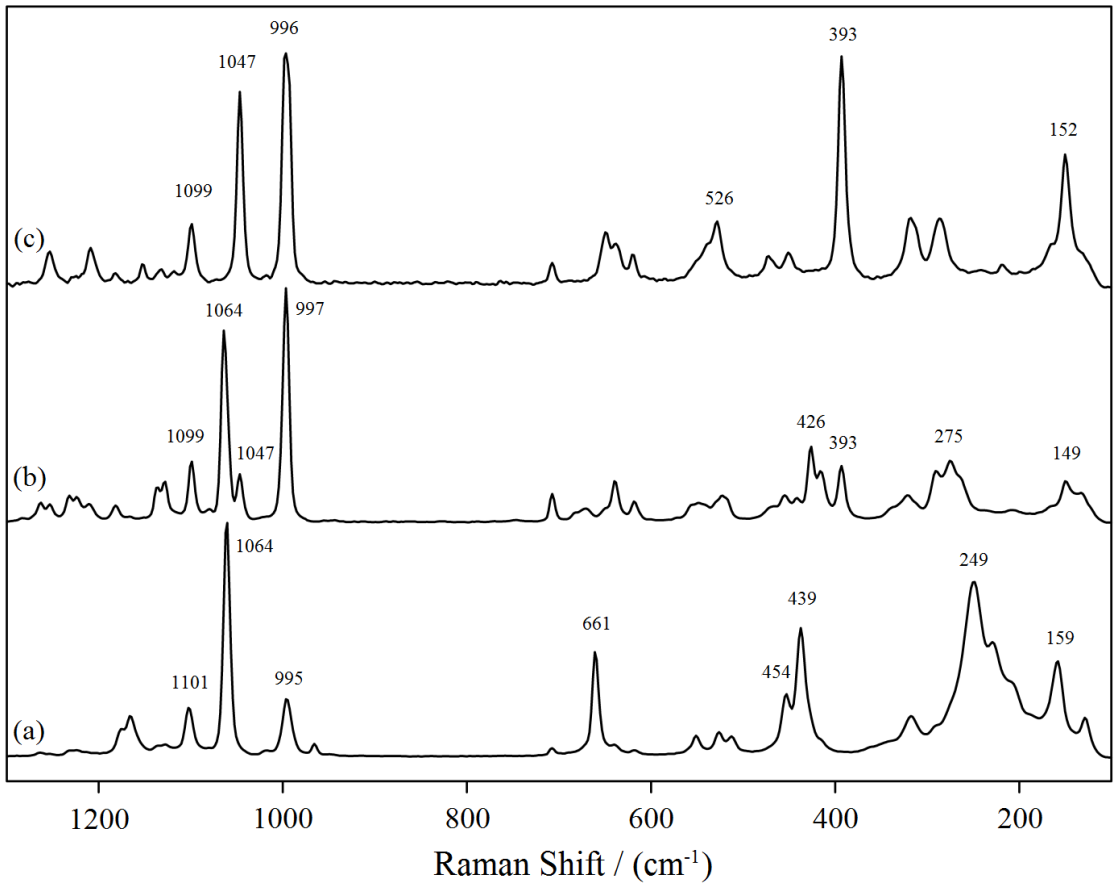

Figure III-1. Raman spectra for three solid samples as a function of age: (a) Sample 1 (Bottom), (b) Sample 3 (Center), and (c) Sample 10 (Top). Clear changes in the Raman can be observed between the purest sample (a) and the two older samples (b) and (c).

Figure III-1 shows Raman solid-state spectra for the newest sample (Sample 1, December 2010), an older sample (Sample 3, May 2010), and the oldest (Sample 10, 1963) sample. For the most pure dithionite sample (Figure III-1a), the strongest peaks were those of dithionite (249, 1061 cm^{-1}) and bisulfite/metabisulfite (660, 1064 cm^{-1}). Given the 4 cm^{-1} resolution of the spectrometer, the 1061 cm^{-1} peak for dithionite and the 1064 cm^{-1} peak characteristic of bisulfite/metabisulfite cannot be resolved. Also present were peaks indicating the presence of small amounts of sulfate (995 cm^{-1}), thiosulfate (439, 454 cm^{-1}), dithionate (1101 cm^{-1}) and possibly sulfur (159 cm^{-1}), though this could

be due to vibrations in the S-S bond of dithionite. Commercially available sodium dithionite typically has purity below 90% and many of these compounds are expected to be present in the material. As the age of the samples increased (see Figure III-1b), a decrease was seen in the strongest dithionite peak (249 cm^{-1}) without a decrease of the 1061 cm^{-1} peak, possibly signifying the creation of bisulfite/metabisulfite as a decomposition product of dithionite. Consistent with dithionite decomposition, there was a noticeable increase in the thiosulfate and sulfate peak intensities with sample age as well as the appearance of tetrathionate (393, 1047 cm^{-1}). Interestingly, the spectrum of Sample 8 contained strong dithionite peaks with weaker peaks for decomposition products, signifying less decomposition of the dithionite. Despite being over 30 years old, Sample 8 was well sealed with tape and subsequently had significantly less atmospheric exposure with respect to other samples of similar age or even younger. Present in every solid sample was a peak between 1098 and 1101 cm^{-1}, characteristic of dithionate (1099 cm^{-1}). While a minor feature in the newest samples, dithionite was one of the primary features in the oldest sample (Sample 10, 1963). Besides this, the oldest sample also contained additional features not present in the other samples. Raman spectroscopy identified tetrathionate (394, 1046 cm^{-1}) and sulfate (996 cm^{-1}) with smaller peaks possibly indicating bisulfite or metabisulfate. The identity of the species responsible for the peak at 526 cm^{-1} is undetermined.

Additional analyses of aqueous samples produced form these solids were performed to determine if any substantial changes occur during the solution preparation. Samples were prepared by dissolving 0.10 g of solid in 8 mL of water. Although the intensities and wavenumbers of the various species will change once solvated (Table III-2), the

composition of the solution should remain unchanged within the measurement time. Consistent with the solid sample, the strongest peak present in solution for samples less than one year old was that of dithionite (226, 579 cm^{-1}). However, illustrating the importance of not interpreting relative peak intensities as differences in concentration, the thiosulfate (457 cm^{-1}) was also one of the strongest peaks in the liquid sample as opposed to bisulfite/metabisulfite in the solid sample. Titration and ion chromatograph results (Tables III-3 and III-4) discussed below show that thiosulfate comprises less than 2% of Sample 1 by mass. Additional peaks characteristic of thiosulfate (447 cm^{-1}), sulfate/bisulfate (981 cm^{-1}), and bisulfite/metabisulfite (1052 cm^{-1}) were also present. Most samples show an additional peak at 1091 cm^{-1}, characteristic of dithionate, which increases with the age of the sample. This pattern is consistent with the results obtained from the solids. Also consistent with the solid-state spectroscopy, the spectrum for a solution of the oldest sample was distinguishing. The only peaks present in the spectrum were identified as sulfate/bisulfate (981 cm^{-1}), tetrathionate (389, 1039 cm^{-1}) and dithionate (1091 cm^{-1}) with no other signal peaks present.

C.2. Titration and Chromatography Results

A three-step iodometric titration was used to determine the composition of the dithionite samples. The titration methodology was performed as previously described in Kilroy and the previous Chapter.[56] The use of three titrations was required to accurately determine the dithionite composition in the presence of the additional reducible species, thiosulfate and sulfite. Of the ten samples analyzed, the most recently produced samples were expected to contain more dithionite and less decomposition products than older

samples. While every other sample was in use at the time of this study, Sample 1 was kept sealed when received and immediately analyzed upon opening. This was done to prevent sample degradation. The analysis results are summarized in Table III-3.

Table III-3. Sample composition as a percent of anion mass in the sample mass measured by a three-step iodometric titration. The subtractions described by the titration methodology result in a negative value for dithionite in the oldest sample (Sample 10), possible due to an unidentified species (see text for details). Error bars were determined by the standard deviation of the analyses, followed by error propagation.

Sample	Production Date	Dithionite	Thiosulfate	Sulfite
1	Dec-2010	61.37 ± 1.16%	0.84 ± 0.07%	2.12 ± 1.73%
2	Sep-2010	49.86 ± 0.99%	3.95 ± 0.09%	3.98 ± 1.73%
3	May-2010	35.78 ± 0.69%	5.87 ± 0.11%	18.08 ± 1.35%
4	Aug-2003	16.16 ± 0.43%	15.85 ± 0.24%	28.61 ± 1.00%
5	Mar-1998	14.94 ± 0.42%	16.44 ± 0.25%	31.43 ± 1.23%
6	Feb-1985	0.37 ± 0.26%	21.17 ± 0.31%	36.92 ± 0.61%
7	Feb-1985	1.13 ± 0.24%	22.83 ± 0.34%	37.16 ± 0.59%
8	Sep-1978	33.00 ± 0.66%	9.77 ± 0.16%	22.16 ± 1.48%
9	Aug-1978	0.40 ± 0.23%	15.07 ± 0.23%	27.57 ± 0.61%
10	Sep-1963	-5.40 ± 0.22%	21.64 ± 0.34%	4.40 ± 0.74%

The newest sample (Sample 1) had the highest dithionite anion composition by mass and very little decomposition products. However, once opened, sample purity deteriorated, losing up to half of its dithionite composition in less than a year, i.e. Samples 2 and 3. The deterioration was likely a result of decomposition due to water adsorption, which is accompanied by an increase in thiosulfate and sulfite. This trend became especially apparent in older samples, with the exception of Sample 8, which was well sealed. The need for a three-step titration is clearly seen by the increase thiosulfate and sulfite. For examples, other than the first two, the decomposition leads to errors exceeding 30% using the one step titration method of Merriman,[49] which the American Association of Textile Chemists and Colorists recommends only for relatively pure

samples.[51] These quantitative results are consistent with the Raman spectra above; the composition of the dithionite samples can be clearly seen to shift to thiosulfate and sulfite as the samples age. Being the oldest dithionite sample tested, it was expected that Sample 10 would have the lowest measured dithionite composition and the highest composition of thiosulfate and sulfite. However, when determined through titration, not only was the dithionite composition for this sample found to be negative, but the sulfite composition was also extremely low (4.40%) compared to the samples preceding it (≥20%). These unexpected results can be understood when reviewing the titration method. In this method, the dithionite concentration is calculated as the difference between two titrations, one for thiosulfate and one for dithionite and thiosulfate.[56] However, the thiosulfate titration assumes that no additional products that can reduce iodine are present. In fact, Raman spectroscopy for this sample indicated the presence of dithionate and tetrathionate in the sample. It has been established that in the presence of sulfite under basic conditions, tetrathionate reacts to form thiosulfate and trithionate (Equation I-16). It is likely that this species decomposed during the solution preparation for titration and produced a reducible compound, most likely thiosulfate or possibly another anion through a different mechanism, which reacted with iodine and affected the results. The sulfite could have been consumed by tetrathionate to produce thiosulfate, or it is also possible that the sulfite composition is extremely low for this sample, having been converted to a more stable decomposition product (e.g. sulfate).

Ion chromatography can directly analyze anions and cations in solution by chemical separation. This allows the dithionite and thiosulfate in the dithionite samples to be determined independently (see Table III-4). Solutions were produced by dissolving

1.0000 g of material in 70 mL of a basic formaldehyde solution followed by dilution (see Experimental Section). Each sample was measured four times. In addition, chemical standards were utilized to independently verify the retention time.

Table III-4. Sample composition of dithionite and thiosulfate as percent anion of sample mass, measured by ion chromatography. Error bars were determined by the standard deviation of four analyses, followed by error propagation.

Sample	Production Date	Dithionite	Thiosulfate
1	Dec-2010	62.87 ± 0.71%	0.25 ± 0.01%
2	Sep-2010	51.23 ± 0.75%	3.28 ± 0.06%
3	May-2010	36.72 ± 0.44%	5.03 ± 0.07%
4	Aug-2003	15.84 ± 0.16%	16.13 ± 0.20%
5	Mar-1998	14.76 ± 0.19%	16.52 ± 0.28%
6	Feb-1985	0.13 ± 0.01%	22.17 ± 0.31%
7	Feb-1985	0.18 ± 0.01%	23.16 ± 0.25%
8	Sep-1978	32.81 ± 0.48%	8.95 ± 0.16%
9	Aug-1978	0.06 ± 0.01%	15.33 ± 0.31%
10	Sep-1963	0.04 ± 0.01%	3.12 ± 0.07%

With the exception of Sample 10, the two methods are found to be in excellent agreement for dithionite and thiosulfate within 2% and 1%. As was seen with the sample titrations, the dithionite composition was found to be extremely low for samples older than 20 years, with the exception of the well-sealed Sample 8, indicating the nearly complete decomposition of dithionite at these ages.

Unlike ion chromatography, the titration produced an impossible negative concentration for dithionite for Sample 10. As discussed above, dithionite concentration is calculated as the difference between two titrations and additional products can affect the result. This issue also results in a much higher thiosulfate composition measured by titration (21.64%) with respect to ion chromatography (3.12%). In addition to the

increased simplicity of ion chromatography with respect to the labor insensitive three-step titration method, the ability to separate the ions can remove these interferences and give more reliable results for highly decomposed samples. For Sample 10 (the oldest sample), ion chromatography was able to confirm the presence of dithionate and tetrathionate, at retention times of approximately 80 and 210 minutes, respectively. Prepared standards established the identities of these peaks.

Ion chromatography was also used to determine the sodium composition for each sample. It was expected that as the decomposition of the dithionite occurred due to atmospheric exposure, the associated sodium composition would decrease due to the absorption of water. The sodium concentration as a percent by mass are listed in Table III-5. Pure sodium dithionite has a sodium percent composition by mass of 26.41%.

Table III-5. Sodium sample content as measured by ion chromatography. Error bars were determined by the standard deviation of four analyses, followed by error propagation.

Sample	Production Date	Measured Sodium Content
1	Dec-2010	26.11 ± 0.56%
2	Sep-2010	25.38 ± 0.37%
3	May-2010	25.57 ± 0.49%
4	Aug-2003	25.75 ± 0.55%
5	Mar-1998	25.19 ± 0.68%
6	Feb-1985	24.35 ± 0.27%
7	Feb-1985	25.43 ± 0.22%
8	Sep-1978	25.67 ± 0.51%
9	Aug-1978	23.21 ± 0.36%
10	Sep-1963	22.63 ± 0.33%

Although the effect is small, the measured sodium composition did seem to decrease with increasing sample age (see Table III-6).

Table III-6. Sodium dithionite compositions as a mass percent of the ionic compound in the samples, taken from lot analyses, ion chromatography and iodometric titrations. Error bars were determined by the standard deviation of four analyses, followed by error propagation.

Sample	Production Date	Sodium Dithionite Composition		
		Lot Analysis	*Titration*	*IC*
1	Dec-2010	88%	83.39 ± 1.58%	85.43 ± 0.97%
2	Sep-2010	90.3%	67.76 ± 1.35%	69.61 ± 1.02%
3	May-2010	83.6%	48.62 ± 0.94%	49.90 ± 0.60%
4	Aug-2003	84%	21.96 ± 0.58%	21.52 ± 0.22%
5	Mar-1998	82.5%	20.30 ± 0.57%	20.06 ± 0.26%
6	Feb-1985	-	0.50 ± 0.35%	0.18 ± 0.01%
7	Feb-1985	-	1.54 ± 0.33%	0.24 ± 0.02%
8	Sep-1978	-	44.84 ± 0.90%	44.58 ± 0.65%
9	Aug-1978	-	0.54 ± 0.31%	0.08 ± 0.01%
10	Sep-1963	-	-7.34 ± 0.30%	0.05 ± 0.01%

This is a result of the adsorption and reaction of water with dithionite, resulting in an increased sample mass and extent of decomposition with a concomitant decrease in the associated sodium composition. Sample 1, being the most recently produced, had the highest measured sodium content due to the lack of exposure to atmosphere and subsequent degradation; both titration and ion chromatography gave a value within 5% of the reported content. However, Sample 10, being nearly fifty years old, had the lowest sodium content. Consistent with other results, the well-sealed Sample 8 had slightly higher sodium content than expected for its age, comparable to samples less than one year old. Again, the high sodium content supports the hypothesis that lack of sample exposure to atmosphere prevented the adsorption of water and subsequent decomposition of dithionite.

D. Conclusion

Ten samples of sodium dithionite at various ages and stages of degradation were analyzed to determine the sample compositions. It was determined that as a sample aged, various degradation products were formed due to water adsorption. For new samples, the primary species found were dithionite, thiosulfate and sulfite (possibly as bisulfite), with dithionite composition decreasing as the age of the sample increased. For the oldest samples, there was the appearance of sulfate and dithionate. Unique to the oldest sample was the presence of tetrathionate, indicative of the more advanced stage of sample decomposition. When these oxidized byproducts are present, analysis through iodometric titration can be problematic.

CHAPTER IV

TITANIA-HYDROXYPROPYL CELLULOSE THIN FILMS FOR THE DETECTION OF PEROXIDE VAPORS

A. Introduction

Titania nanoparticles in a hydroxypropyl cellulose matrix produced using a sol-gel method was utilized to prepare films on polycarbonate slides and coatings on cellulose filter papers. The exposure of these colorless films to hydrogen peroxide vapor leads to the development of an intense yellow color. Using a tungsten lamp and an inexpensive web camera to measure the reflected light, first-order behavior in the color change was observed when exposed to peroxide vapor of less than 50 ppm. For 50 mass percent titania nanoparticles in hydroxypropyl cellulose films on polycarbonate, the detection limit was estimated to be 90 ppm after a one minute measurement and 1.5 ppm after a one hour integration. The coatings on the filter paper had a threefold higher sensitivity compared to the films, with a detection limit of 5.4 ppm peroxide for a one minute measurement and 0.09 ppm peroxide after a one hour integration. The high sensitivity and rapid response of these films makes them a promising material for use as a sensitive peroxide detector.

B. Experimental Details

B.1. Preparation of Titanium(IV) Isopropoxide-Hydroxypropyl Cellulose Solution

A solution of titanium(IV) isopropoxide with hydroxypropyl cellulose in 2-propanol was produced following the procedure outlined by Kozuka and coworkers.[141] Briefly, 1 g of hydroxypropyl cellulose (Alfa Aesar, M.W. = 100,000) was dissolved in 70 mL of 2-propanol (Pharmco-Aaper, ACS Reagent). A measured amount of titanium(IV) isopropoxide (Alfa Aesar, 97 %) was then added dropwise while stirring. After stirring for one hour under nitrogen, 1.5 g of concentrated hydrochloric acid (Pharmco-Aaper, ACS Reagent) diluted with 20 mL of 2-propanol was added to the titanium-cellulose solution while swirling the solution. The final solution was stirred under nitrogen for 24 hours before use. Solutions with varying quantities of titania were prepared up to the point where sufficient titania was present to yield a 60 mass percent titania/(titania+cellulose) film, assuming that the titanium(IV) isopropoxide was completely converted to titania. After production, the solutions were pale yellow and stored under nitrogen. Film preparation was typically performed within 12 hours after the initial 24-hour mixing period.

B.2. Preparation of Sol-Gel Films on Polycarbonate and Filter Papers

Polycarbonate slides (2.54 x 7.62 x 0.152 cm) were sonicated in ethanol for 30 minutes and dried in air. Once dried, an excess volume of the titanium(IV) isopropoxide-cellulose solution was applied to a slide held in an aluminum slide holder (0.040" deep). A Gardco 8-path wet film applicator was used to remove the excess solution and produce

films of the precursor solutions with a homogeneous thickness of 0.020". The procedure was standardized for the reproduction of homogenous films (see Figure IV-1).

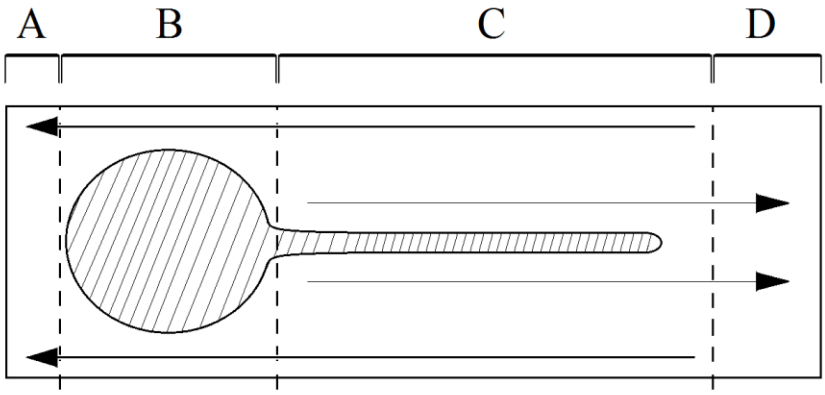

Figure IV-1. Layout and deposition method for production of films on glass and polycarbonate slides.

First, a pool of 12 drops of the titania-cellulose solution (Section B) was made 0.5 cm from one end of the slide (Section A). Next, a line of 13 drops was extended down (Section C) to the other end of the slide (Section D). The Gardco 8-path wet film applicator, with a selected height of 40 mils (0.040 in), was pulled from the tip of Section B to the end of Section C, lifted, and pushed from the end of Section D through Sections C, B, and A, past the end of the slide. The slides were then placed under a watch glass to air dry for one hour. The resulting films were used as prepared without the implementation of the calcination stage.

Coatings were produced on cellulose filter paper (VWR 415) by coating one side of the paper (see Figure IV-2).

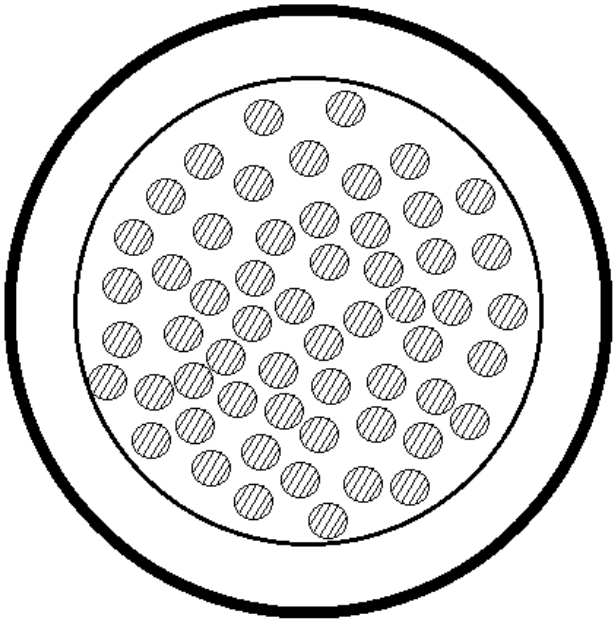

Figure IV-2. Diagram for the production of coated filter papers. Shown are drops of the titanium isopropoxide-cellulose in crystallization dish (thick line) with placement of the 3" filter paper (thin line).

To produce coated papers similar in loading to the glass and polycarbonate films, an equal volume-per-area between the slides and papers was used. With 25 drops being used to coat a slide 2.54 cm wide by 7.62 cm long, the filter paper, with a diameter of 7.5 cm, would require 57 drops for equal volume-per-area coverage. To apply this volume of solution, 57 drops were placed in the bottom of a crystallization dish in a traced outline of the filter paper underneath. Once added, the filer paper was placed on the solution, absorbing the drops on the paper's surface. To ensure uniform coverage, the paper was rotated and slid across the surface of the crystallization dish in order to absorb as much as possible. The papers were then removed and hung vertically to air dry for one hour. In the first 5 minutes of drying, the filter papers were constantly rotated to ensure a uniform thickness (i.e. homogenous distribution of the solution throughout the paper).

B.3. Titanium(IV) Oxysulfate Solution for Peroxide Quantification

The colorimetric procedure developed by OSHA was utilized to measure the peroxide vapor concentration.[97] This method requires a solution of titanium(IV) oxysulfate in sulfuric acid. This was produced by dissolving a mixture of 5.5 g of dehydrated $TiOSO_4 \cdot xH_2O$ (Strem Chemicals) and 20 g of ammonium sulfate (Spectrum, A.C.S. Reagent) in a heated solution of 100 mL of sulfuric acid (Pharmco-Aaper, A.C.S. Reagent). After cooling, the resulting pale yellow solution was added to 350 mL of ultrapure water, again cooled to room temperature, filtered through a 0.40 μm filter to remove any suspended materials, and diluted to a final volume of 500 mL.

B.4. Peroxide Solutions for Gas Exposure

Peroxide solutions of various concentrations were made through dilution of a 30% hydrogen peroxide stock solution (BDH). Given that the uptake of hydrogen peroxide gas from the solution phase in the bubbler is a turbulent process, direct control of the created vapor concentration is not possible; both solution concentration and temperature as well as carrier gas flow rate can greatly affect the concentration of the produced peroxide vapor. For these reasons, solutions with numerous concentrations (1, 2, 5, 10, 15, and 20% hydrogen peroxide by volume) were made and stored in a refrigerator at 4 ^{o}C when not being used. When used, each solution was warmed to room temperature over the course of one hour and then poured into the bubbler. While these actions did not ensure reproducible behavior of peroxide uptake, standardization of the method was important for similar exposure conditions.

B.5. Film Testing Apparatus

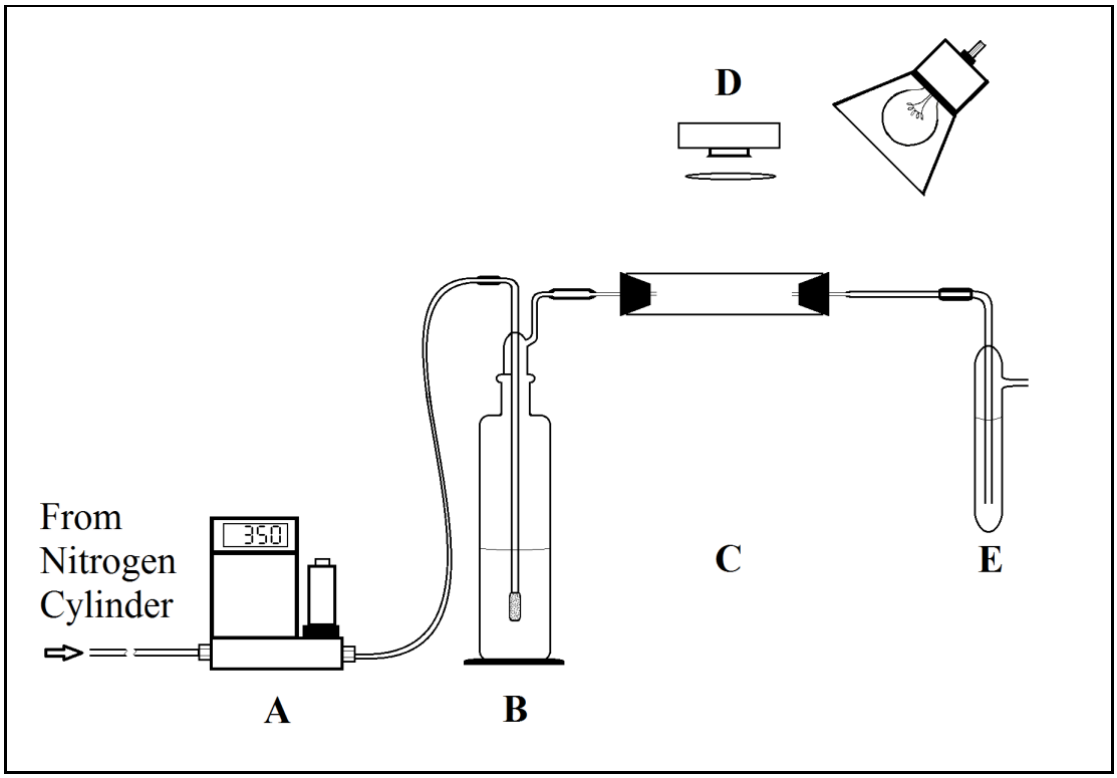

Figure IV-3. Schematic diagram of the peroxide exposure apparatus. Depicted are the (A) flow controller, (B) bubbler to entrain peroxide vapor, (C) exposure chamber, (D) detection system, and (E) a bubbler used to determine the total concentration of peroxide in the flow.

Figure IV-3 shows a schematic diagram of the apparatus that was used to expose and monitor the films. The apparatus was assembled in a hood, and the window was blocked to negate the effects of outside light. A nitrogen cylinder (Airgas, Ultrahigh Purity) was used to supply nitrogen as the carrier gas. A gas regulator was set to a backing pressure of 20 psi and the flow was regulated at 350 standard cubic centimeters per minute using an Omega FMA 5500 mass flow controller (**A**). To ensure the reported flow was accurate, an HP soap film flowmeter was used repeatedly; it was found to be within 5% of the reported flow for all experiments. The nitrogen flow was then directed through a 250 mL bubbler containing the peroxide solution (**B**). The gas was dispersed

into the solution using a sintered glass head, which distributed the gas through the solution to ensure a steady uptake of the peroxide vapor. Next, the peroxide-enriched gas was directed into a glass cell containing the sample, either a coated polycarbonate slide or a cellulose filter paper. The glass cell (**C**) had a piece of white paper attached on its outside bottom to create a white background. A 20 W incandescent light was positioned above the cell to provide homogenous lighting for the slide and a Logitech Pro 9000 USB camera recorded images of the sample during exposure to peroxide vapor (**D**). Between the camera and the cell was a Leiz Wetzlar BG 12 blue bandpass filter, which isolated the wavelengths between 300 and 500 nanometers. After leaving the cell, the gas progressed through a bubbler containing 25 mL of the titanium(IV) oxysulfate solution (**E**), which reacted with the peroxide in the gas and produced a color change that was proportional to the total quantity of peroxide in the gas. A second bubbler was attached following the first one to confirm complete reaction of entrained peroxide vapor with the titanium(IV) oxysulfate solution. There was no measured absorbance change in the second bubbler's solution when run with 30% peroxide solution for 30 minutes, which indicated that the peroxide vapor was completely reacted in the first bubbler. The total peroxide concentration was determined using a colorimetric method that utilized the absorption of the titanium(IV) oxysulfate solution at 410 nm.[97] A Cary 50 Bio UV-VIS spectrometer was used for the absorption measurement and was calibrated as per this colorimetric method. The peroxide concentration in the gas was computed using the total concentration in titanium(IV) oxysulfate solution, the flow rate which was fixed at 350 sccm for all experiments, and the exposure time of the films to the flowing gas. This process was performed for every exposure to determine the vapor concentration. The

referenced OSHA VI-6 method describes the hydrogen peroxide quantification procedure for gas phase sampling.[97]

The total volume of N_2 gas passed through the apparatus is 21 L for an hour-long exposure. Since N_2 gas bubbles through an aqueous solution of hydrogen peroxide, the addition of water vapor could slightly increase the total volume of gas volume passed. Since this was not corrected for in the computation of the gas phase concentration of hydrogen peroxide, a slight underestimation could possibly occur. Running the bubbler for an extended time (18 hours) resulted in a water mass loss of 0.5 g/hour. This mass of water corresponds to approximately 0.6 L of water vapor in 21 L of N_2 gas, given a maximum 3% error towards lower ppm.

Before each experimental run, the targeted gas phase concentration was obtained by varying the concentration of hydrogen peroxide in the bubbler solution. For precise values, some iteration is required due to variability in the stock hydrogen peroxide concentration with time. Once started, each experimental run was recorded as an MJPG video and saved to a disk. The video was shortened using the open-source program MEncoder by extracting one frame every ten seconds for the duration of the exposure, typically 0.5 to 1 hour. Data reduction was performed using ImageJ, an open-source analysis software package developed by the National Institute of Health.[151] The imported video was split into red, blue, and green channels. As discussed above, the BG 12 blue bandpass filter limited the range of recorded wavelengths from 300 to 500 nm. In these experiments, the reflected light saturated the blue channel and, therefore, the red channel, which had much lower sensitivity in the blue region, was used to quantify the reflected light. The response of the red channel to the desired analytical wavelengths was

confirmed using a broad band light source and a monochromator. Intensities were extracted from the video using ImageJ. Except when noted, the intensity was determined by an average center section area of the samples and the results were used to generate all plots.

B.6. Particle Size Measurement

A Malvern HPP5001 particle size analyzer was used for size characterization of particulates in the solution. Twenty-five measurements were performed for each sample, which were undiluted and measured at 25 ºC. Scans of 0% and 50% mass ratio titanium-cellulose solutions were performed daily over a period of two weeks.

B.7. Electron and Force Microscopies

Scanning electron microscopy (SEM) analysis of the films was performed with a Quanta 600F ESEM, using a spot size of 3.5 and a potential voltage of 20 kV. Additionally, a Bruker Multimode 8 atomic force microscope with an Ultrasharp silicon cantilever (NSC 14/50) was used for surface roughness measurements. A 10 μm by 10 μm scan area was used with the cantilever operating in tapping mode, and Research Nanoscope 7.2.0 was used for image analysis and production of false color images.

C. Results and Discussion

C.1. Stability and Characterization of the Films and Coatings

Films and coatings were prepared as described in the Experimental section. As the films air-dried, there was a tendency for the films, produced from the titanium(IV)

isopropoxide-cellulose solutions with high titania mass loading, to crack or peel away from the slide. This cracking was especially prevalent for films deposited on glass slides, which lead to the use of polycarbonate slides in this investigation. On the polycarbonate substrates, virtually all of the 40 and 50 mass percent titania coatings produced high quality films upon drying. However, films with 60 mass percent titania could not be produced without cracking (see Table IV-1).

Table IV-1. Film quality after drying on polycarbonate slides as a function of the titania mass percent or loading. The titania mass percent is determined by the titanium isoproproxide-cellulose solution used to create the film.

Mass Percent Ti	Initial Film Quality
0% (Control)	Smooth
20%	Smooth
40%	Smooth
50%	Smooth
60%	Cracking, Peeling

The decrease in adherence of the films to the slide with high titania content may be due to the lower hydroxypropyl cellulose content and increased stress within the film, which results in a greater propensity for cracking. These findings are in agreement with the previous description of film cracking at higher titania loadings by Kozuka and coworkers.[141] Additional films were made that were either thicker or layered. With layering or increasing the thickness of the 60 mass percent titania films, the tendency of the films to pull away from the slides became more pronounced, with peeling manifesting in the thickest films (see Table IV-2). Cracking was still present, but peeling was the main contributor of the films' instability.

Table IV-2. Effects of layering and thickness on stability of 60 mass percent titania films on polycarbonate.

Film Characteristic	Peeling or Cracking
1 Layer	Cracking
1 Layer, 2X as Thick	Both
2 Layers	Both

Therefore, the majority of the work described herein was performed with single-layered films with a 50 mass percent titania loading or lower. The greatest color change was obtained for films and coatings with 50 mass percent titania content. These films also displayed excellent overall stability on the polycarbonate slides before peroxide exposure. Although films with 40 and 50 mass percent titania loading developed stress cracks after reacting with the peroxide vapor, the degree of cracking had little influence on the observed color evolution upon exposure to hydrogen peroxide. There was no observable cracking or peeling of coatings applied on the filter paper.

To measure the surface roughness of the prepared films, atomic force microscopy (AFM) was utilized. A film produced from 50 mass percent titania loading was formed onto a glass slide and a 10 μm by 10 μm section of the surface was analyzed (see Figure IV-4).

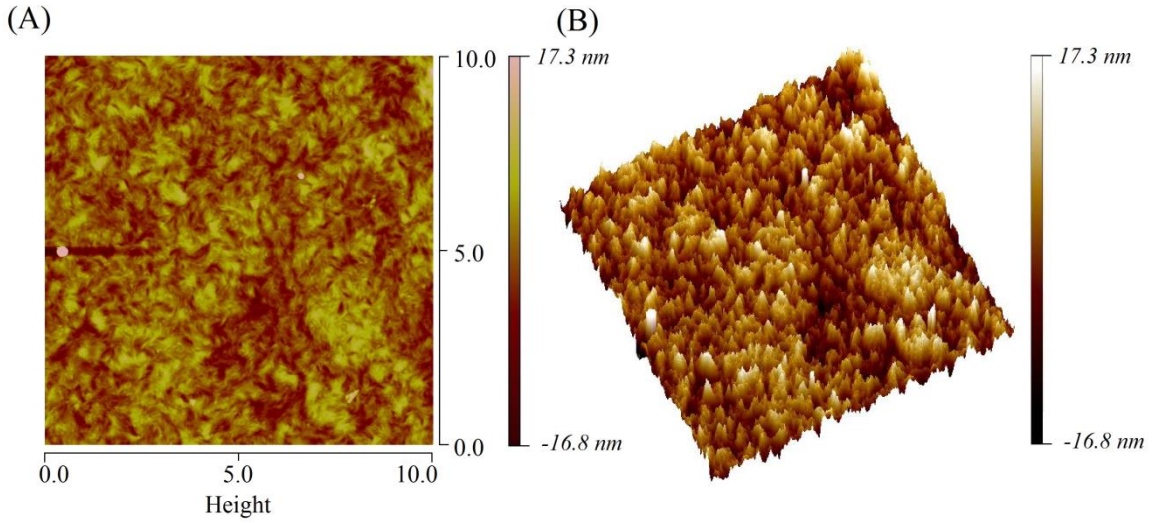

Figure IV-4. False-color images of (A) the height and (B) surface roughness of a 50 mass percent titania-cellulose film, measured by AFM.

For the measured film, the root mean square roughness (R_q) was measured to be 5.23 nm. For comparison, the measured R_q value for Si(100) etched using the RCA method (a method used to produce clean, planar silicon surfaces for integrated circuitry) has been found to be 0.09 nm, extremely small given the expected flatness of the surface.[152] At the other extreme, superhydrophobic films of trimethylsilanized silica using the sol-gel process have been found to be close to 30 nm, highlighting the large peak to valley difference which imparts the films with the hydrophobic tendencies.[153] Such titania films can be characterized as moderately smooth as a result of the slow evaporation of the solvent and congealing of the cellulose matrix.

As the titania-cellulose solutions aged, there was an observable increase in the turbidity of the solution. This increase was attributed to continual particle growth and aggregation with time. Dynamic light scattering (DLS) analysis was used to measure the growth of the titania nanoparticles in freshly prepared solutions as they aged for up to 1 week (see Figure IV-4 and IV-5). DLS measurements of the precursor solution for 50

mass percent titania films were performed immediately (i.e., within 5 minutes) after preparation and one day of mixing.

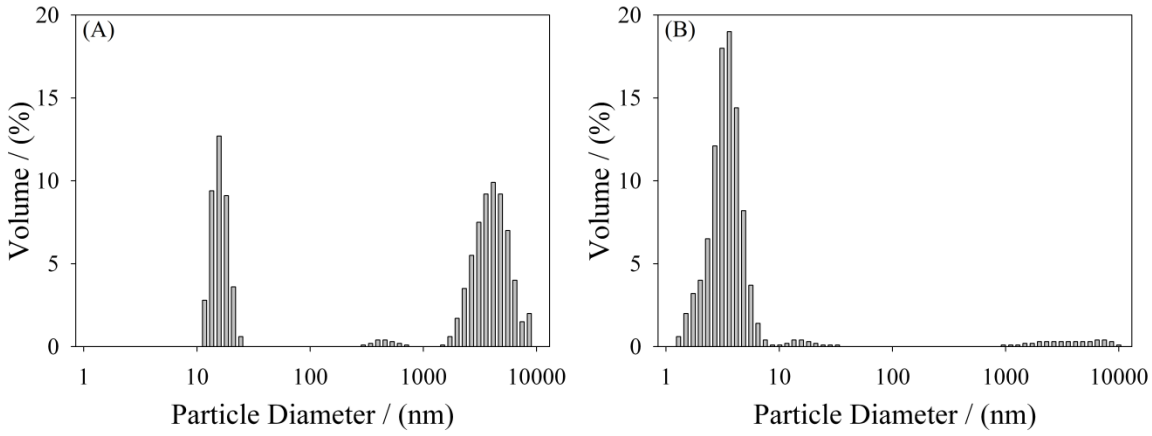

Figure IV-5. DLS analyses of cellulose solution before addition of titanium isoproproxide (A) and immediately after addition of titanium isoproproxide (B).

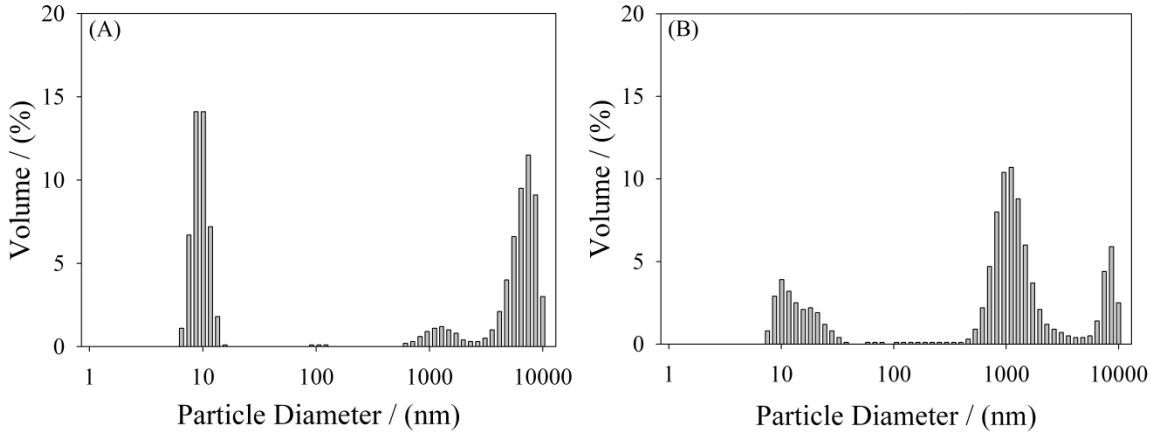

Figure IV-6. DLS analyses of titania-cellulose solution after stirring for one day (A) and for one week (B).

The hydroxypropylcellulose solution lacking titanium isoproproxide (Figure IV-5A) showed distributions centered around 12 nm and 4000 nm, with the larger diameter distribution containing over 60% of the total particle volume. This larger distribution was attributed to the agglomeration of the hydroxypropyl cellulose without a well-defined mean particle size. Upon the addition of titanium isoproproxide, a large

distribution centered between 3 nm and 4 nm appeared, comprising nearly 94% of the measured particle volume (Figure IV-5B). This distribution was assigned to nanoparticulate titania forming in the solution. The remaining volume was as seen before in the hydroxypropylcellulose control. The population of the nanoparticles in this size range decreased over a 24 hour mixing period, by the end of which the mean particle size had increased to approximately 10 nm (Figure IV-6A). This distribution is noticeably shifted to lower particle sizes, with respect to the hydroxypropylcellulose control. There is also a new, much smaller, distribution around 1000 nm or 1 μm. After one week, the titania particles reached a mean size distribution of 1 μm (Figure IV-6B).

As an additional check of particle sizing, scanning electron microscopy (SEM) was used to analyze a film made from a two-week old solution. SEM analysis on this film showed a large population of uniformly sized 1 μm titanium particles, in agreement with the previous DLS measurements (see Figure IV-7).

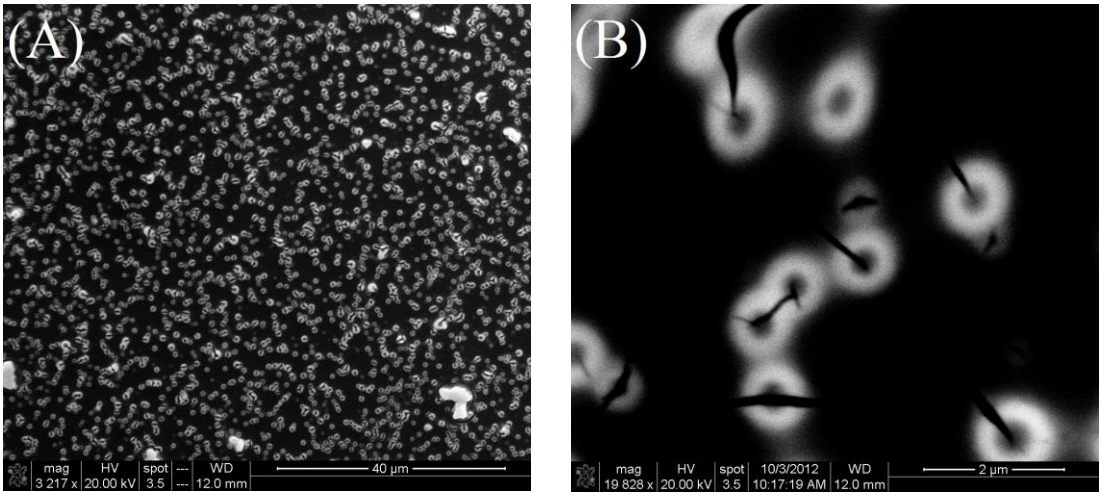

Figure IV-7. Scanning electron micrograph of two week-old titania-cellulose films at magnifications of (A) 3000X and (B) 20000X.

Experimentally, the films made within 24 hours of solution preparation had slightly higher sensitively, or a more rapid color change, to hydrogen peroxide vapor. To

maintain consistency, all films and coatings were prepared and tested within 24 hours of preparation of the precursor solution, while the titania particle size remains within the 5 to 10 nm distribution.

The films and coatings were also used shortly after preparation to ensure consistency. Over a week, both the films and coatings remain stable. For the films, there is very little difference in the sensitivity between a fresh film and one stored in a covered petri dish and exposed to light for six months. The dense sol-gel film combined with the lack of water that can produce radicals via photochemistry is believed to contribute to the observed stability. However, the coatings on filter paper are less stable and become brittle with time. Over a six months period in a covered petri dish, the coatings lose approximately 50% of their initial sensitivity. However, they are still more sensitive than the films even after six months of storage. Although not a focus of this study, it is thought that better storage conditions could extend the lifetime of the coatings.

C.2. Reaction Kinetics

Upon exposure to gaseous hydrogen peroxide, the films and coatings changed from colorless to yellow wherein the intensities are dependent on the peroxide concentration and the exposure time. Figures IV-8A and IV-8B show the recorded images after filtering the light with a BG 12 blue bandpass filter before and after exposure of the films on polycarbonate slides to hydrogen peroxide. When the intensities were examined in detail, it was found that the images initially saturated the blue channel. As the coatings and films react with hydrogen peroxide, the absorption of light between 300 and 500 nm began to occur (observed through UV spectra of exposed films), which caused less light

to be reflected and resulted in a darker image of the film or coating. A control film and coating created without the addition of titanium isoproproxide did not have an observed color change during exposure to peroxide vapors.

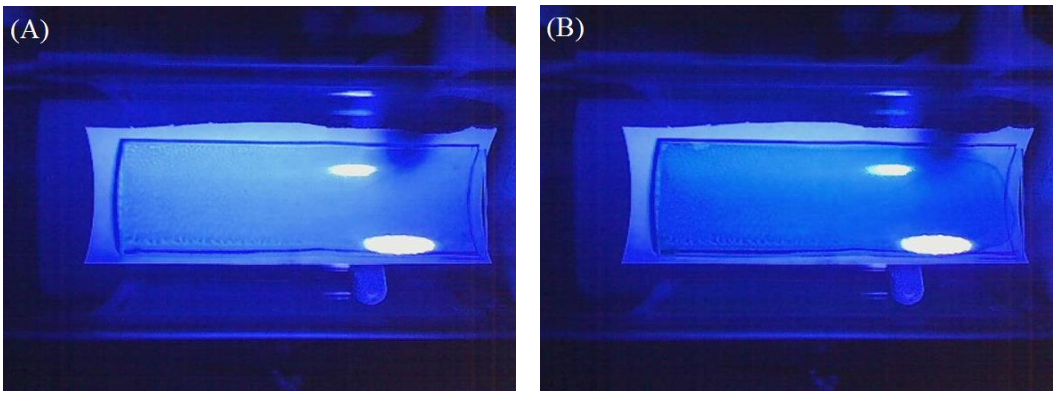

Figure IV-8. Original recording of film on polycarbonate slide (A) before and (B) after peroxide exposure.

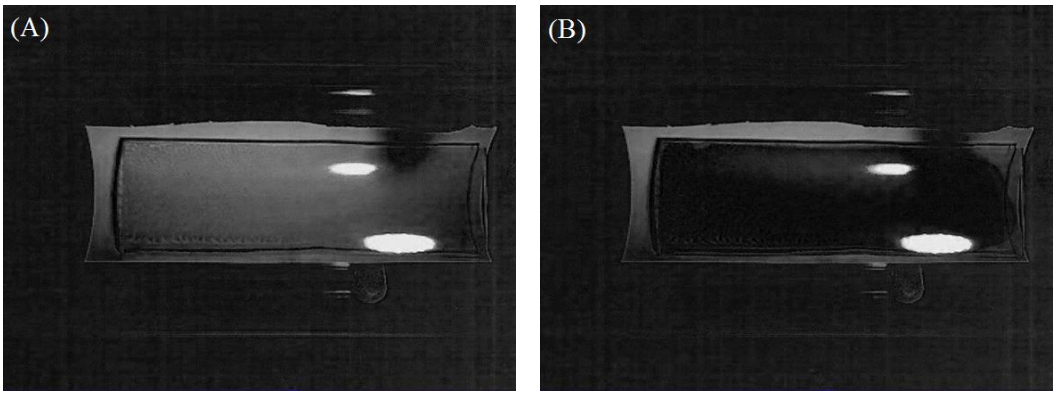

Figure IV-9. Isolated red channel of film on polycarbonate slide (A) before and (B) after peroxide exposure.

The particular red dye used in the web camera has reasonable absorbance in the blue region of the spectra, as confirmed using a broadband light source combined with a 1/8-m monochromator. Therefore, the red channel has an increased dynamic range and lower sensitivity. The resulting image after splitting the color channels using ImageJ and focusing only on the red channel is shown in Figure IV-9A and IV-9B. As shown in this figure, a dramatic decrease in the intensity was readily observed. The measured response

of the camera to the films and coatings changing color is considered to be reproducible, as was recently reviewed by Kehoe and Penn.[154]

As discussed in the experimental section, ImageJ was used to extract the intensity as a function of time from the video. A typical decrease in reflected intensity with time is shown in Figure IV-10A. The intensity appears to exponentially decline with time or peroxide exposure. This observation was confirmed by plotting the natural logarithm of the intensity versus exposure time (Figure IV-10B), yielding a linear plot that is characteristic of an exponential time dependence. Additional intensity data can be found in Appendix C.

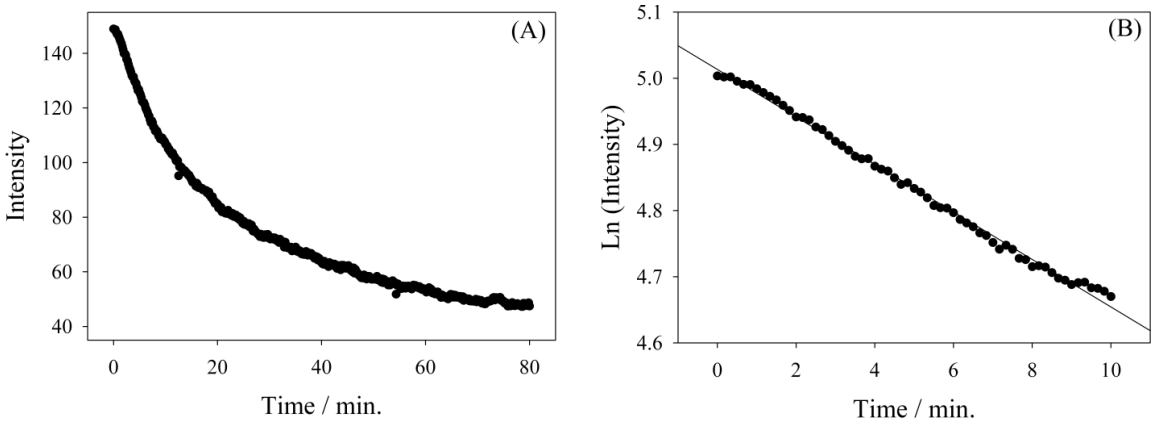

Figure IV-10. (A) Intensity versus exposure time for a 50 mass percent titania film and (B) the first-order behavior of the first 10 minutes of exposure.

The negative slope of this plot (Figure IV-10B), determined by linear regression, is the phenomenological first-order rate constant. At later time points, the decrease in reflected intensity slows and then stops as the active titania particles in the film and coating are consumed. The saturation intensities for 25 and 50 mass percent titania coatings on filter paper were 44.7 ± 5.5 and 16.2 ± 0.3, respectively. These intensities were determined by the averaging of three experiments, two 60 minute exposures to hydrogen peroxide gas with concentrations of 37.3 and 38.5 ppm and one 80 minute exposure of 10.7 ppm. The

raw saturation intensities for each experiment was performed by averaging of the last 5 minutes of each exposure and differed by less than 2% from that computed from the previous 5 minutes. As expected, higher titania loading resulted in a smaller intensity value as a result of more light being absorbed. While a higher mass loading is important for the magnitude of the final absorption value, the substrate is also extremely important. The saturation intensity for the 50 mass percent titania films on polycarbonate was determined from an average of three 60 minute exposures to hydrogen peroxide gas with concentrations of 72.6, 19.3 and 8.6 ppm, and was found to be 42.0 ± 15.0. The standard derivation of the saturation intensity of the 50 mass percent titania polycarbonate film is significantly higher than the similar 50 mass percent titania coating on filter paper.

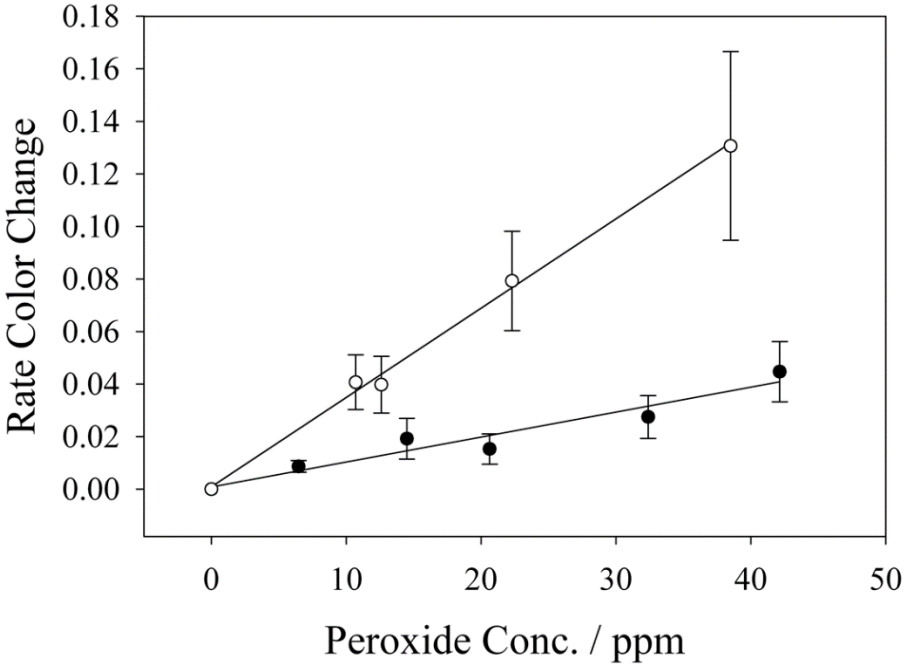

Figure IV-11. Phenomenological first-order rate constants obtained from the 50 mass percent titania films on polycarbonate (●) and coatings on filter paper (o) substrates as a function of the peroxide concentration. Error bars were determined from film homogeneity, as discussed in the text.

To determine the color change dependence on peroxide concentration or, equivalently, the rate of the peroxide flux to the surface, six films on polycarbonate and five coatings on cellulose filter paper were exposed to peroxide concentrations ranging from 0 to 50 ppm. Figure IV-11 shows the phenomenological first-order rate constants, which were determined using the methodology described above, plotted against the measured peroxide concentrations. Experimentally, the error in the measurement was dominated by the small inhomogeneity of the coating. The error bars shown in Figure IV-11 were estimated first by dividing the films and coatings into four equally sized sections to determine the rate constants for each section and then computing the standard deviation of the rate constant in each quadrant. The resulting rate constants were linearly dependent on the concentration peroxide vapor. With a constant concentration of the encapsulated titanium(IV) species within the film, the color change was linearly proportional to the hydrogen peroxide concentration or the flux of hydrogen peroxide molecules to the surface.

The responses of both films and coatings to hydrogen peroxide were first order with respect to the gas phase concentration of hydrogen peroxide. The linear regression of the phenomenological first-order rate constant versus hydrogen peroxide concentration obtained from the films on polycarbonate and coatings on filter paper were 1.0×10^{-3} per ppm with an R^2 of 0.98 and 3.4×10^{-3} per ppm with an R^2 of 1, respectively. These results demonstrate that coatings on cellulose filter paper are over three times as sensitive as the films on polycarbonate, meaning that the filter paper is a superior substrate for both sensitivity and reproducibility. Given that the difference is only a factor of three and the surface area and porosity of the filter paper is significantly greater than that of the

polycarbonate substrate, the porous nature of the filter paper is not likely the cause of the different rates. The coating was prepared using a similar amount of the sol-gel precursor solution per unit area as that of the films, eliminating one advantage of a porous substrate. In addition to sensitivity, the background noise for the films and coatings were measured to be 5.2 and 1.1 intensity units, respectively. One major difference between the films and coatings is that the films are transparent and require a white background material to be placed under the slide, resulting in loss in the reflected intensity. The coatings are white and require no additional background material to reflect the light. Thus, some of the difference between the films and coatings could result from small differences in the experimental setup. Importantly, our measurements show that the chemistry that occurs on these materials is similar. Finally, for higher hydrogen peroxide concentrations, the measured errors for the phenomenological first-order rate constants in Figure 6 were larger than those found for lower concentrations. This was a result of the films and coatings close to the peroxide inlet exhibiting a greater initial rate of coloration.

The effect of titania mass loading on the phenomenological first-order rate constant of the coatings was studied using 0, 25 and 50 mass percent titania mass, where the 0 mass loading was used as a control. Figure IV-12 shows the response of these coatings to exposures of various peroxide concentrations.

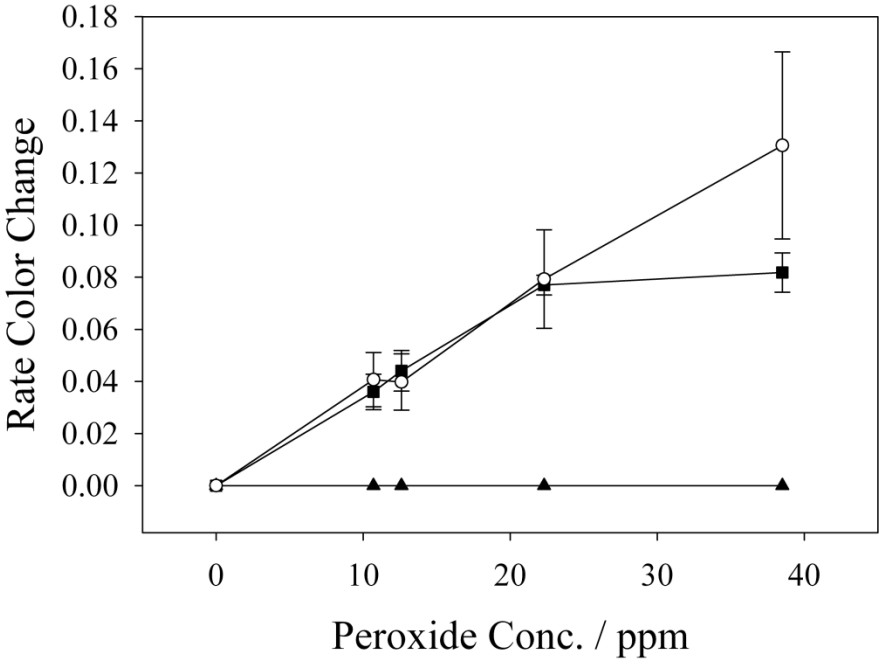

Figure IV-12. Phenomenological first-order rate constants of 0 (▲), 25 (■) and 50 (○) mass percent titania coatings as a function of gas phase hydrogen peroxide concentration. Error bars were determined from film homogeneity as discussed in the text.

The control films without titania showed no reactivity towards peroxide. At lower concentrations of hydrogen peroxide vapor (0 – 20 ppm), the 25% and 50% by mass titania films displayed similar rates of color change at a constant hydrogen peroxide concentration. When exposed to more concentrated vapor, the 25% by mass titania coatings loading leveled off to a constant rate of color change independent of the hydrogen peroxide concentration. Leveling off at higher concentrations of hydrogen peroxide was not observed for the 50% titania coatings, which implied that the rate of intensity change of these films could be used to quantify peroxide concentrations greater than 40 ppm.

C.3. Peroxide Sensitivity and Reaction Mechanism

The experimental results (Figures IV-11 and IV-12) can be qualitatively understood by a reaction mechanism that depends on the flux of hydrogen peroxide to the surface. The phenomenological first-order rate constant at each peroxide concentration appears to depend only on this flux (flux of hydrogen peroxide to the surface). Therefore, the surface reaction rate for the formation of the color species is fast relative to the arrival rate. The final coloration depends only on the concentration of available sites, presumably the encapsulated titanium(IV) species within the film that are completely consumed at later time points. This hypothesis is further supported by the linear dependence of the rate constant on hydrogen peroxide concentration because the flux of hydrogen peroxide molecules to the surface has a linear dependence on the gas phase concentration or partial pressure. Additionally consistent with this model is the independence of the phenomenological rate constant with titania loading (Figure IV-12). The fast surface reaction rate implies that, at these peroxide concentrations, the measured rate should be independent of the number of reactive sites within the films and coatings. However, the ultimate capacity of these films is limited by the number of active sites provided by the encapsulated titanium(IV) species; thus, higher loading is associated with greater ultimate color change in the presence of peroxide vapor.

The slope of the phenomenological rate constant versus peroxide concentration (Figures IV-11 and IV-12) is an indicator of film and coating sensitivity to peroxide vapor. Color change per ppm of hydrogen peroxide directly correlated with film and coating sensitivity to peroxide vapor wherein a larger color change resulted in greater the sensitivity. Using the concentrations tested herein, the cellulose coatings clearly

provided greater sensitivity. A more quantitative estimate was obtained using the slopes and the background noise of the detection system. The background noise for the films and coatings was measured to be 5.2 and 1.1 intensity units, respectively. The major limiting factor is the sensitivity of the web camera. Using 3σ as an estimate of the limit of detection for the intensity measurements combined with predetermined measurement times, the minimum detectible slope or intensity change was estimated. The minimum detectible slope, in turn, was used to identify the detection limit in ppm. For the 50 mass percent titania films on polycarbonate, the detection limit was estimated to be 90 ppm hydrogen peroxide for a 1-minute measurement and 1.5 ppm for a 1-hour integration. The coatings on filter paper had a much lower detection limit of 5.4 ppm hydrogen peroxide for a 1-minute measurement minute and 0.09 ppm hydrogen peroxide for a 1-hour integration.

D. Conclusion

Sol-gel methods were used to produce titania in a hydroxypropyl cellulose matrix as films on polycarbonate or coatings on cellulose. These films and coatings had reactivity toward hydrogen peroxide and changed color from colorless to an intense yellow when exposed to hydrogen peroxide. The films on polycarbonate with a titania/(titania+cellulose) mass percent greater than 50% had a tendency to crack. Using an inexpensive web camera and a tungsten lamp to measure the reflected light, it was determined that the films exhibited a first-order behavior with regard to color change when exposed to peroxide vapor of less than 50 ppm. As the titania content present in the films increased, less light was reflected at saturation. However, the mass ratio in the

solution did not affect the response rate for hydrogen peroxide concentrations below 25 ppm. For the 50 mass percent titania films on polycarbonate, the detection limit was estimated to be 90 and 1.5 ppm for a 1-minute measurement and a 1-hour integration, respectively. The coatings on cellulose provided a threefold increase in sensitivity compared to the films on polycarbonate, with a detection limit of 5.4 ppm hydrogen peroxide for a 1-minute measurement and 0.09 ppm hydrogen peroxide for an hour-long integration. The major limiting factor was the sensitivity of the web camera. Using a more sensitive detection technique, it may be possible to use the reflected intensity from these films as an extremely sensitive hydrogen peroxide detector. Ongoing studies are being conducted to determine the response of these films to organic peroxides. Nevertheless, a sensor utilizing the titania-cellulose coating may be constructed to monitor peroxide vapor exposure in workplaces to determine whether exposure levels are within the OSHA permissible average exposure limit of 1 ppm of peroxide vapor over an 8-hour day.[96]

CHAPTER V

THE OPTIMIZATION OF SENSING COATINGS FOR THE DETECTION OF ORGANIC PEROXIDE VAPORS

A. Introduction

After optimizing and determining the sensitivities of titania-cellulose films and coatings to peroxide vapors in the previous Chapter, it was decided to see if these sensing materials could be utilized to detect organic peroxide (e.g. triacetone triperoxide – TATP; hexamethylene triperoxide diamine - HMTD) vapors in a similar fashion. Notably more difficult to detect due to the lower reactivity and vapor pressure, organic peroxides are of great concern due to their historical use as the materials for the main charge in terrorist improvised explosive devices (IEDs).[112-115] Current methods for detection of these compounds include many approaches utilizing air sampling and ion-mobility spectroscopy,[119-122] laser-induced breakdown spectroscopy,[123-125] and mass spectrometry.[130-133] However, these methods are difficult and require complicated operating parameters. By comparison, detection of organic peroxide vapors through a color-change mechanism (such as the sol-gel coatings to hydrogen peroxide discusses last Chapter) would be ideal, as this would provide a clear yes-no indicator for their presence.

However, when the sol-gel coatings studied the last chapter were exposed to organic peroxides, it was found that they were not extremely sensitive to organic peroxide vapors, and only displayed a color change after an extended amount of exposure time (e.g. more than 3 hours). It was discussed in a recent article that reaction of TATP with acid produced hydrogen peroxide, to which the films and coatings are already sensitive.[155] With this in mind, a variety of solutions with titanium(IV) and high acid content were produced to evaluate propensity for organic peroxide vapor detection. Solutions produced include the titania sol-gel in cellulose solution described last Chapter, but with higher acid concentrations. It was observed that the sensitivity of these coatings increased dramatically to TATP vapor ($P_{vapor} \sim 10^{-2}$ torr at 25 °C) while vapors from HMTD remain difficult to detect, possibly due to HMTD's much lower vapor pressure ($P_{vapor} \sim 10^{-4}$ torr at 25 ºC).[118] Additional coatings of an acidified solution of titanyl sulfate on a silica substrate were produced containing an ionic liquid in place of isopropanol as the solvent and either sulfuric or trifluoromethanesulfonic acid. Through this substitution of an ionic liquid, the coatings were protected against drying out; thus, as the acidic environment was maintained, the usable lifetime of the produced coatings was extended. The most sensitvite coating with the ionic liquid was found to be that made with trifluoromethanesulfonic acid, which showed an equal sensitivity to organic peroxides as the sol-gel coatings, with the added benefit of long-term stability.

B. Experimental Details

B.1. Preparation of Titanium(IV) Isoproproxide-Hydroxylpropyl Cellulose Solutions

Solutions of titanium(IV) isopropoxide with hydroxypropyl cellulose in 2-propanol and of titanyl sulfate (i.e. titanium(IV) oxysulfate) in buffered ionic liquid solutions with sulfuric or trifluoromethanesulfonic acid were produced following the procedure outlined in the Experimental section of Chapter IV. The only alteration was in the amount of acid added following the addition of titanium(IV) isoproproxide for the sol-gel coatings. In place of 1.5 g of concentrated hydrochloric acid (Pharmco-Aaper, ACS Reagent), the acid content was quadrupled to be 6.0 g of hydrochloric acid in one solution. For the second solution, concentrated sulfuric acid (Pharmco-Aaper, ACS Reagent) was substituted for hydrochloric acid and the amount added was 6.2 g (for pH equivalence).

B.2. Preparation of Titanyl Sulfate in Buffered Ionic Liquid Solutions

Solutions of titanyl sulfate (i.e. titanium(IV) oxysulfate) in a buffered ionic liquid solution were produced. First, 1.69 g of H_2O (RO, 18 MΩ-cm) was mixed with either 0.38 g of concentrated sulfuric acid (Pharmco-Aaper, ACS Reagent) or 0.58 g of trifluoromethanesulfonic acid (Alfa Aesar, 98+%) in a test tube. To these solutions, 0.50 g of solid titanium(IV) oxysulfate was added and the tube was immersed in a boiling water bath for five minutes to dissolve the solid. The tube was removed and cooled to room temperature, after which the solution was filtered through a 0.22 μm syringe filter to remove any undissolved particulates. Following this, 0.81 g of 1-ethyl-3-methylimidzolium hydrogen sulfate (Aldrich, 95%), acting as an ionic liquid in the

solution, was added and stirred. The resulting solutions were sealed under nitrogen and Parafilm until use.

B.3. Preparation of Sol-Gel Coatings on Glass Filter Paper and Ionic Liquid Coatings on Silica Slides

Sol-gel coatings were produced on glass filter paper source by coating one side of the paper with a known volume-per-area amount of the titanium isopropoxide-cellulose solution as was used in the previous Chapter (see Figure IV-2). Glass was chosen in place of cellulose-based filter papers as the increased hydrochloric acid content of the first solution could possibly decompose the cellulose. For the second solution, sulfuric acid has long been known to decompose cellulose, leading to a brown, burnt appearance.

Silica thin layer chromatography plates (Baker-flex silica gel 1B, 2.5 cm x 7.5 cm, J.T. Baker) were used as the substrate for the produced coatings. To ensure no mixing of the detection solutions occurred, channels between silica strips were created (see Figure V-1).

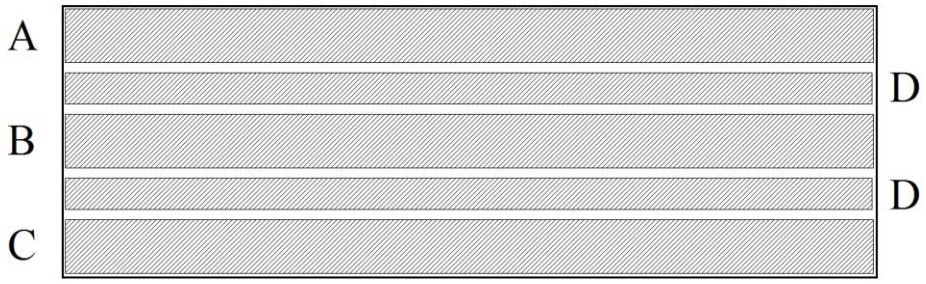

Figure V-1. Layout of silica strips used for film exposures. Solutions of the (A) titania sol-gel as well as titanyl sulfate in (B) sulfuric acid and (C) trifluoromethanesulfonic acid in the ionic liquid were applied equally. (D) Emtpy spaces (0.1 cm each in diameter) and sections of blank silica (0.3 cm in diamter) were created to prevent mixing of the applied solutions.

Equal amounts of each titanium solution (between 0.10 and 0.12 g) were applied to the each section (A, B and C) of the silica slides and were dried in air under a watch glass for varying amounts of time, ranging from 1 hour to 1 month. Through this aging of the coatings and subsequent exposure to peroxide, the longevities of the sol-gel and ionic liquid coatings could be determined through the change in the sensitivities over time.

B.4. Surface Area Analysis of Filter Paper and Silica Substrates

In order to determine the surface area available in each of the substrates, surface area analysis via Brunauer-Emmett-Teller (BET) theory was utilized.[156] A Quantachrome Autosorb-1 system was utilized for surface area analysis. Ultrapure nitrogen (Airgas) was used as the measuring gas, with liquid nitrogen used for sample cooling during analysis. Uncoated samples of glass filter paper and silica (both in contact with the polycarbonate slide and removed in the form of a powder) were analyzed by five-point measurements. All samples were outgassed for 24 hours before analysis of surface area.

B.5. Setup and Testing Methodology of the High Acid Content Coatings

The detection solution preparation, exposure apparatus, peroxide quantification and intensity measurements were all used as previously described. The sole difference in these exposures was the removal of gas flow from the apparatus and the placement of solid samples of TATP and HMTD inside the glass chamber. Solid samples of TATP and HMTD were synthesized and provided by XploSafe LLC. For exposure, 0.10 g of solid TATP or HMTD was weighed and placed in the glass cell approximately 2 cm from the coated filter papers, which were present as strips adhered to a polycarbonate slide or

the silica bonded to the polycarbonate substrate. The mechanism for exposure was the evolution and diffusion of vapor from the solid peroxides to the filter paper surface; for this reason, exposures were extended to six hours to ensure high gas diffusion throughout the cell. Quantification of organic peroxide concentrations in gas phase was not attempted. However, the sensitivities of the high acid content coatings to gaseous organic peroxides were directly compared to the associated gaseous hydrogen peroxide sensitivities that were quantified in the previous Chapter: this concept is denoted the peroxide sensing equivalency - the higher the value, the more sensitive the coating is to organic peroxide vapor.

C. Results and Discussions

C.1. Sol-Gel Film Reactivity to Organic Peroxides

As was seen with the previously tested films and coatings, there is a distinct color change in the coatings when exposed to peroxide vapors. When exposed to TATP vapors, the titania solution containing the increased hydrochloric acid concentration displayed the characteristic yellow color change as discussed previously; however, the titania coating with sulfuric acid was observed to turn a more dark shade of orange when exposed. However, when exposed to HMTD vapors, the sulfuric acid coating showed a very subdued color change, with the hydrochloric acid coatings showing no visible change (see Figure V-2).

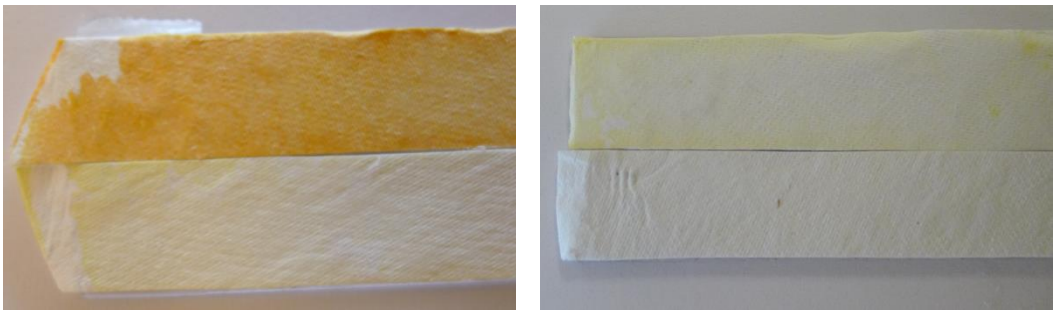

Figure V-2. Picture of titania coatings on glass filter paper with (top) sulfuric acid and (bottom) hydrochloric acid following exposure to (left) TATP and (right) HMTD for six hours.

With the lack of HMTD sensitivity observed in Figure V-2, a contact study of HMTD to the coating surface was performed to ascertain whether any reaction occurred with the hydrochloric acid coating and HMTD. In this study, a small amount of solid HMTD was placed onto the surfaces of the hydrochloric and sulfuric acid coatings for a two hour period, at the end of which the coating was examined for color change (see Figure V-3).

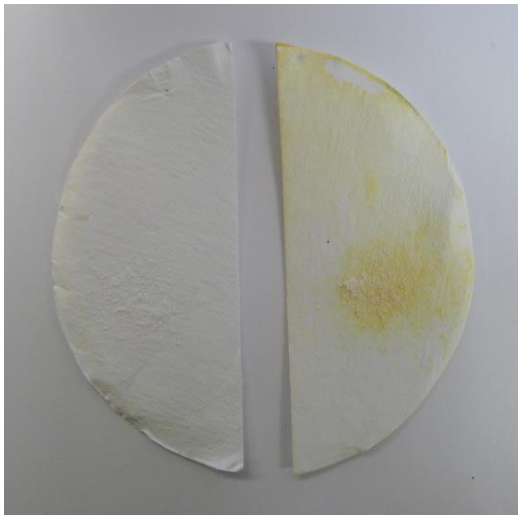

Figure V-3. (Left) Hydrochloric and (right) sulfuric acid coatings following a surface contact test with HMTD.

As can be seen, there was a strong color change following the two hour contact test for the sulfuric acid coating, with no observable color change across the hydrochloric acid coating. It is possible that the reaction is extremely slow, and that exposure over a

greater time (e.g. >1 day) may result in a color change; however, this supposition has not been explored further.

C.2. Surface Area Analyses of Substrates

BET analysis was used to measure the surface areas of the uncoated substrates. While numerous attempts were made, the surface area for the glass filter papers was unmeasurable. It is unknown as to the reason for this outcome, but it is possible that the surface area was below the measurement limit of the instrument. For the silica substrate, the measured surface area was found to be 2.53×10^2 m^2/g when still applied to the polycarbonate slide. In terms of slide area, this equates to 2.80 m^2/cm^2 silica slide. When removed from the slide and in a purely powder form, the surface area was found to increase to 3.24×10^2 m^2/g, likely due to the less dense nature of the powder versus the plated form. Given this high surface area, the substrate of choice was switched from glass filter paper to silica slides.

C.3. Solution Sensitivities to Hydrogen Peroxide Vapor

To ascertain how the higher acid content of the sulfuric sol-gel and buffered ionic liquid coatings would affect peroxide reactivity, the produced films and coatings were exposed to hydrogen peroxide at four concentrations. This was completed to give a point of reference of comparison between the lower acid content films and coatings (Chapter IV) and the higher acid content coatings made for organic peroxides. These measurements also can be used to determine the minimum possible concentration of TATP vapor, as it has been detailed that three molecules of hydrogen peroxide (or

peroxide anion) form for every molecule of TATP decomposed in an acidic environment. The coatings were made and air dried for 24 hours before use. As the ionic liquid coatings do not dry out, the estimated sensitivity is viable for strips dried for more than one day. The first five minutes of each peroxide exposure were used to determine the color change rate dependency on peroxide concentration (Figure V-4).

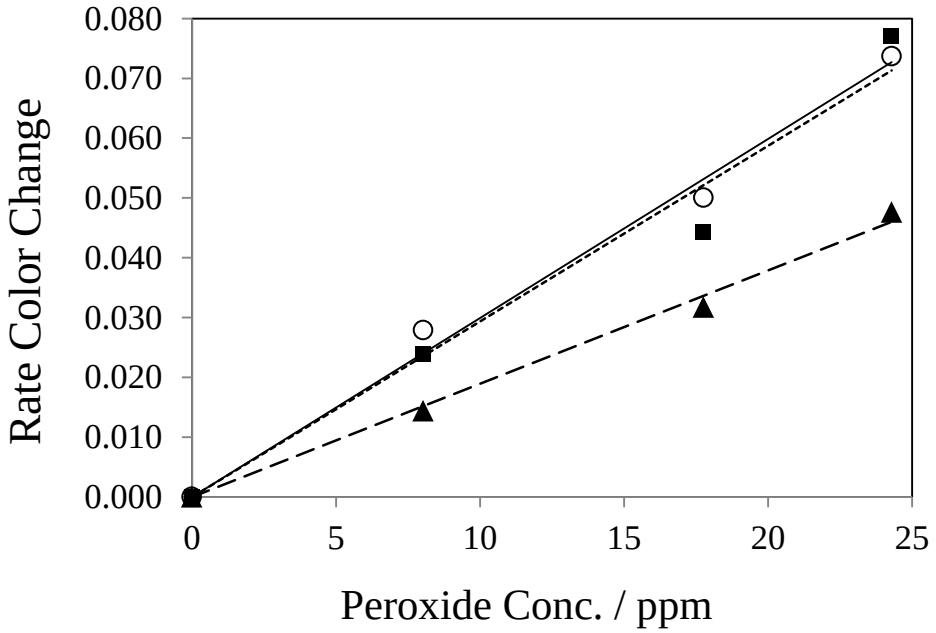

Figure V-4. Phenomenological first-order rate constants of the sulfuric acid, titania sol-gel films (■ and dotted line) and the titanyl-ionic liquid coatings with sulfuric (▲ and dashed line) and trifluoromethanesulfonic acids (○ and solid line). As can be seen, the sol-gel and trifluoromethanesulfonic acid coatings were found to be equally sensitive over the tested range.

When graphed with an enforced zero-intercept, the sol-gel and ionic liquid coatings showed virtually equal sensitivities of 3.0×10^{-3} ($R^2 = 0.992$) and 2.9×10^{-3} ($R^2 = 0.989$) per ppm peroxide, respectively. It is worth noting that the sensitivity of the sol-gel coatings with high sulfuric acid content was extremely close to the previously estimated sol-gel / hydrochloric acid coating sensitivity of 3.4×10^{-3} per ppm peroxide, which were

used after being dried for 1 hour (see Figure IV-11). This is important as it validates that both the solution preparation and testing environment are stable and reproducible, that eh sol-gel coating behavior is stable for over 1 hour, and that the various coatings can be compared with minimal concerns of experimental change or indeterminate error.

C.4. Long Term Stability and Sensitivities of Sol-Gel and Ionic Liquid Coatings

To determine the long term stabilities and sensitivities of the coatings to peroxide vapors, coatings on silica slides were produced and air dried for one day, two weeks, and four weeks (24, 336, and 672 hours) before being exposed to hydrogen peroxide vapor. The color change responses of the aged coatings were normalized to the concentrations of peroxide vapor to which they were exposed (rate color change / hour ·ppm peroxide). Two coatings were exposed every period and the responses were averaged (Figure V-5).

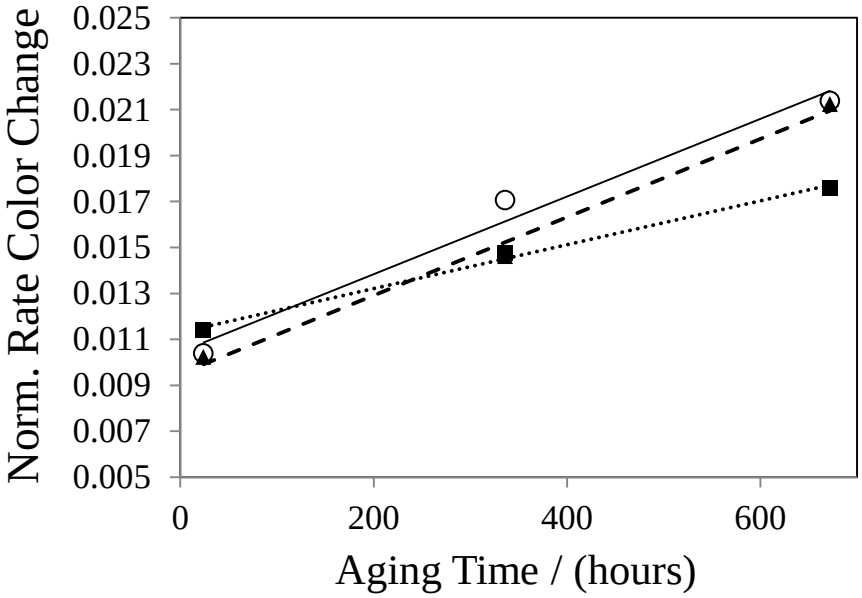

Figure V-5. Normalized color change rates for coatings of the sulfuric acid, titania sol-gel films (■ and dotted line) and the titanyl-ionic liquid coatings with sulfuric (▲ and dashed line) and trifluoromethanesulfonic acids (○ and solid line). The ionic liquid coatings are seen to increase in sensitivity at an equal rate while the sol-gel coatings increase more slowly.

It was seen that over the four week aging period the sensitivity to peroxide of each type of coating was seen to increase, with the ionic liquid coatings showing the most increase. The ionic liquid coatings were both seen to increase by 1.7×10^{-5} intensity units per ppm per hour while the sol-gel coating increased at 9.6×10^{-6} intensity units per ppm per hour, roughly half that of the ionic liquid coatings. It is thought that the increase of sensitivity for both types of coatings results from the increasing acidity of the applied solution as the evaporation process occurs. It was discussed previously that at pH < 1, the peroxo titanium complex exists in a mononuclear arrangement with a more intense orange coloration than the yellow that exists at between pH = 1 and 3. As the evaporation process occurs for these coatings, it is believed that the pH of the coatings decreases and the associated sensitivity to peroxide increases as mononuclear form of the titanium complex increases and the observed color shifts from yellow to orange. This shift can be seen in Figure V-6.

Figure V-6. Coatings exposed to peroxide after aging for (left) one day and (right) two weeks. The strip was made in accordance with the described layout in Section B.3 of this Chapter. The increased orange content of the older coating can be clearly seen.

An additional benefit of the ionic liquid coating is its attribute of not dehydrating completely as quickly as the sol-gel coatings. After the solvent evaporates from the

coatings, the ionic liquid coatings retain some amount of moisture, likely increasing their sensitivity to peroxide vapors compared to the sol-gel coatings.

C.5. TATP and HMTD Reaction Kinetics with the Acidic Sol-Gel Coatings

Similar to hydrogen peroxide experiments, ImageJ was used to extract the intensity as a function of time from the video. A plot of the raw intensity of the entire coating from the exposures is seen in Figure V-7.

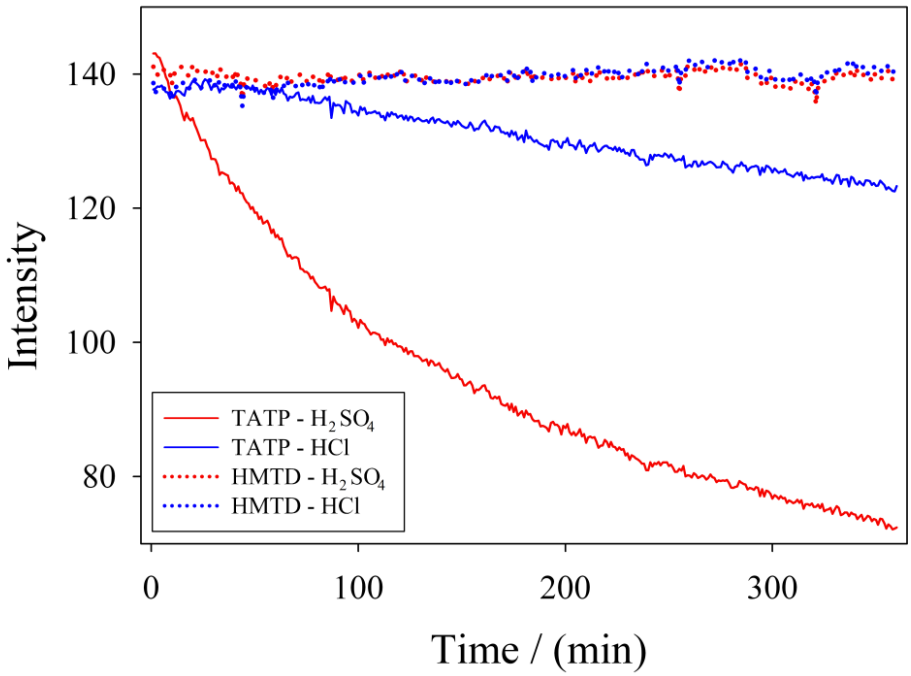

Figure V-7. Intensity versus exposure time for hydrochloric and sulfuric acid coatings.

As can be seen, the greatest changes in intensity occurred when the coatings were exposed to TATP vapors, with the sulfuric acid coating showing the greatest sensitivity (i.e. color change). The color change of the sulfuric acid coating resembles the first-order behavior seen from the coatings described in the previous Chapter. When exposed to HMTD vapors, both sets coatings showed little to no color change. However, as the

contact test proved that the sulfuric acid coatings react with HMTD, the analysis parameters were reevaluated. It was found that as the reaction of the organic peroxides is diffusion-dependent (i.e. no exterior flow pushing the gas forward), there was a noticeable gradient across the coatings (see Figure V-8).

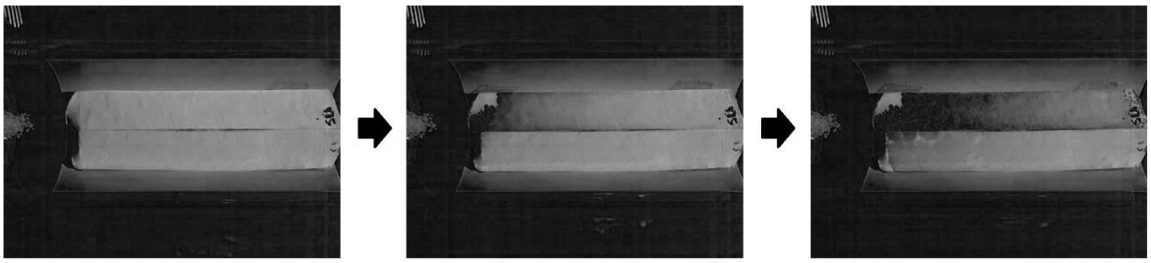

Figure V-8. TATP exposure to acid coatings. A color change gradient is clearly visible for the (top) sulfuric acid coating one hour into exposure, showing reduced reflected intensity at the left side of the papers but high intensity on the right side; at the end, a similar gradient is seen on the (bottom) hydrochloric acid coating.

Given that as the peroxide vapor diffuses, it will contact the side closest to the solid sample first; therefore, the reaction kinetics of the coatings were measured using the leftmost quarter of the coatings. The resulting measured intensities from this alteration are seen below in Figure V-9.

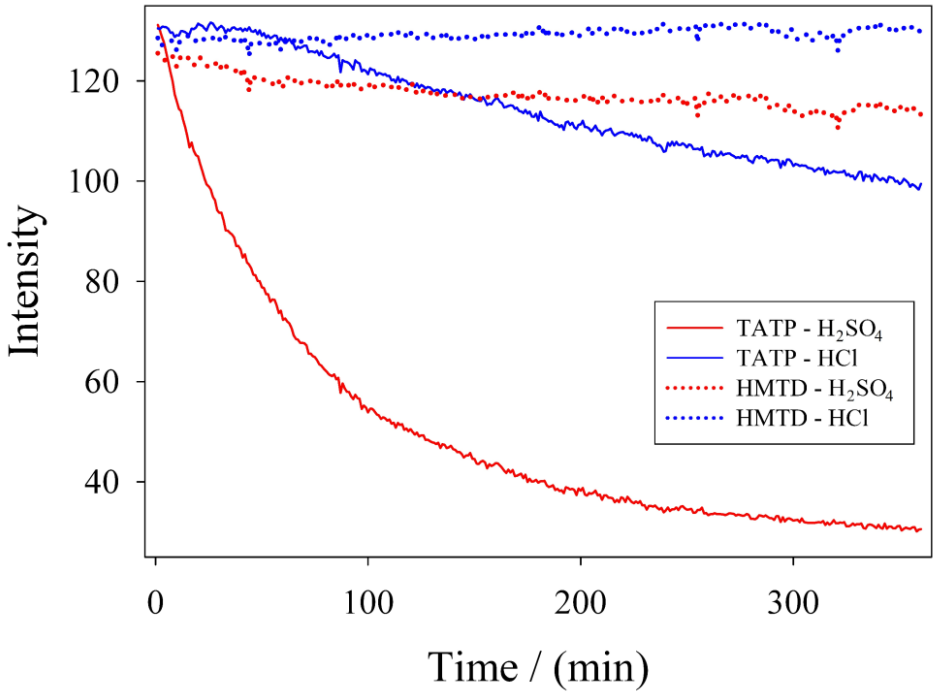

Figure V-9. Intensity versus exposure time of the closest quarter of hydrochloric and sulfuric acid coatings to the solid organic peroxides.

It is seen that the sulfuric acid coating displays first-order reactivity to TATP. It can also be seen that after approximately one hour, the hydrochloric acid coatings begin to decrease in intensity in a somewhat linear fashion. The cause for this delayed reaction is not known. The coatings exposed to HMTD vapors showed less reactivity with only a slight decrease seen for the sulfuric acid coating and no observable decrease for the hydrochloric acid coating.

The first-order behavior of the exposures was modeled by taking the natural log of the intensity for the first two hours of exposure (i.e. Figure V-10). The absolute value of all calculated slope values was taken for comparison purposes to Figure IV-11.

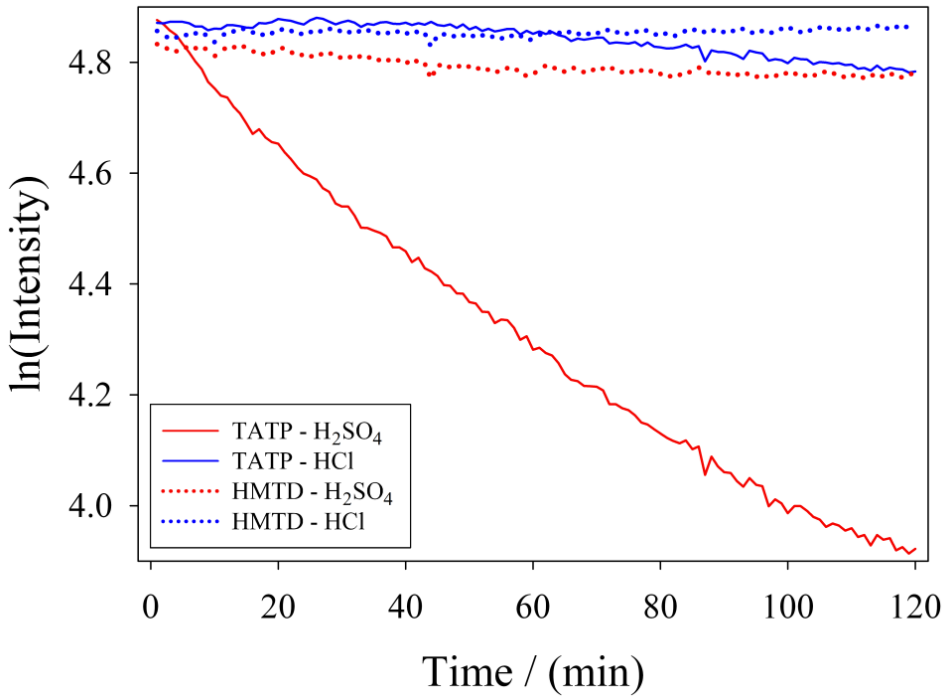

Figure V-10. First-order behavior of the first two hours of acid coating exposure to organic peroxides.

The first-order approximation for the sulfuric acid coating exposed to TATP showed a very linear relationship ($y = 8.0 \cdot 10^{-3}(x)$, $R^2 = 0.99$), characteristic of a first-order reaction. Assuming these coatings react through a mechanism similar to the films and coatings discussed last Chapter with the reaction rate being dependent on the number of available surface sites, the sulfuric acid coatings have a peroxide sensing equivalency of 2.35 ppm. The hydrochloric acid coating was found to be less an order of magnitude less sensitive than the sulfuric acid coatings ($y = 8.0 \cdot 10^{-4}(x)$, $R^2 = 0.88$), having a peroxide sensing equivalency of 0.24 ppm. For the HMTD exposures, the coatings showed subdued reactivity, with the hydrochloric acid coating showing no discernable change in intensity. The sulfuric acid coating showed slight reactivity ($y = 4.7 \cdot 10^{-4}(x)$, $R^2 = 0.83$), having a peroxide sensing equivalency of 0.14 ppm. Given the low sensitivity to HMTD, this results should not be taken as statistically validated.

The diffusion of the organic peroxides in the glass cell is a complicating factor: for this reason, a new testing method was tried to minimize the diffusion gradient across the cell. To accomplish this, a 0.10 g sample of TATP was left to diffuse in the airtight glass exposure cell for 12 hours or more, with one end of the tube sealed with Parafilm. To insert the coatings for testing, a thin slice was made in the Parafilm with a razor blade. Through this cut the slide was pushed into position under the camera using a spatula, and the end was resealed with another piece of Parafilm. From sample introduction and positioning to recording the exposure, the process took less than 15 seconds, minimizing the loss of vaporized TATP. However, possibility due to the reactivity of the TATP with the cell, the diffusion gradient could not be eliminated.

Using this procedure, the sol-gel coatings were exposed for two hours for comparison purposes, and the intensities of the closest quarter of the film were analyzed to be comparable to Figure V-10 (see Figure V-11).

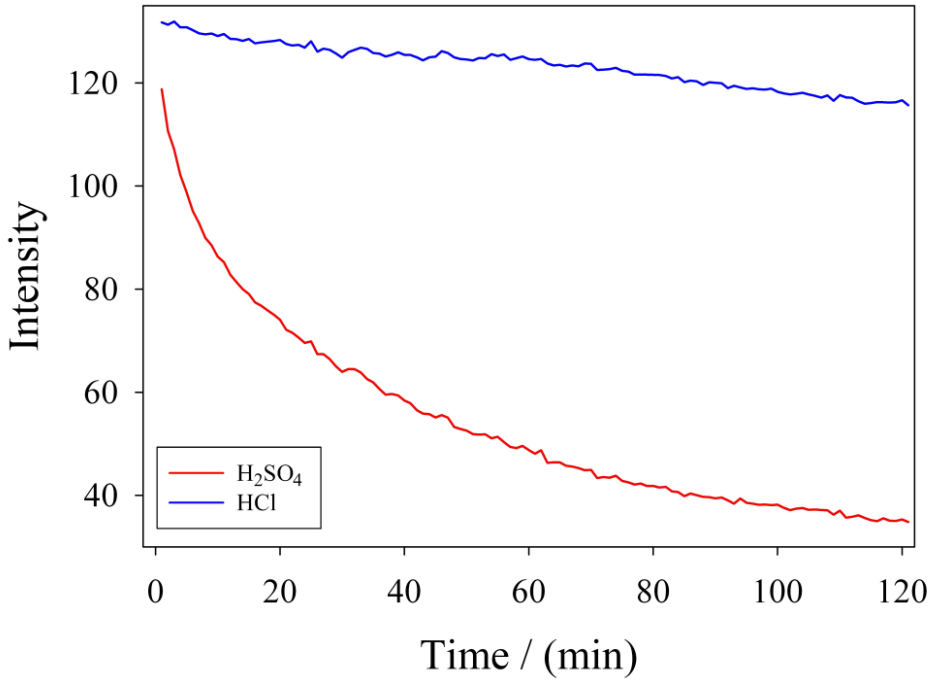

Figure V-11. Intensity versus exposure time of the closest quarter of hydrochloric and sulfuric acid coatings pre-diffused TATP vapors.

For comparison purposes, when modeled as a first-order reaction, the measured rate of color change can give a quantity for comparing the coating sensitivities. For the hydrochloric coating, the calculated peroxide sensing equivalency was found to be 0.29 ppm, statistically non-different from the non-diffusion controlled exposure. For the sulfuric coating, the calculated peroxide sensing equivalency was found to be 2.56 ppm, slightly more sensitive than in the non-diffusion controlled exposure. However, given that diffusion of TATP was still an issue, this numbers should qualitative and not quantitative. When comparing the hydrochloric and sulfuric acid coatings, it is worth noting that the sulfuric acid coatings also detected HMTD vapors, whereas the hydrochloric acid coatings did not. This would seem to indicate that the sulfuric acid coating is superior for organic peroxide detection.

D. Conclusion

The preliminary effect of acid loading on the sensitivity of titania-cellulose coatings to organic peroxide vapors was discussed. Titania-cellulose coatings containing hydrochloric and sulfuric acid were exposed to organic peroxide vapors diffusing from solid samples of TATP and HMTD, with the change in reflected intensity being used to determine the coating sensitivities to the gaseous peroxides. It was observed that both hydrochloric and sulfuric acid coatings displayed first-order kinetics in the presence of diffusing TATP vapor, with peroxide sensing equivalencies of 0.24 and 2.35 ppm, respectively. When exposed to HMTD, the hydrochloric acid coating displayed no reactivity (i.e. color change), a finding supported by a surface contact test with HMTD, which also showed no color change. The sulfuric acid was weakly sensitive to HMTD vapors, with a peroxide sensing equivalency of 0.14 ppm and first-order kinetics similar to TATP exposure; however, this projection suffers from a high amount of uncertainty. When exposed to saturated TATP vapors previously diffused in the exposure cell, the hydrochloric acid coating displayed an unchanged sensitivity and a statistically non-different peroxide sensing equivalency of 0.29 ppm. However, the sulfuric acid coating displayed second-order behavior, indicating a more complicated reaction mechanism for the coating. When modeled as a first-order reaction for comparison purposes, the sulfuric acid coating possessed a peroxide sensing equivalency of 2.56 ppm, slightly increased from the non-diffusion controlled exposure. Additional exposures are required to statistically validate these projected sensitivities.

CONCLUDING REMARKS

A. Sodium Dithionite

Following the Introduction, the first three Chapters of this dissertation review the research accomplished with sodium dithionite. Chapter II details the development and validation of a new method for dithionite and thiosulfate quantification using ion chromatography; it is hoped that this method for analysis could be utilized in industry in place of the standard three iodometric titration approach, which requires both additional time and resources when compared to the new method. During the course of this study, a peculiarity was seen to occur when the oldest sample was titrated – a calculated negative dithionite composition. This finding led the research discussed in Chapter III, where a study of the long-term composition of samples of sodium dithionite was performed. Using Raman spectroscopy in addition to the previously utilized methods, extended S-S bonding compounds were found to form over time, including tetrathionate and possibly trithionate. In such advanced stages of dithionite degradation, it is suggested that the ion chromatographic method be used for composition analysis as the titration method can be affected by the additional reducible species present.

B. Titania-Cellulose Thin Films for Peroxide Detection

Having recognized acidic titanium(IV) solutions as a superior detection method for peroxide vapors, it was decided to ascertain whether or not thin films composed similarly could behave as the solutions did. To this end, thin films on polycarbonate and coatings on filter paper were made and exposed to peroxide concentrations, which was described in Chapter V. These materials were found to be reactive to hydrogen peroxide vapor, with the most sensitive coatings showing a one minute limit of detection of 5.4 ppm peroxide. However, these coatings showed only slight reactivity to organic peroxides (*i.e.* TATP, HMTD). A literature review found that higher acid content resulting in the production of hydrogen peroxide following decomposition of organic peroxide vapors. With this in mind, higher acid content coatings and their sensitivities to TATP and HMTD were evaluated, as reviewed in Chapter VI. Coatings with higher acid concentrations were found to be moderately sensitive to TATP, with sulfuric acid coatings showing a peroxide sensing equivalency of 2.35 ppm. For HMTD however, while reactive when in contact with the solid organic peroxide, very low sensitivity was seen in exposures. This is likely as result of the much lower vapor pressure of HMTD relative to TATP, but additional work negating the effects of diffusion and solely quantifying the sensitivities of these coatings is continuing. It is intended for these materials to be manufactured for industrial safety and national security purposes.

REFERENCES

1. Barbera, J. J.; Metzger, A.; Wolf, M. In *Ullmann's Encyclopedia of Industrial Chemistry* 2000; Vol. 34, p 695.

2. Suess, H. U. *Restaurator* **2009**, *30*, 245.

3. Gorenšek, M.; Gorjanc, M.; Recelj, P.; Meden, A. *Text. Res. J.* **2008**, *78*, 524.

4. Kunttou, K.; Hongyo, S.; Maeda, S.; Mishima, K. *Text. Res. J.* **2005**, *75*, 149.

5. Carter, H. A. *J. Chem. Educ.* **1996**, *73*, 1068.

6. Torimoto, N. *J. Chem. Educ.* **1987**, *64*, 332.

7. Fox, M. R. *Vat Dyestuffs and Vat Dyeing*; 1st ed.; John Wiley & Sons: New York, 1947.

8. Matthews, J. M. *Bleaching and Related Processes*; 1st ed.; J. J. Little & Ives Co.: New York, 1921.

9. Yoe, J. H.; Edgar, G. *J. Phys. Chem.* **1923**, *27*, 65.

10. Anonymous *Chemical Market Reporter* **1997**, *251*, 45.

11. Anonymous *Chemical Market Reporter* **2000**, *257*, 33.

12. Kirschner, M. *Chemical Market Reporter* **2003**, *263*, 27.

13. Kirschner, M. *Chemical Market Reporter* **2006**, *269*, 26.

14. De Vries, J. G.; Kellogg, R. M. *J. Org. Chem.* **1980**, *45*, 4126.

15. Kazmi, S. A.; Shorter, A. L.; McArdle, J. V. *Inorg. Chem.* **1984**, *23*, 4332.

16. Jeong, Y. U.; Manthiram, A. *Inorg. Chem.* **2001**, *40*, 73.

17. Boparai, H. K.; Shea, P. J.; Comfort, S. D.; Snow, D. D. *Environ. Sci. Technol.* **2006**, *40*, 3043.

18. Langell, M. A.; Kadossov, E.; Boparai, H.; Shea, P. *Surf. Interface Anal.* **2009**, *41*, 941.

19. Su, C.; Ludwig, R. D. *Environ. Sci. Technol.* **2005**, *39*, 6208.

20. Xie, Y.; Cwiertny, D. M. *Environ. Sci. Technol.* **2010**, *44*, 8649.

21. de Carvalho, L. M.; Schwedt, G. *Electroanal.* **2001**, *13*, 596.

22. Novakov, M.; Krivankov, L.; Bartos, M.; Urbanova, V.; Vytras, K. *Talanta* **2007**, *74*, 183.

23. de Carvalho, L. M.; Schwedt, G. *J. Chromatogr. A* **2005**, *1099*, 185.

24. Rinker, R. G.; Lynn, S.; Mason, D. M.; Corcoran, W. H. *Ind. Eng. Chem. Res.* **1965**, *4*, 282.

25. De Groot, D. C. *Fresenius J. Anal. Chem* **1967**, *229*, 335.

26. Brown, L.; Szekeres, L. *Talanta* **1979**, *26*, 414.

27. DePoy, P. E.; Mason, D. M. *Faraday Symp. Chem. S.* **1974**, *9*, 47.

28. Steudel, R.; Munchow, V. *J. Chromatogr. A* **1992**, *623*, 174.

29. Kovacs, K. M.; Rabai, G. *Chem. Commun.* **2002**, 790.

30. Čermák, V.; Smutek, M. *Collect. Czech. Chem. Commun.* **1975**, *40*, 24.

31. Lister, M. W.; Garvie, R. C. *Can. J. Chem.* **1959**, *37*, 1567.

32. Kolthoff, I. M.; Miller, C. S. *J. Am. Chem. Soc.* **1941**, *63*, 2818.

33. Rinker, R. G.; Gordon, T. P.; Mason, D. M.; Sakaida, R. R.; Corcoran, W. H. *J. Phys. Chem.* **1960**, *64*, 573.

34. Wayman, M.; Lem, W. J. *Can. J. Chem.* **1970**, *48*, 782.

35. Takahashi, H.; Kaneko, N.; Miwa, K. *Spectrochim. Acta. A. - M.* **1982**, *38*, 1147.

36. Nehb, W.; Vydra, K. In *Ullmann's Encyclopedia of Industrial Chemistry*; Wiley-VCH: Weinheim, 2012; Vol. 35, p 5.

37. Greenwood, N. N.; Earnshaw, A. *Chemistry of the Elements (2nd Edition)*; Elsevier, 1997.

38. Janzen, E. G. *J. Phys. Chem.* **1972**, *76*, 157.

39. Kumar, M. *Mar. Chem.* **1981**, *10*, 475.

40. Sillén, L. G. *Oceanography* **1961**, 32.

41. Shriver, D.; Atkins, P.; Overton, T.; Rourke, J.; Armstrong, F.; Weller, M. *Inorganic Chemistry*; W. H. Freeman and Company: New York, 2006.

42. Wong, G. T. F. *Mar. Chem.* **1980**, *9*, 1.

43. Frank, M. *Textile Colorist* **1915**, *37*, 4.

44. Bernthsen, A. *Ber. Dtscu. Chem. Ges.* **1881**, *14*, 438.

45. Schönbein, C. F. *J. Prakt. Chem.* **1854**, *61*, 193.

46. Schützenberger, M. P. *Compt. Rend.* **1869**, *69*, 6.

47. Bazlen, M.; Google Patents: 1907.

48. Bernthsen, A. In *The Chemical News and Journal of Physical Science*; Crookes, W., Ed.; Edwin John Davey: London, 1881; Vol. 43, p 79.

49. Merriman, R. W. *J. Soc. Chem. Ind.* **1923**, *42*, 290.

50. Wollak, R. *Fresenius J. Anal. Chem* **1930**, *80*, 1.

51. Wood, P. J.; Wiest, E. G.; Apsey, C. W.; Brubaker, C. H.; Fernald, B. B.; Kelton, S. C.; Petschow, J.; Pond, W. F.; Simpson, C. T. *Assay of Sodium Hydrosulfite,* American Association of Textile Chemists and Colorists, 1957.

52. Zocher, H.; Saechtling, H. *Fresenius J. Anal. Chem.* **1939**, *117*, 392.

53. Danehy, J. P.; Zubritsky, C. W. *Anal. Chem.* **1974**, *46*, 391.

54. Kilroy, W. P. *Talanta* **1978**, *25*, 359.

55. Kilroy, W. P. *Talanta* **1979**, *26*, 111.

56. Kilroy, W. P. *Talanta* **1980**, *27*, 343.

57. Kilroy, W. P. *Talanta* **1983**, *30*, 419.

58. Stutts, K. J. *Anal. Chem.* **1987**, *59*, 543.

59. de Carvalho, L. M.; Schwedt, G. *Anal. Chim. Acta* **2001**, *436*, 293.

60. Weiß, J.; Göbl, M. *Fresenius J. Anal. Chem* **1985**, *320*, 439.

61. Drude, P. *Ann. Phys.* **1889**, *272*, 532.

62. Leaver, K. D.; Chapman, B. N. *Thin Films*; Wykeham Publiations: London, 1971.

63. Secundus, G. P.; T., H. H.; Bostock, J. *Natural History*; H. G. Bohn: London, 1855; Vol. 6.

64. Ohring, M. *Materials Science of Thin Films*; Academic Press, 2002.

65. Eishanbini-Riad, A.; Barlow, F. D. *Thin Film Technology Handbook*; McGraw-Hill Professional: New York, 1997.

66. Smart, L. E.; Moore, E. A. *Solid State Chemistry: An Introduction*; CRC Press, 2005.

67. Dimitriev, Y.; Ivanova, Y.; Iordanova, R. *Journal of the University of Chemical Technology and Metallurgy* **2008**, *43*, 12.

68. Dislich, H.; Hinz, P. *J. Non-Cryst. Solids* **1982**, *48*, 11.

69. Bowman, J. E. *Memoirs and Proceedings of the Chemical Society* **1845**, *3*, 248.

70. Geffcken, W.; Berger, E.; Reichspatent, D., Ed.; Jeaner Glaswerk Schott & Gen.: Germany, 1939.

71. Sibum, H.; Güther, V.; Roidl, O.; Habashi, F.; Wolf, H. U. In *Ullmann's Encyclopedia of Industrial Chemistry*; Wiley-VCH Verlag GmbH & Co. KGaA: 2000.

72. Kamat, P. V. *J. Phys. Chem. Lett.* **2011**, *2*, 839.

73. Fujishima, A.; Honda, K. *Nature* **1972**, *238*, 37.

74. O'Regan, B.; Gratzel, M. *Nature* **1991**, *353*, 737.

75. Reisch, M. *Chem. Eng. News* **2001**, *79*, 8.

76. Remillard, J. T.; McBride, J. R.; Nietering, K. E.; Drews, A. R.; Zhang, X. *J. Phys. Chem. B* **2000**, *104*, 4440.

77. Xi, B.; Verma, L. K.; Li, J.; Bhatia, C. S.; Danner, A. J.; Yang, H.; Zeng, H. C. *ACS Appl. Mater. Interfaces* **2012**, *4*, 1093.

78. Rajeshwar, K.; Ibanez, J. G. *J. Chem. Ed.* **1995**, *72*, 1044.

79. Daghrir, R.; Drogui, P.; Robert, D. *Ind. Eng. Chem. Res.* **2013**, *52*, 3581.

80. Gaikwad, V. B.; Jain, G. H. In *Sensing Technology (ICST), 2011 Fifth International Conference on* 2011, p 239.

81. Hu, P.; Du, G.; Zhou, W.; Cui, J.; Lin, J.; Liu, H.; Liu, D.; Wang, J.; Chen, S. *ACS Appl. Mater. Interfaces* **2010**, *2*, 3263.

82. Kim, I.-D.; Rothschild, A.; Hyodo, T.; Tuller, H. L. *Nano Lett.* **2006**, *6*, 193.

83. Su, J.; Zou, X.-X.; Zou, Y.-C.; Li, G.-D.; Wang, P.-P.; Chen, J.-S. *Inorg. Chem.* **2013**, *52*, 5924.

84. Tolmachoff, E.; Memarzadeh, S.; Wang, H. *J. Phys. Chem. C* **2011**, *115*, 21620.

85. Munz, M.; Langridge, M. T.; Devarepally, K. K.; Cox, D. C.; Patel, P.; Martin, N. A.; Vargha, G.; Stolojan, V.; White, S.; Curry, R. J. *ACS Appl. Mater. Interfaces* **2013**, *5*, 1197.

86. Hage, R.; Lienke, A. *Angew. Chem. Int. Ed.* **2006**, *45*, 206.

87. Chen, H.-W.; Chen, C.-Y.; Wang, G.-S. *Chemosphere* **2011**, *85*, 591.

88. Meneses, M.; Pasqualino, J. C.; Castells, F. *Chemosphere* **2010**, *81*, 266.

89. Shintani, H. *Biocontrol Sci.* **2009**, *14*, 39.

90. Demirkol, O.; Cagri-Mehmetoglu, A.; Qiang, Z.; Ercal, N.; Adams, C. *J. Agric. Food Chem.* **2008**, *56*, 10414.

91. Qiang, Z.; Demirkol, O.; Ercal, N.; Adams, C. *J. Agric. Food Chem.* **2005**, *53*, 9830.

92. Castle, L.; Mercer, A. J.; Gilbert, J. *J. Food. Protect.* **1995**, *58*, 5.

93. Reidmiller, J. S.; Baldeck, J. D.; Rutherford, G. C.; Marquis, R. E. *J. Food. Protect.* **2003**, *66*, 8.

94. Fichet, G.; Antloga, K.; Comoy, E.; Deslys, J. P.; McDonnell, G. *J. Hosp. Infect.* **2007**, *67*, 278.

95. Pottage, T.; Richardson, C.; Parks, S.; Walker, J. T.; Bennett, A. M. *J. Hosp. Infect.* **2010**, *74*, 55.

96. OSHA; Labor, U. S. D. o., Ed. 1910.

97. OSHA; U. S. Department of Labor: 1978; Vol. 2012.

98. OSHA; U. S. Department of Labor: 2004.

99. Abo, M.; Urano, Y.; Hanaoka, K.; Terai, T.; Komatsu, T.; Nagano, T. *J. Am. Chem. Soc.* **2011**, *133*, 10629.

100. Ohta, T.; Yamauchi, Y.; Takitani, S. *Fresenius J. Anal. Chem.* **1992**, *343*, 550.

101. Qi, B.; Zhu, Y. Z.; Hu, M.; Zhang, Y.; Tang, X. *Anal. Lett.* **2001**, *34*, 1247.

102. Luo, W.; Li, Y.-S.; Yuan, J.; Zhu, L.; Liu, Z.; Tang, H.; Liu, S. *Talanta* **2010**, *81*, 901.

103. Toniolo, R.; Geatti, P.; Bontempelli, G.; Schiavon, G. *J. Electroanal. Chem.* **2001**, *514*, 123.

104. Kuwata, S.; Sadaoka, Y. *Sensor. Actua. B: Chemical* **2000**, *65*, 325.

105. Wiedemair, J.; van Dorp, H. D. S.; Olthuis, W.; van den Berg, A. *Electrophoresis* **2012**, *33*, 3181.

106. Kulys, J. *Sensors and Actuators B: Chemical* **1992**, *9*, 143.

107. Lewis, D. *J. Phys. Chem.* **1958**, *62*, 1145.

108. Possanzini, M.; Di Palo, V. *Anal. Chim. Acta* **1995**, *315*, 225.

109. Satterfield, C. N.; Bonnell, A. H. *Anal. Chem.* **1955**, *27*, 1174.

110. Matsubara, C.; Kudo, K.; Kawashita, T.; Takamura, K. *Anal. Chem.* **1985**, *57*, 1107.

111. Huang, H.; Dasgupta, P. K. *Talanta* **1997**, *44*, 605.

112. Amani, M.; Chu, Y.; Waterman, K. L.; Hurley, C. M.; Platek, M. J.; Gregory, O. J. *Sensor. Actua. B: Chemical* **2012**, *162*, 7.

113. Belluck, P.; Chang, K. In *The New York Times*; The New York Times: New York, 2001, p 1.

114. Oxley, J. C.; Smith, J. L.; Moran, J.; Nelson, K.; Utley, W. E. **2004**, 349.

115. Perks, B.; Sanderson, K. Terror plot sparks frenzied speculation about liquid explosives. *Chemistry World* [Online Early Access]. Published Online: 2006. http://www.rsc.org/chemistryworld/News/2006/August/11080602.asp (accessed 6/3/2013).

116. Dubnikova, F.; Kosloff, R.; Almog, J.; Zeiri, Y.; Boese, R.; Itzhaky, H.; Alt, A.; Keinan, E. *J. Am. Chem. Soc.* **2005**, *127*, 1146.

117. Dubnikova, F.; Kosloff, R.; Zeiri, Y.; Karpas, Z. *J. Phys. Chem. A* **2002**, *106*, 4951.

118. Moore, D. *Sens. Imaging* **2007**, *8*, 9.

119. Buttigieg, G. A.; Knight, A. K.; Denson, S.; Pommier, C.; Bonner Denton, M. *Forensice Sci. Int.* **2003**, *135*, 53.

120. Oxley, J. C.; Smith, J. L.; Kirschenbaum, L. J.; Marimganti, S.; Vadlamannati, S. *J. Forensic Sci.* **2008**, *53*, 690.

121. MacCrehan, W.; Moore, S.; Hancock, D. *Anal. Chem.* **2011**, *83*, 9054.

122. Fan, W.; Young, M.; Canino, J.; Smith, J.; Oxley, J.; Almirall, J. *Anal. Bioanal. Chem.* **2012**, *403*, 401.

123. Lazic, V.; Palucci, A.; Jovicevic, S.; Carapanese, M.; Poggi, C.; Buono, E. In *Proceedings of SPIE*; Fountain, A. W., Gardner, P. J., Eds. 2010; Vol. 7665, p 76650V.

124. Lazic, V.; Palucci, A.; Jovicevic, S.; Carpanese, M. *Spectrochim. Acta. B.* **2011**, *66*, 644.

125. Botti, S.; Carpanese, M.; Cantarini, L.; Giubileo, G.; Lazic, V.; Jovicevic, S.; Palucci, A.; Puiu, A. In *Proceedings of SPIE*; Fountain, A. W., Gardner, P. J., Eds. 2010; Vol. 7665, p 76650O.

126. Subarna, B.; Susanta, K. M.; Mano, M.; Indu , B. M. *Nanotechnology* **2009**, *20*, 075502.

127. Chowdhuri, A.; Sharma, A.; Gupta, V. In *Proceedings of SPIE*; Fountain, A. W., Gardner, P. J., Eds. 2011; Vol. 8018, p 80181V.

128. Capua, E.; Cao, R.; Sukenik, C. N.; Naaman, R. *Sensor. Actua. B: Chemical* **2009**, *140*, 122.

129. Wackerbarth, H.; Salb, C.; Gundrum, L.; Niederkrüger, M.; Christou, K.; Beushausen, V.; Viöl, W. *Appl. Opt.* **2010**, *49*, 4362.

130. Wilson, P. F.; Prince, B. J.; McEwan, M. J. *Anal. Chem.* **2005**, *78*, 575.

131. Mullen, C.; Irwin, A.; Pond, B. V.; Huestis, D. L.; Coggiola, M. J.; Oser, H. *Anal. Chem.* **2006**, *78*, 3807.

132. Romolo, F. S.; Cassioli, L.; Grossi, S.; Cinelli, G.; Russo, M. V. *Forensic Sci. Int.* **2013**, *224*, 96.

133. Shen, C.; Li, J.; Han, H.; Wang, H.; Jiang, H.; Chu, Y. *Int. J. Mass. Spectrom.* **2009**, *285*, 100.

134. Sehönn, G. *Z. Anal. Chem. Freseniu.* **1870**, *9*, 41.

135. Patel, C. C.; Mohan, M. S. *Nature* **1960**, *186*, 803.

136. Schwarz, R. *Z. Anorg. Allg. Chem.* **1933**, *210*, 303.

137. Jere, G. V.; Patel, C. C. *Nature* **1962**, *194*, 470.

138. Schwarzenbach, G.; Müehlebach, J.; Müeller, K. *Inorg. Chem.* **1970**, *9*, 2381.

139. Ohya, Y. In *Handbook of Sol-Gel Science and Technology : Processing Characterization and Applications*; 1st ed.; Sakka, S., Ed.; Kluwer Academic Publishers: Norwell, Massachusetts, 2005; Vol. 1, p 109.

140. Vogel, A. I. *Textbook of Quantitative Chemical Analysis*; 5th ed.; Longman Scientific & Technical: New York, 1989.

141. Kusabe, M.; Kozuka, H.; Abe, S.; Suzuki, H. *J. Sol-Gel Sci. Technol.* **2007**, *44*, 111.

142. Harris, D. C. *Quantitative Chemical Analysis*; 7th ed.; W. H. Freeman and Company: New York, 2007.

143. Haga, K.; Iwaya, K.; Kaneko, R. *Bull. Chem. Soc. Jpn* **1985**, *59*, 5.

144. Williams, W. J. *Handbook of Anion Determination*; Butterworths & Co.: London, 1979.

145. Hubaux, A.; Vos, G. *Anal. Chem.* **1970**, *42*, 849.

146. Schlessinger, G. G. *Inorganic Laboratory Preparations*; Chemical Publishing Company: New York, 1962.

147. Wood, A.; Kelly, D. *Arch. Microbiol.* **1986**, *144*, 71.

148. Biltz, H.; Biltz, W. *Laboratory Methods of Inorganic Chemistry*; John Wiley & Sons: New York, 1928.

149. Degen, I. A.; Newman, G. A. *Spectrochim. Acta. A. - M.* **1993**, *49*, 859.

150. Meyer, B.; Ospina, M.; Peter, L. B. *Anal. Chim. Acta* **1980**, *117*, 301.

151. Schneider, C. A.; Rasband, W. S.; Eliceiri, K. W. *Nat. Meth.* **2012**, *9*, 671.

152. Gilicinski, A. G.; Rynders, R. M.; Beck, S. E.; Strausser, Y. E.; Stets, J. R.; Felker, B. S.; Bohling, D. A. *MRS Online Proceedings Library* **1993**, *324*, null.

153. Goswami, D.; Medda, S. K.; De, G. *ACS Appl. Mater. Interfaces* **2011**, *3*, 3440.

154. Kehoe, E.; Penn, R. L. *J. Chem. Ed.* **2013**, *90*, 1191.

155. Sella, E.; Shabat, D. *Chem. Commun.* **2008**, *0*, 5701.

156. Brunauer, S.; Emmett, P. H.; Teller, E. *J. Am. Chem. Soc.* **1938**, *60*, 309.

APPENDICES

APPENDIX A - *Calibration Curves for Ion Chromatography*, **Chapters II and III**

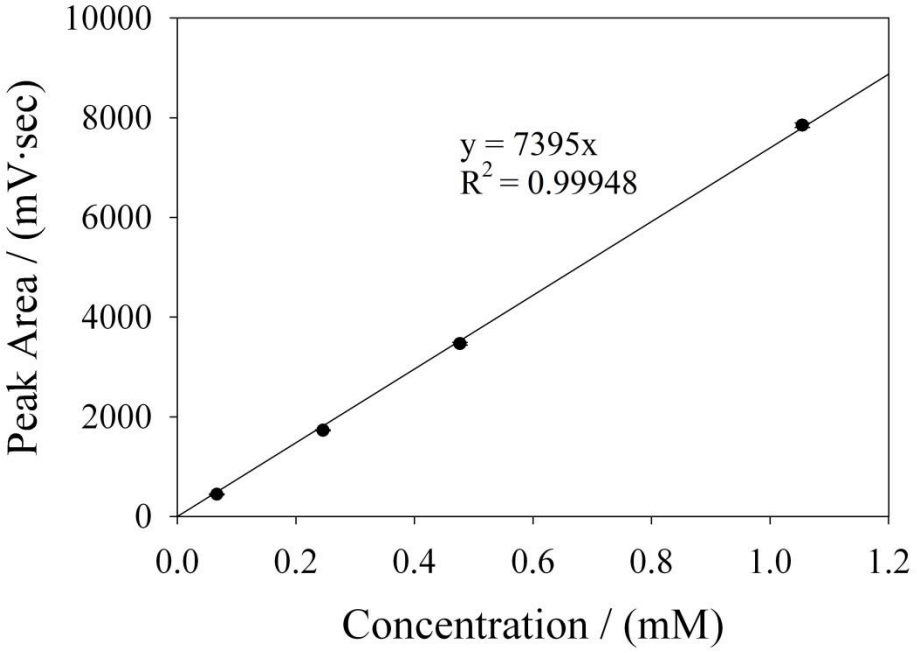

Figure A1. Calibration curve for dithionite anion, produced using IC. Hydroxymethanesulfinate (i.e. Rongalite) anion was used in place of dithionite, as quantification was performed after addition of formaldehyde (see text). The calibration was extremely linear (R^2 = 0.99948), and the zero-intercept is set. Error bars are present, but small and obscured.

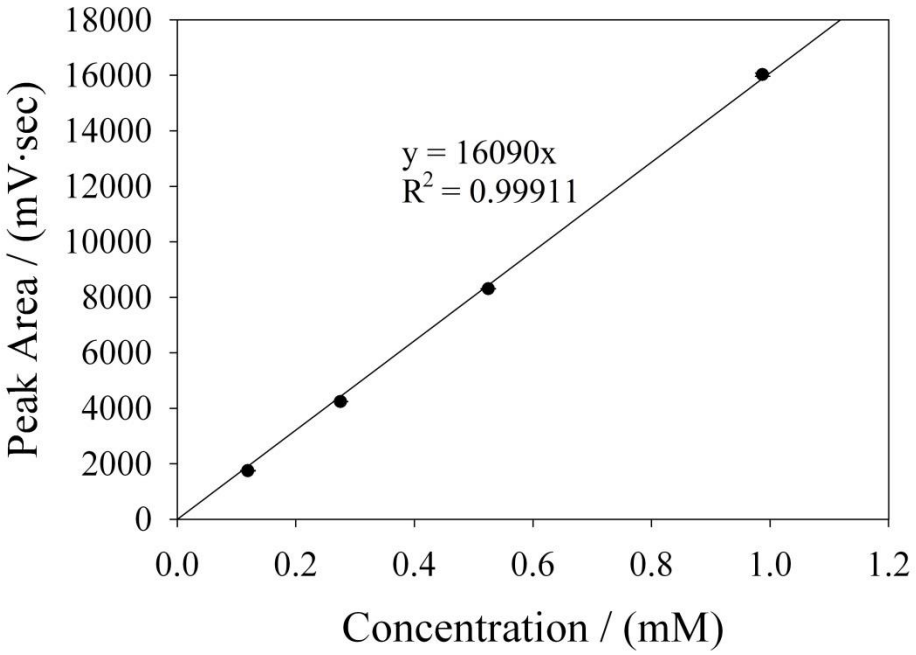

Figure A2. Calibration curve for thiosulfate anion produced using IC. The calibration was extremely linear (R^2 = 0.99911), and the zero intercept is set. Error bars are present, but small and obscured.

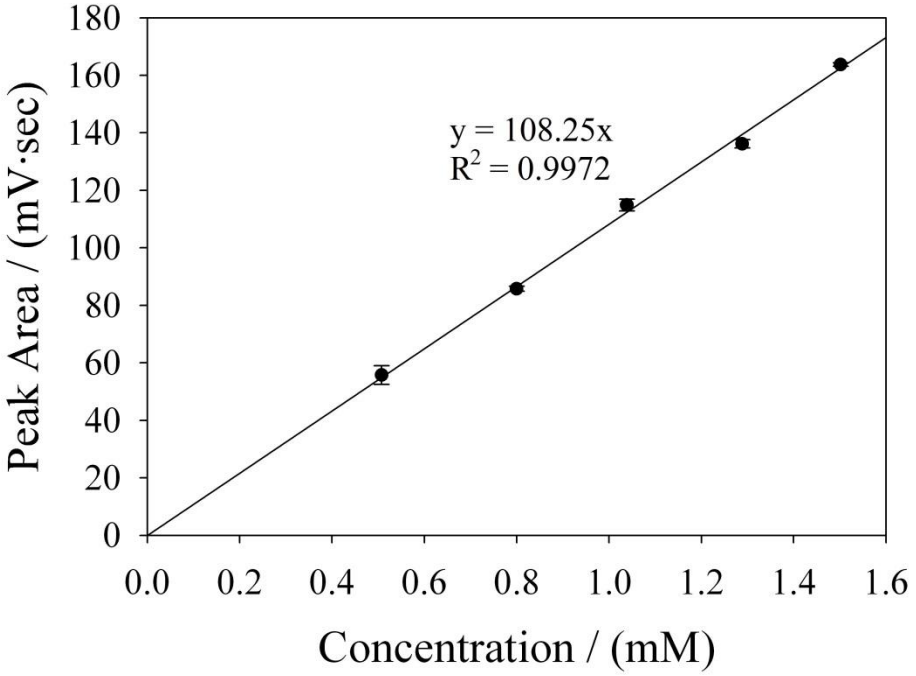

Figure A3. Calibration curve for sodium cation, produced using IC. The calibration was extremely linear (R^2 = 0.9972), and the zero-intercept is set. Error bars are present.

APPENDIX B - *Raman Spectra of Solid Standards*, **Chapter III**

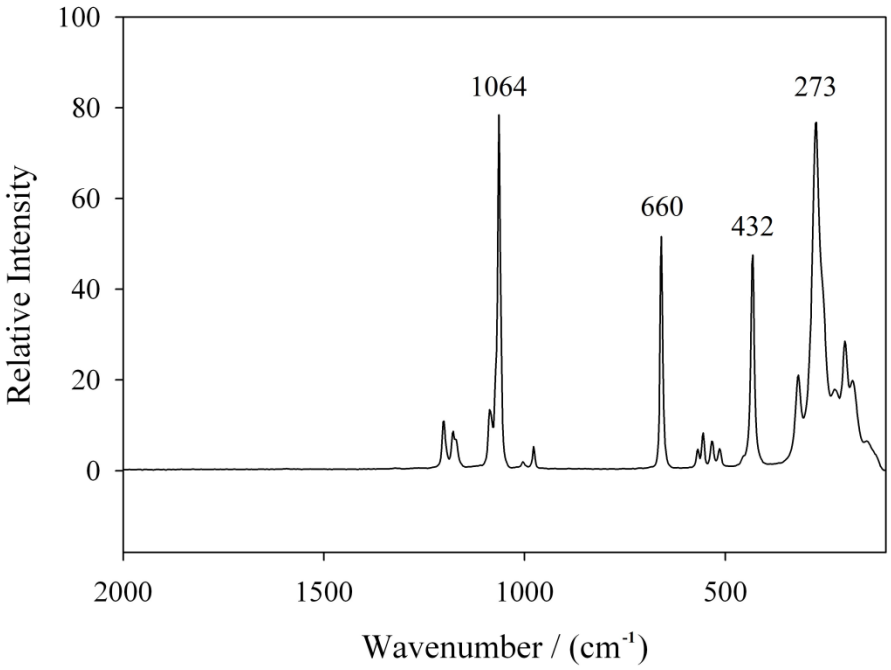

Figure B1. Raman spectrum of solid sodium bisulfite ($NaHSO_3$).

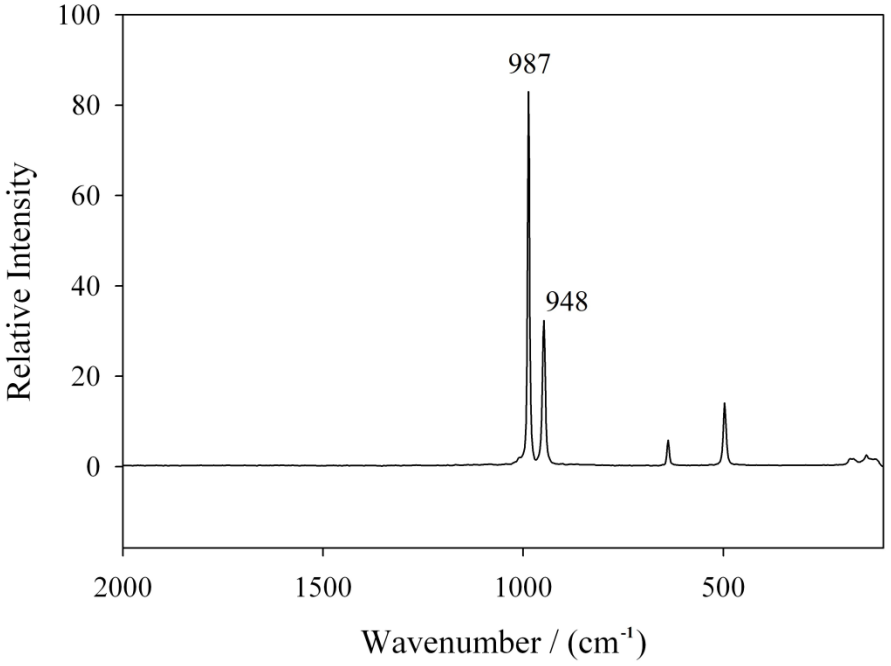

Figure B2. Raman spectrum of solid sodium sulfite (Na_2SO_3).

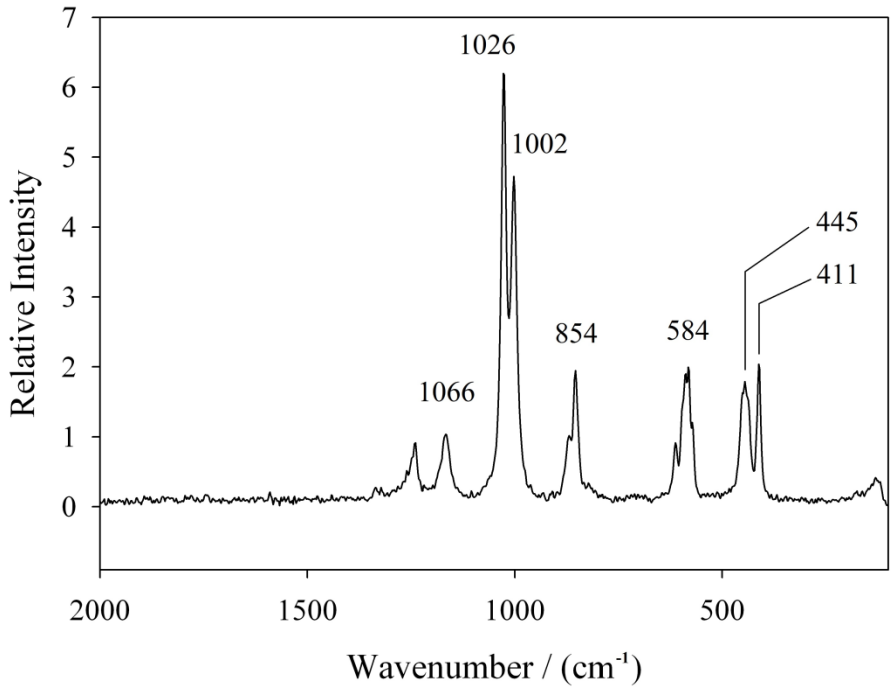

Figure B3. Raman spectrum of solid potassium bisulfate ($KHSO_4$).

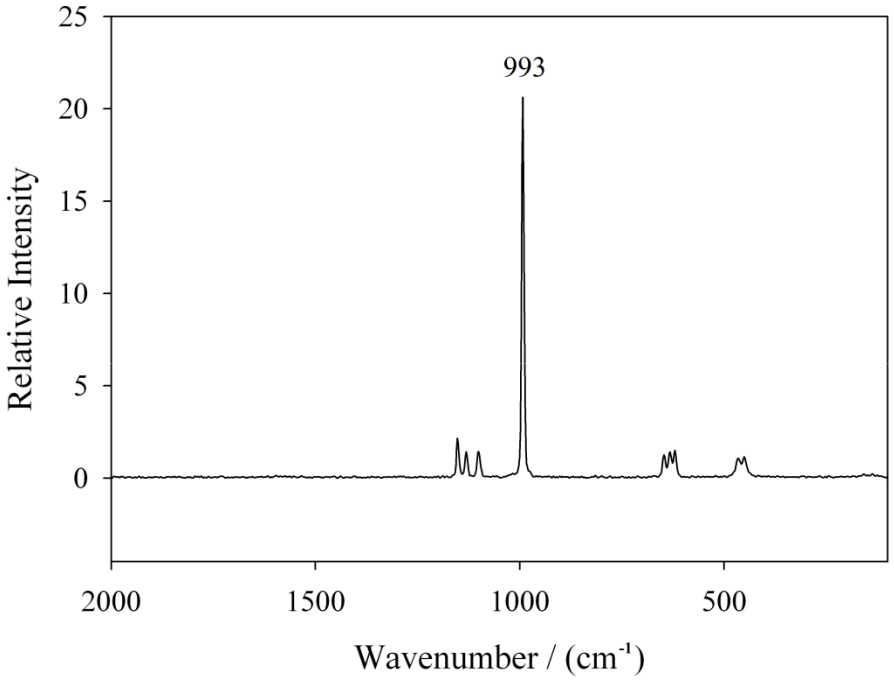

Figure B4. Raman spectrum of solid sodium sulfate (Na_2SO_4).

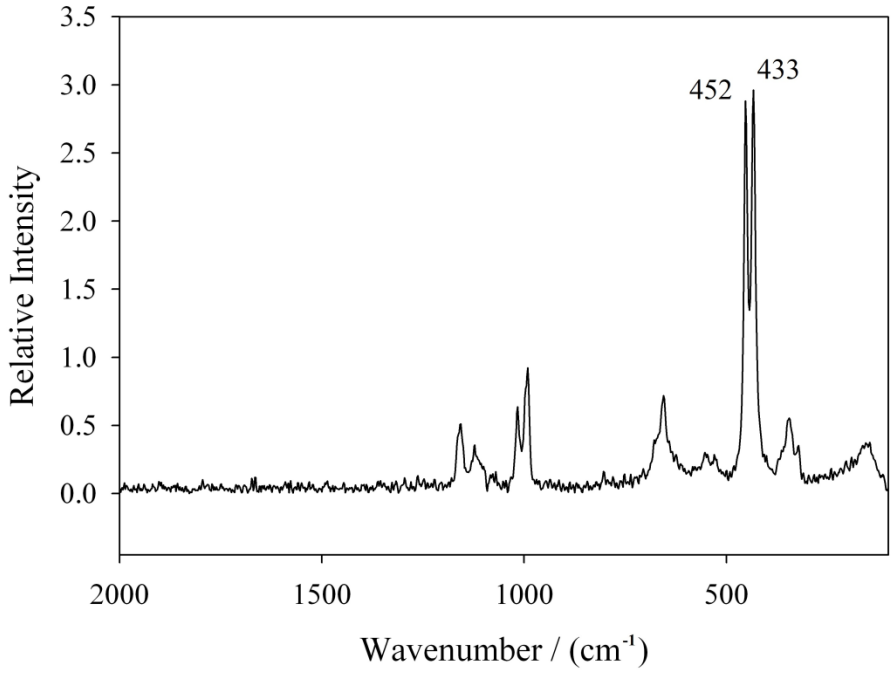

Figure B5. Raman spectrum of solid sodium thiosulfate pentahydrate ($Na_2S_2O_3 \bullet 5H_2O$).

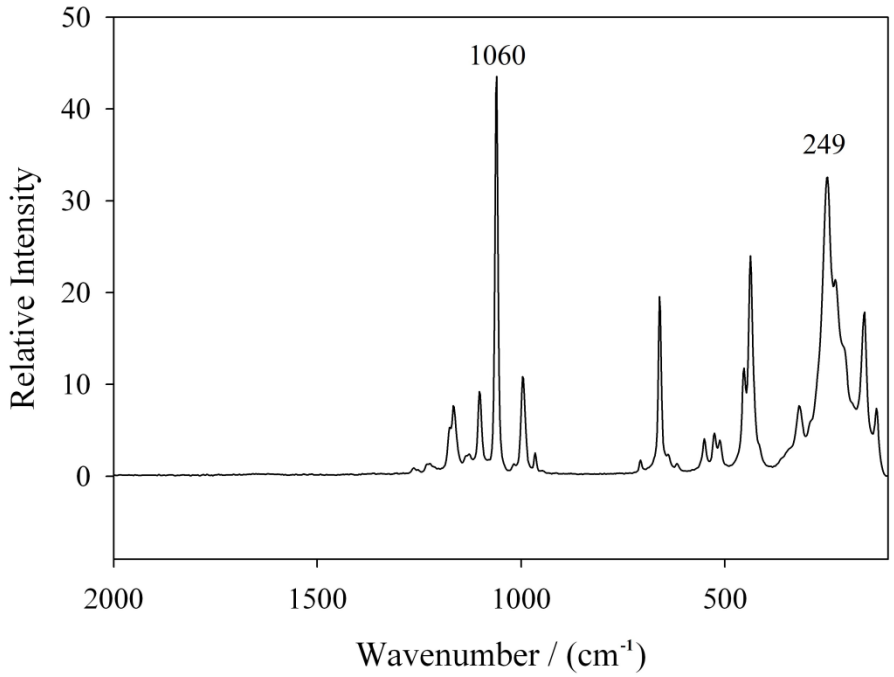

Figure B6. Raman spectrum of solid sodium dithionite (Sample 1).

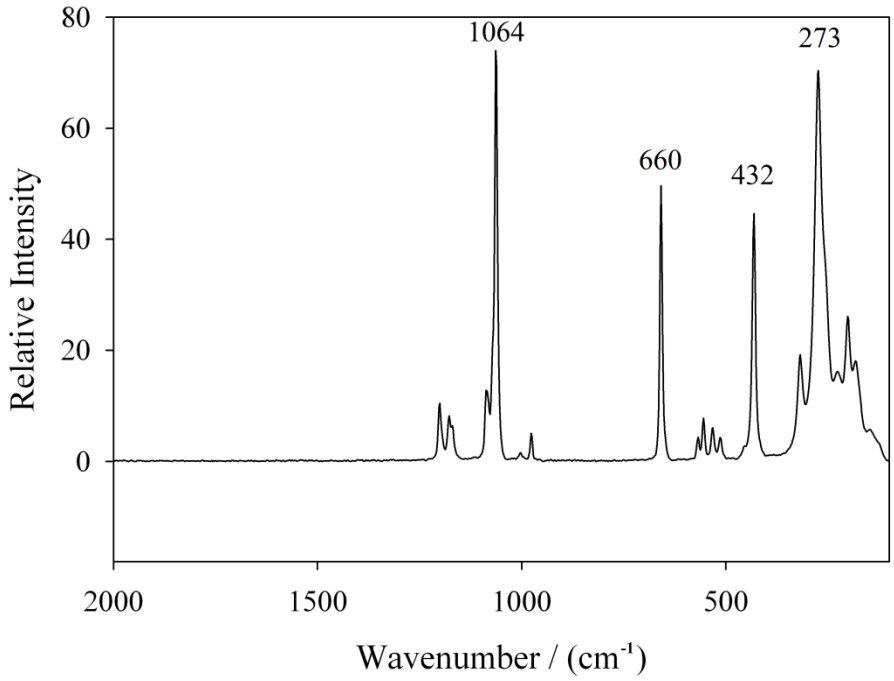

Figure B7. Raman spectrum of solid sodium metabisulfite ($Na_2S_2O_5$).

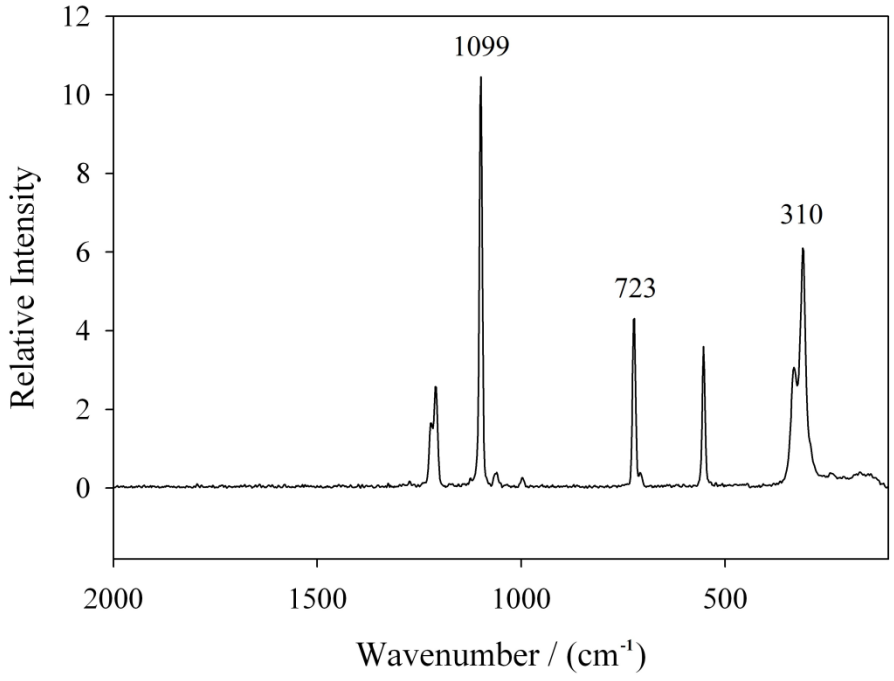

Figure B8. Raman spectrum of solid sodium dithionate ($Na_2S_2O_6$).

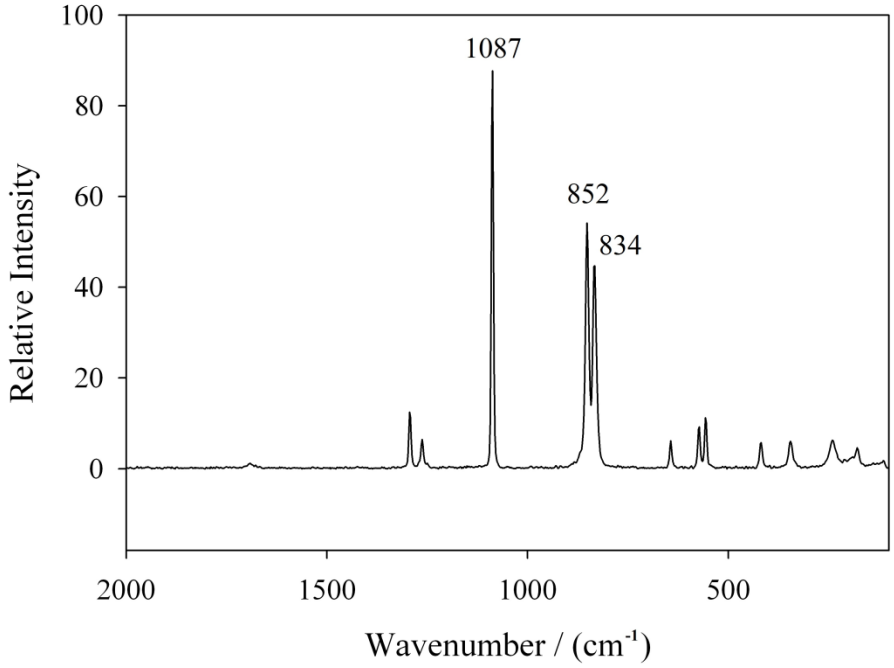

Figure B9. Raman spectrum of solid sodium persulfate ($Na_2S_2O_8$).

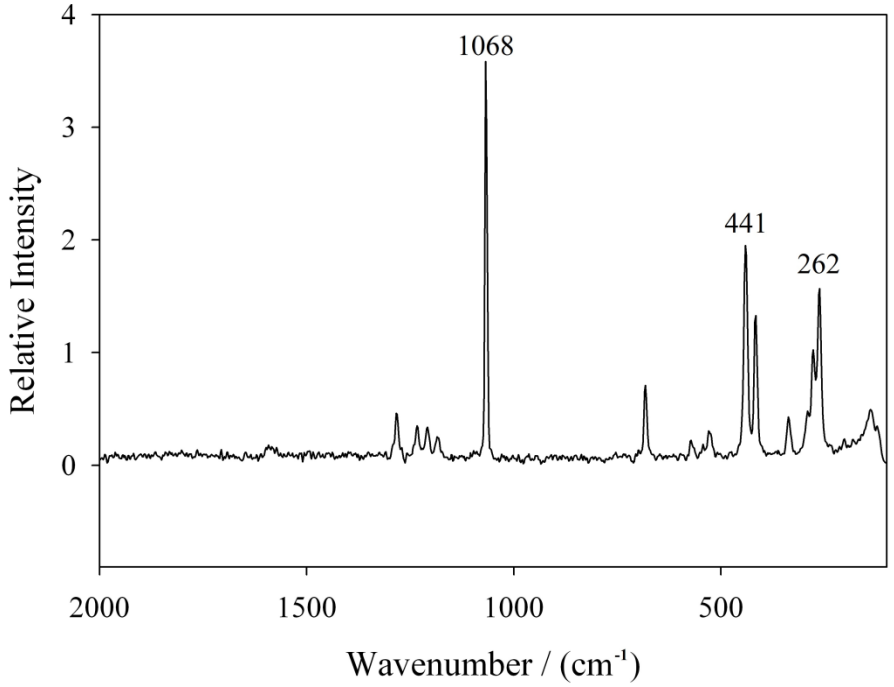

Figure B10. Raman spectrum of solid sodium trithionate ($Na_2S_3O_6$).

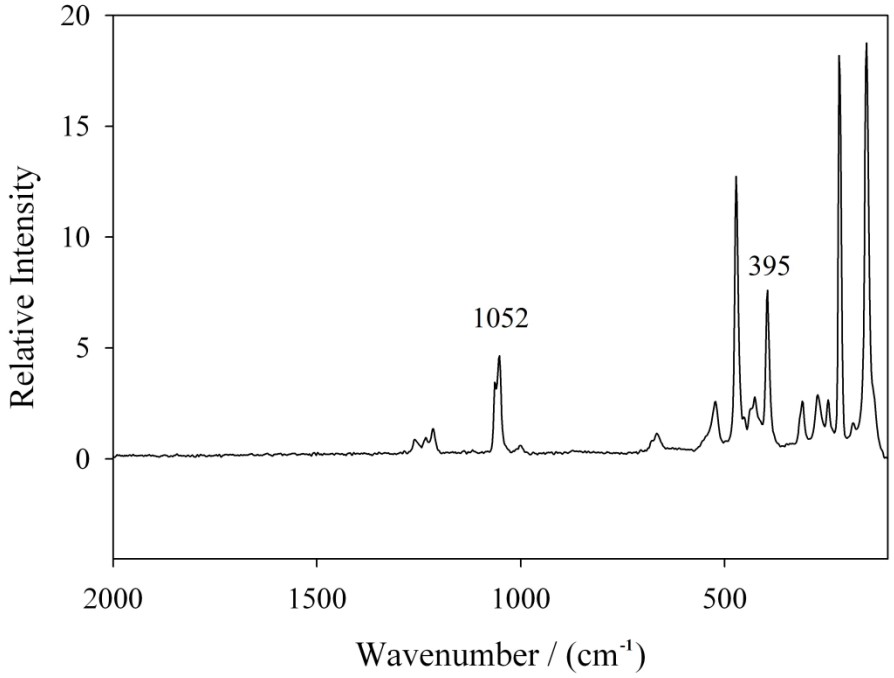

Figure B11. Raman spectrum of solid sodium tetrathionate dihydrate ($Na_2S_4O_6$•$2H_2O$).

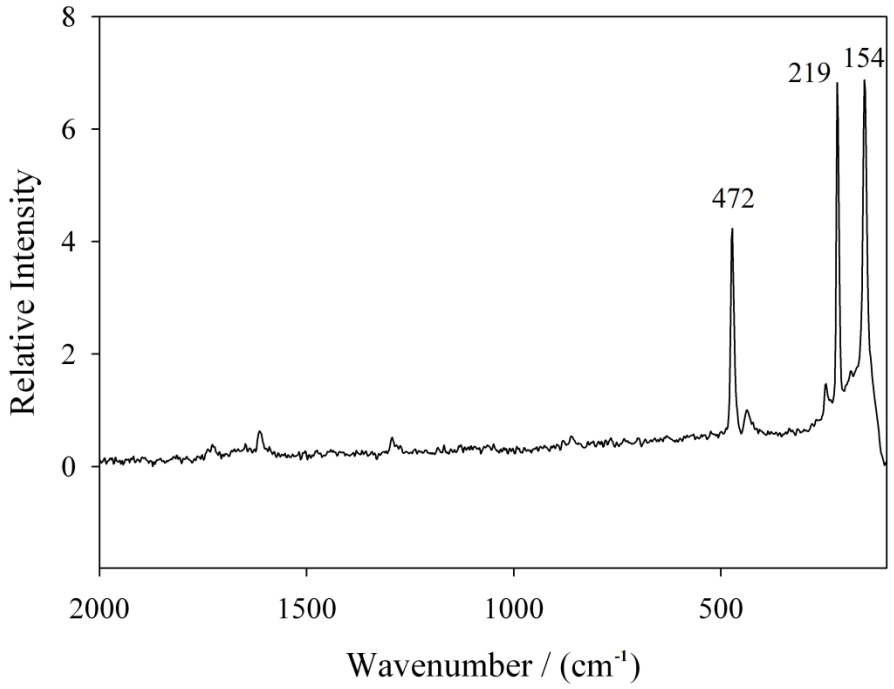

Figure B12. Raman spectrum of solid sulfur (S_8). Given that sulfur does not dissolve in water, no Raman spectrum of a sulfur solution was possible.

Raman Spectra of Solution Standards

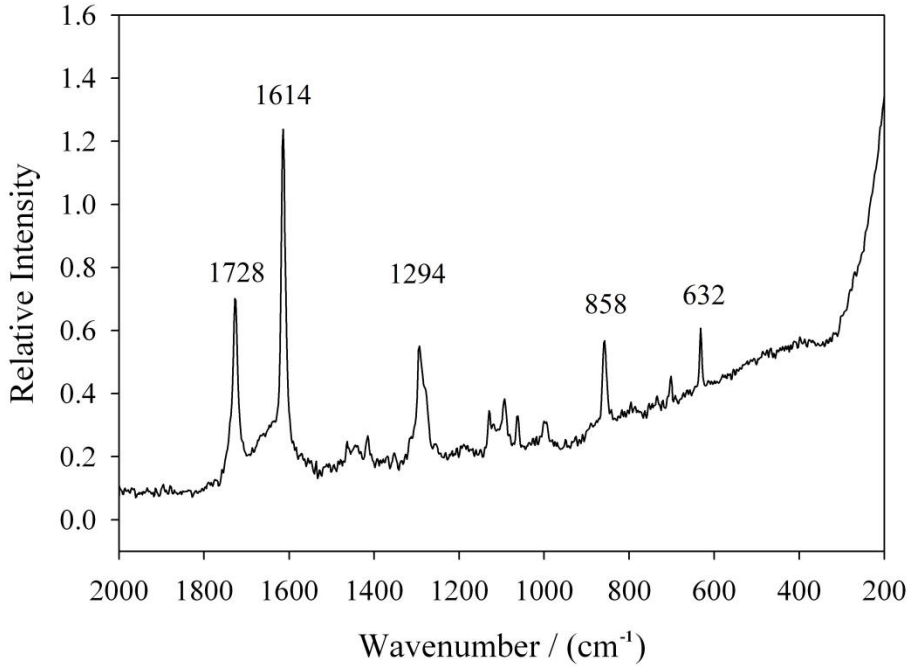

Figure B13. Raman spectrum of blank solution (water behind Mylar window in Mylar cell). The Raman spectra below have all had this blank subtracted, leaving only the peaks of the standards.

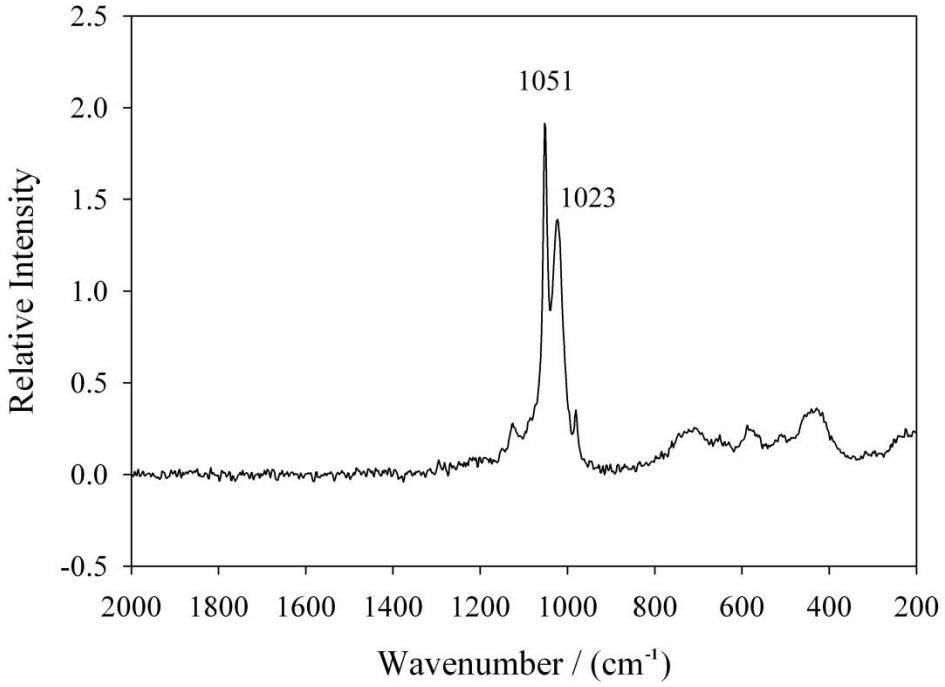

Figure B14. Raman spectrum of sodium bisulfite ($NaHSO_3$) in solution.

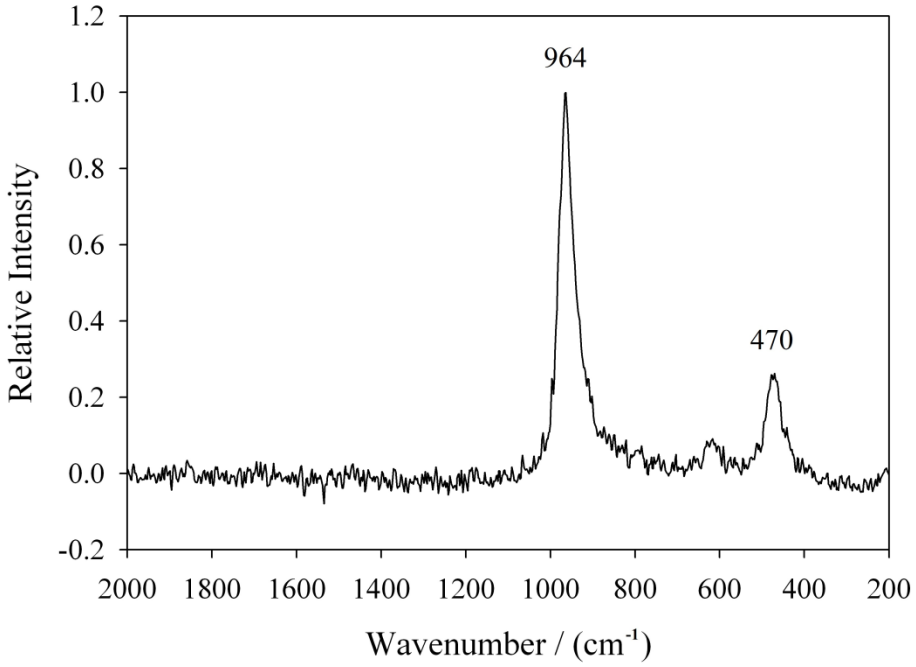

Figure B15. Raman spectrum of sodium sulfite (Na_2SO_3) in solution.

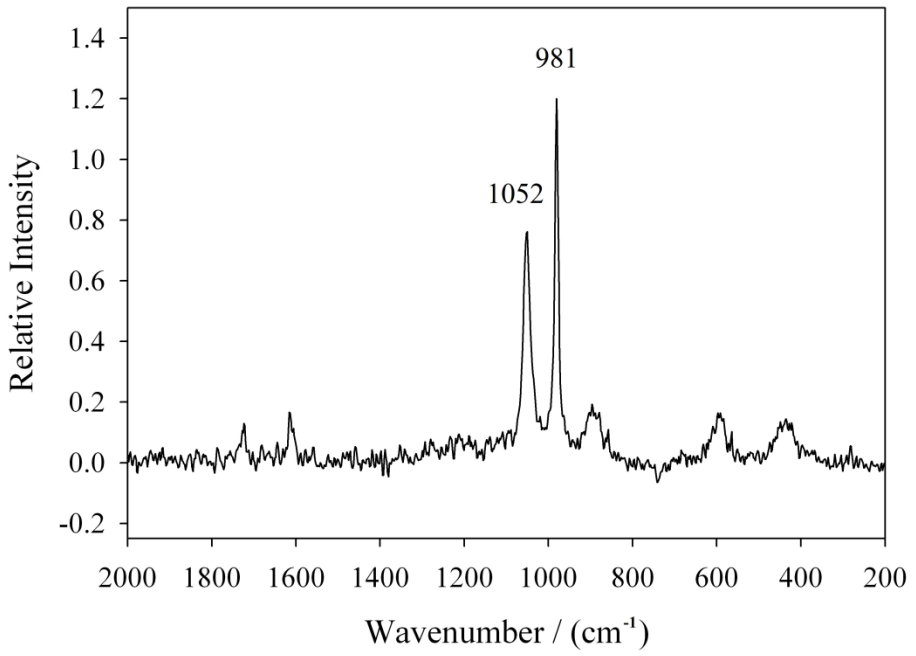

Figure B16. Raman spectrum of potassium bisulfate ($KHSO_4$) in solution.

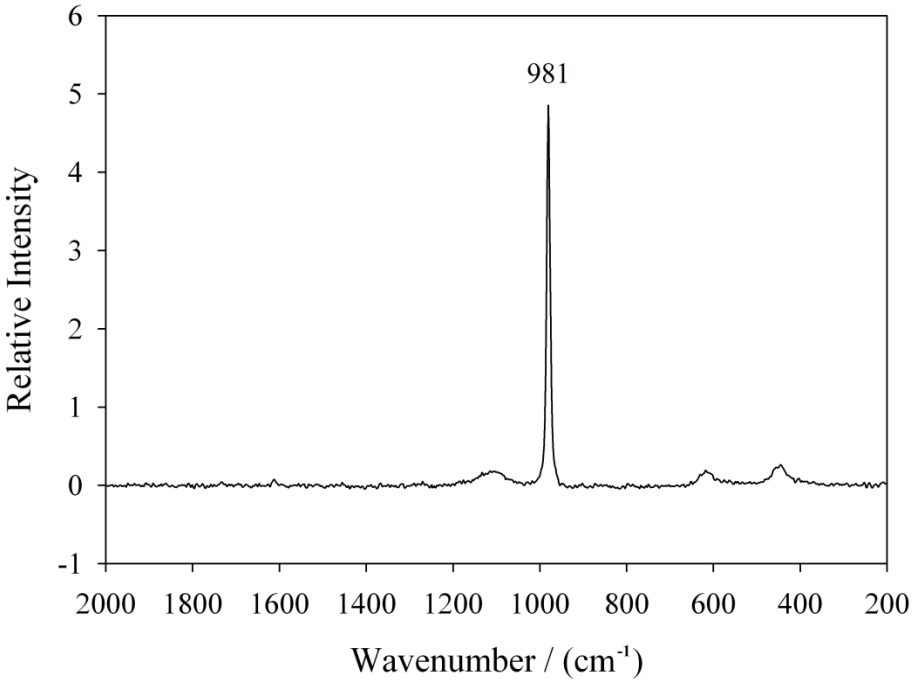

Figure B17. Raman spectrum of sodium sulfate (Na_2SO_4) in solution.

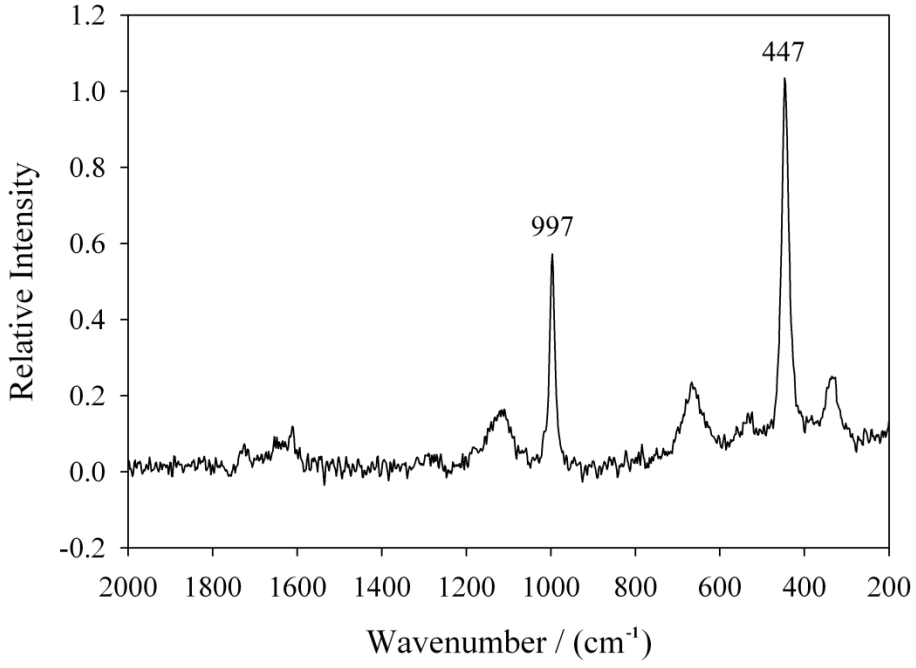

Figure B18. Raman spectrum of sodium thiosulfate pentahydrate ($Na_2S_2O_3 \bullet 5H_2O$) in solution.

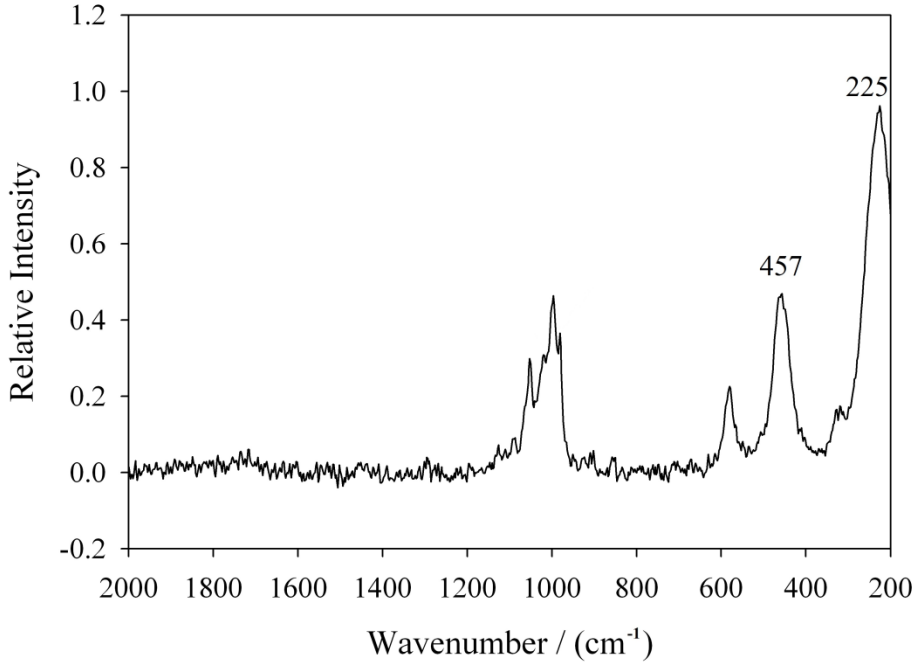

Figure B19. Raman spectrum of sodium dithionite ($Na_2S_2O_4$, Sample 1) in solution.

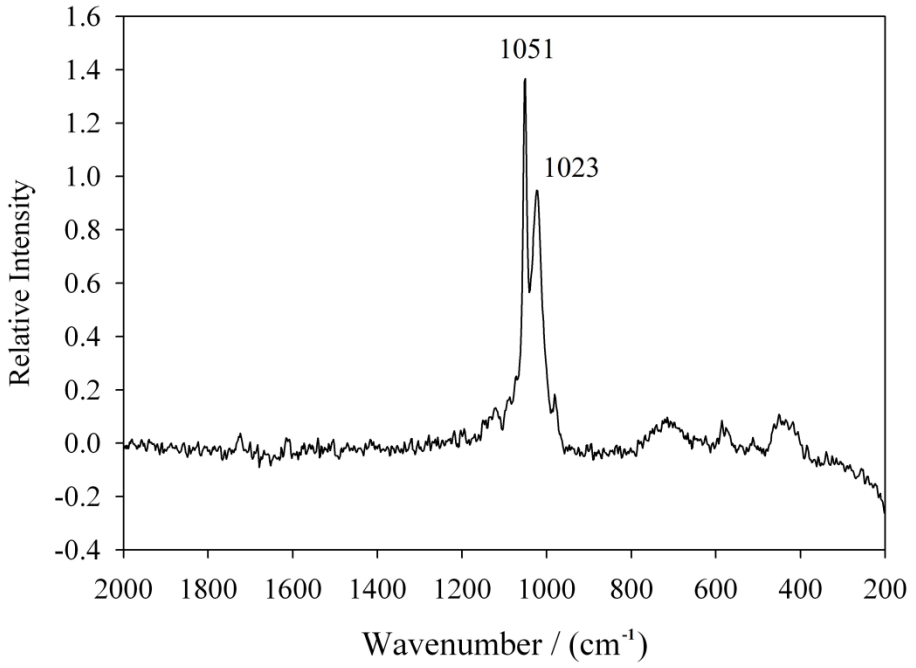

Figure B20. Raman spectrum of sodium metabisulfite ($Na_2S_2O_5$) in solution.

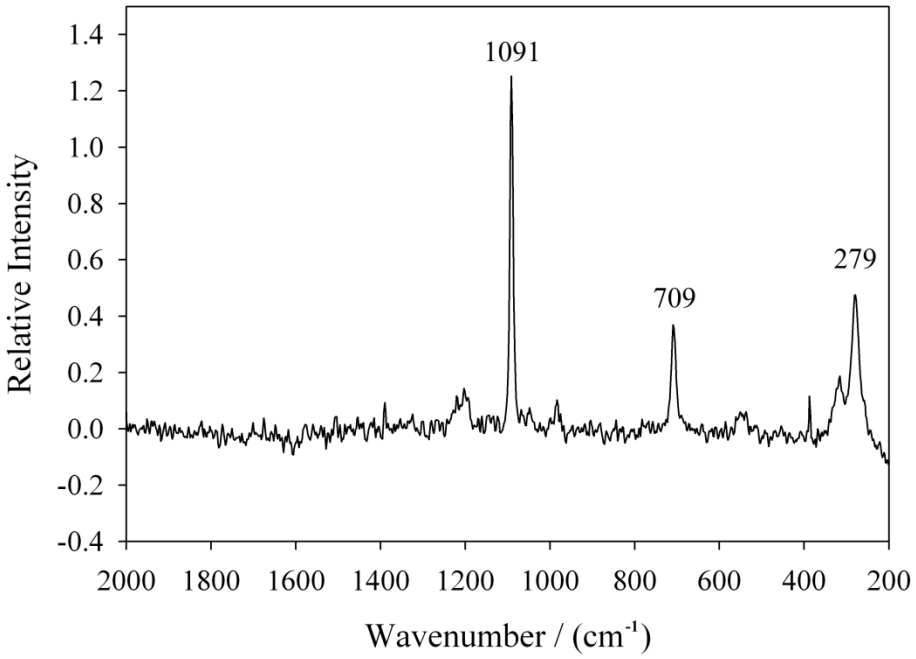

Figure B21. Raman spectrum of sodium dithionate ($Na_2S_2O_6$) in solution.

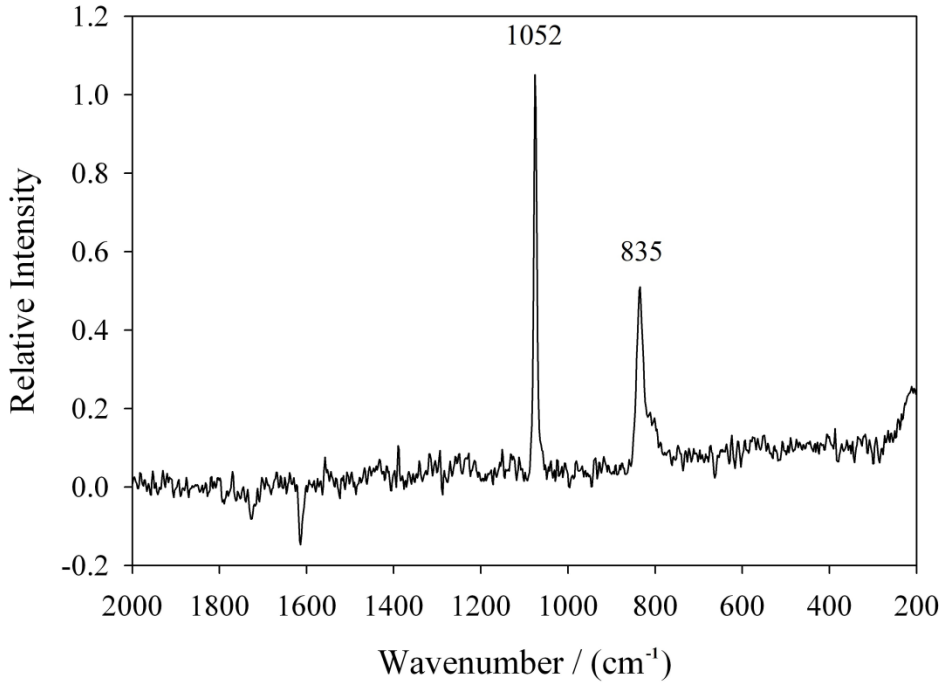

Figure B22. Raman spectrum of sodium persulfate ($Na_2S_2O_8$) in solution.

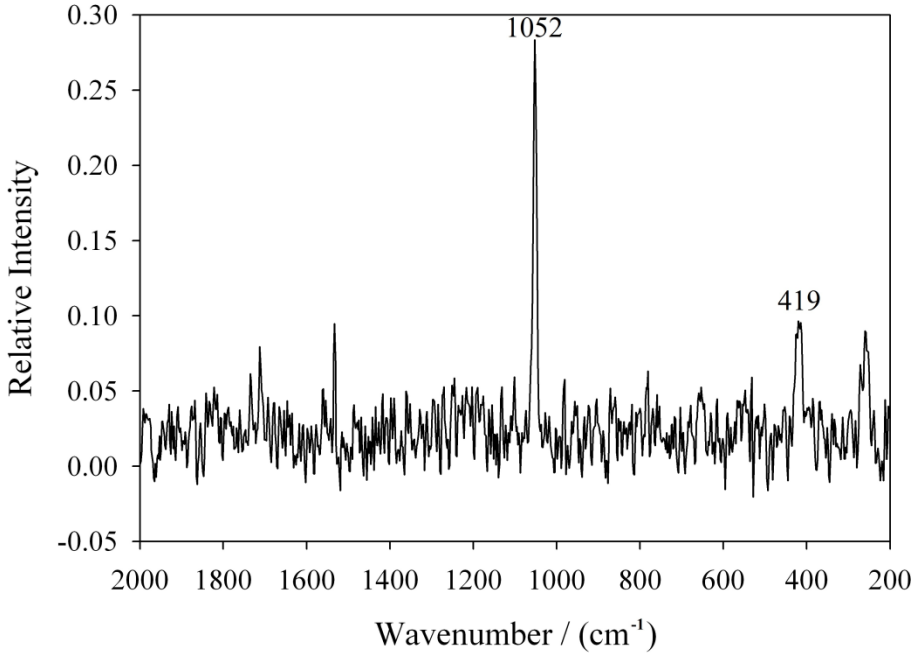

Figure B23. Raman spectrum of sodium trithionate ($Na_2S_3O_6$) in solution.

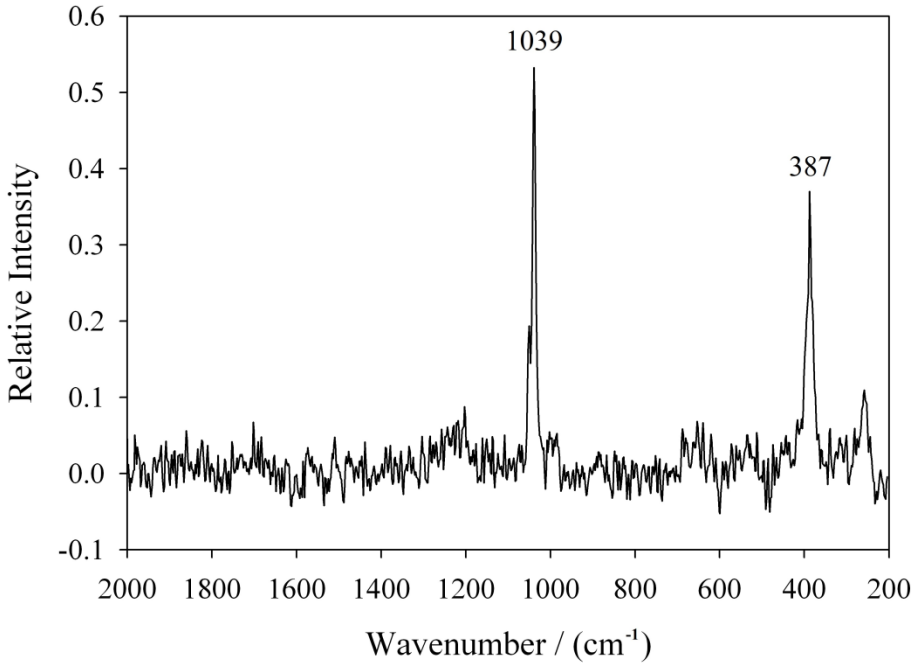

Figure B24. Raman spectrum of sodium tetrathionate ($Na_2S_4O_6$) in solution.

Raman Spectra of Dithionite Samples

Sample 1 – Produced December 2010, J. T. Baker

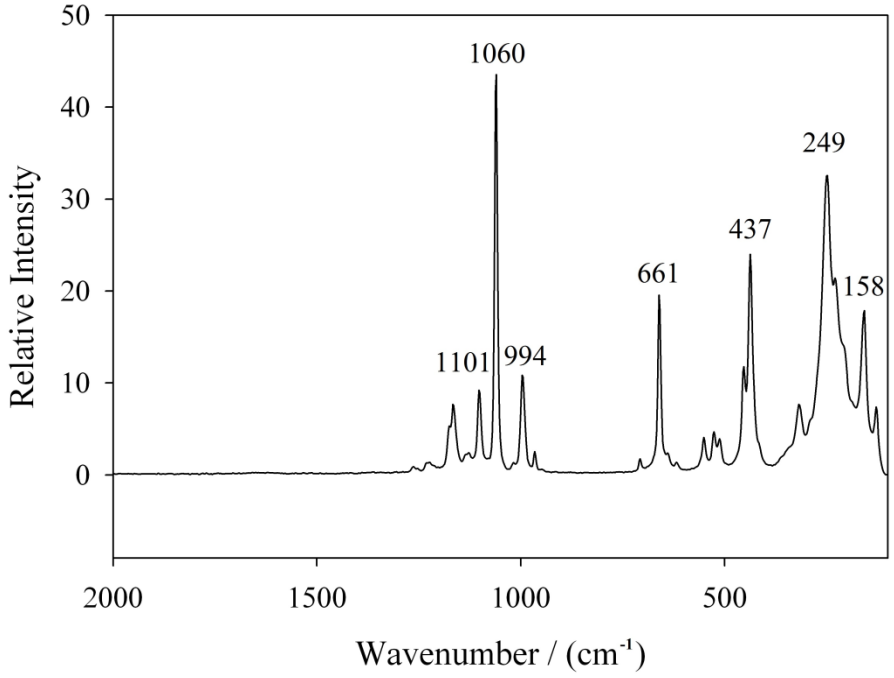

Figure B25. Raman spectrum of solid Sample 1.

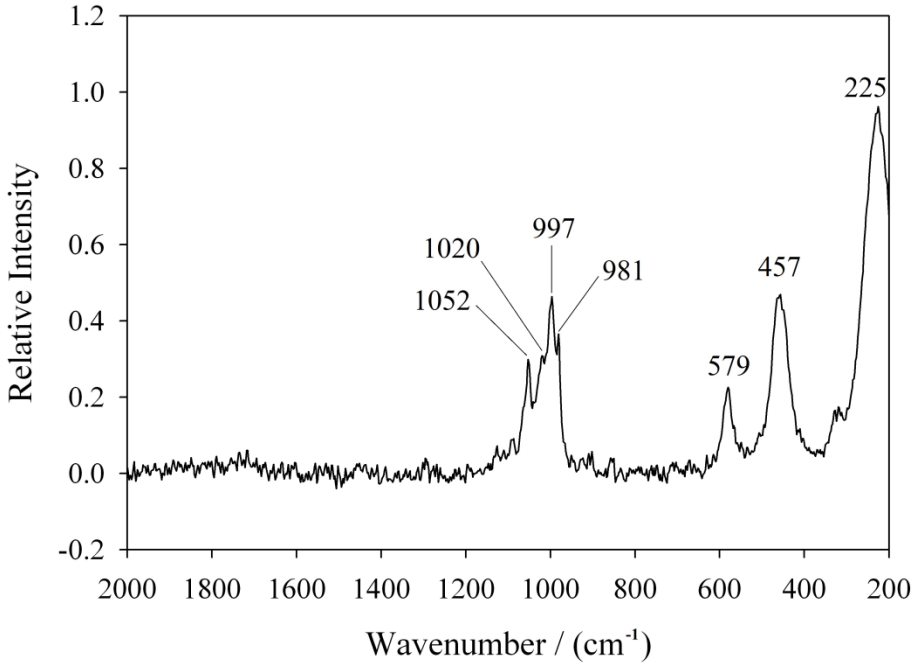

Figure B26. Raman spectrum of Sample 1 in solution.

Sample 2 – Produced September 2010, Alfa Aesar

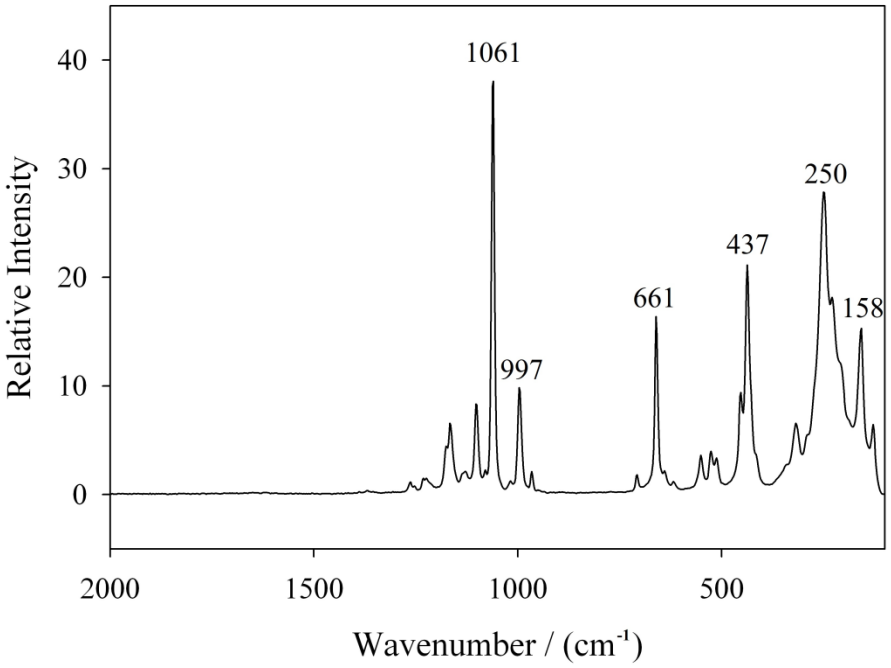

Figure B27. Raman spectrum of solid Sample 2.

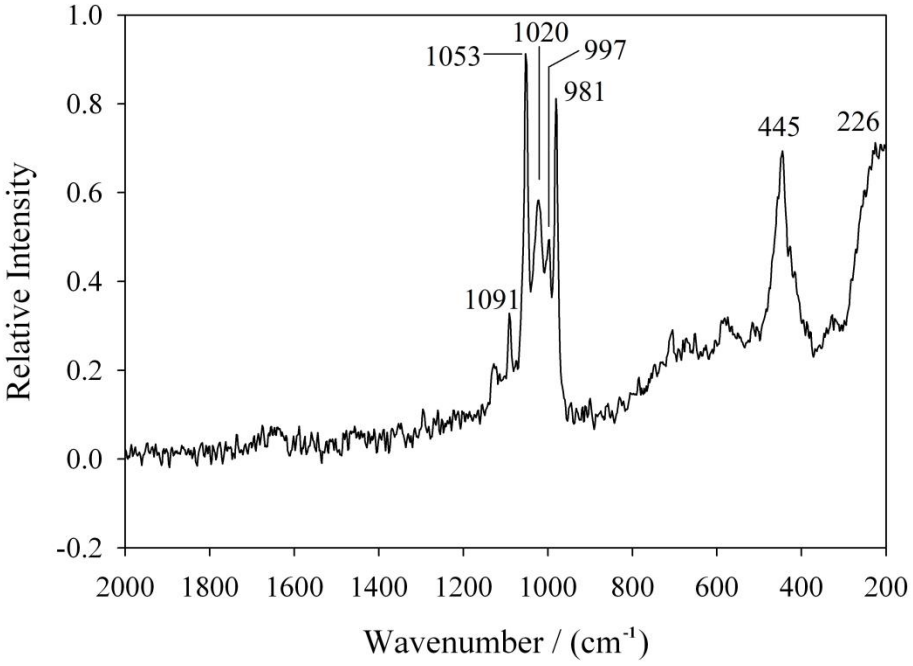

Figure B28. Raman spectrum of Sample 2 in solution.

Sample 3 – Produced May 2010, Sigma-Aldrich

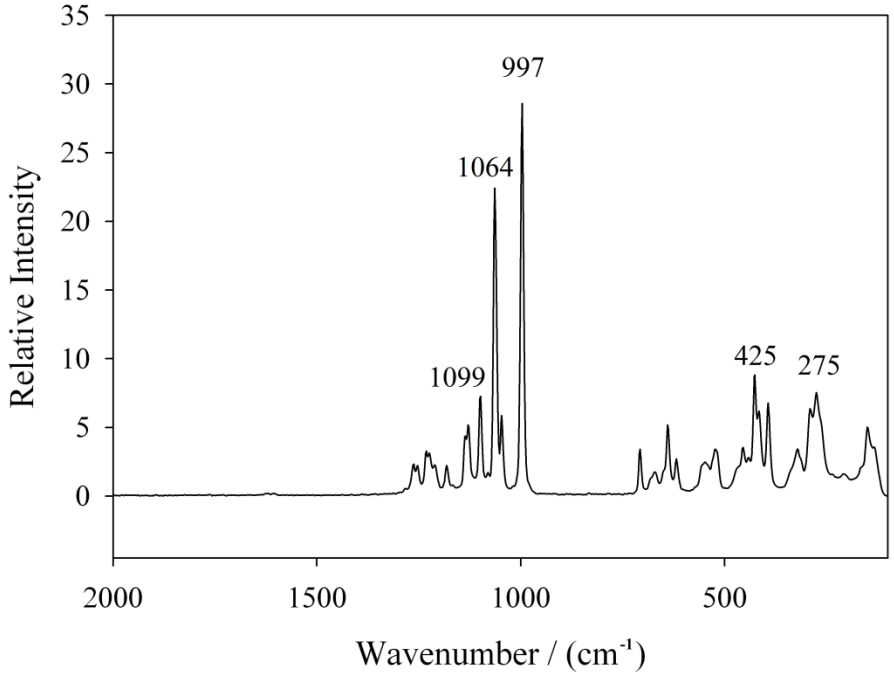

Figure B29. Raman spectrum of solid Sample 3.

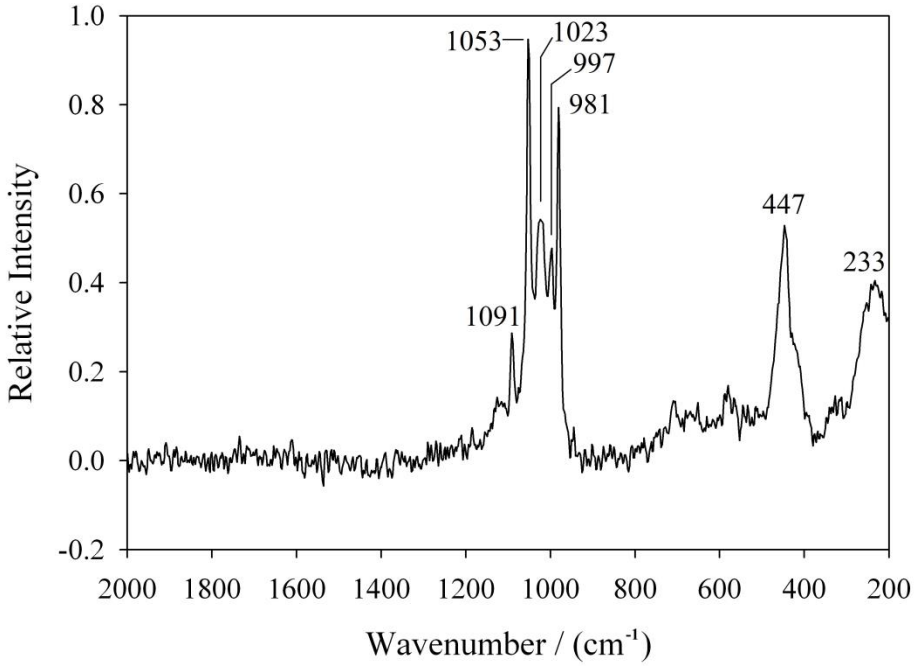

Figure B30. Raman spectrum of Sample 3 in solution.

Sample 4 – Produced August 2003, GFS Chemicals

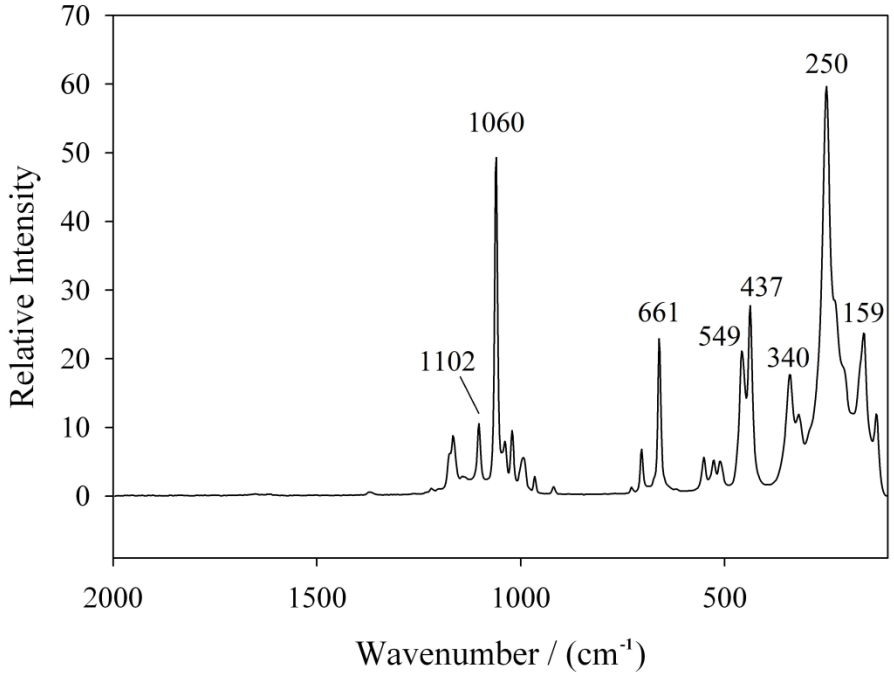

Figure B31. Raman spectrum of solid Sample 4.

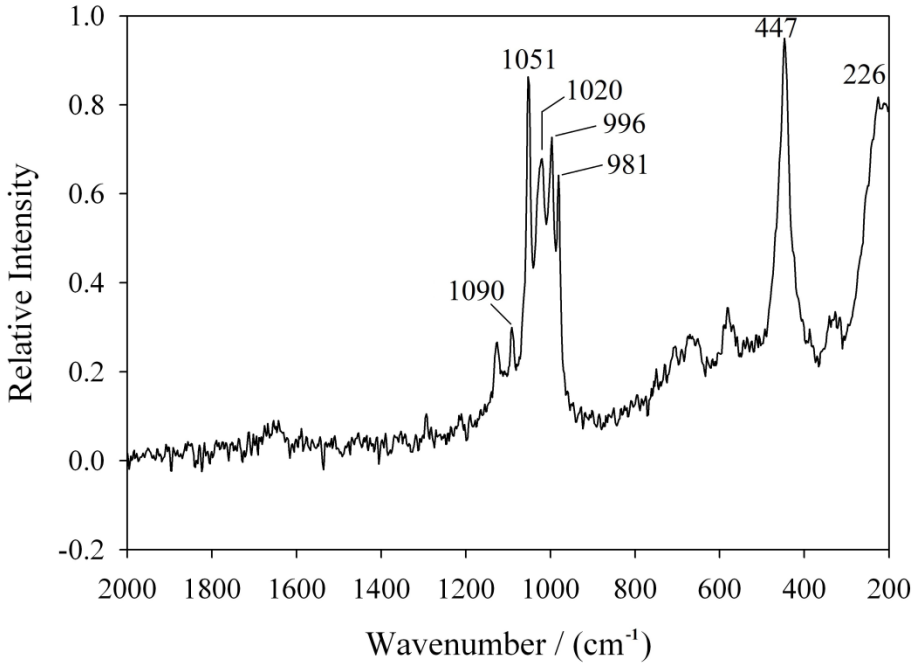

Figure B32. Raman spectrum of Sample 4 in solution.

Sample 5 – Produced March 1998, Aldrich Chemical Company

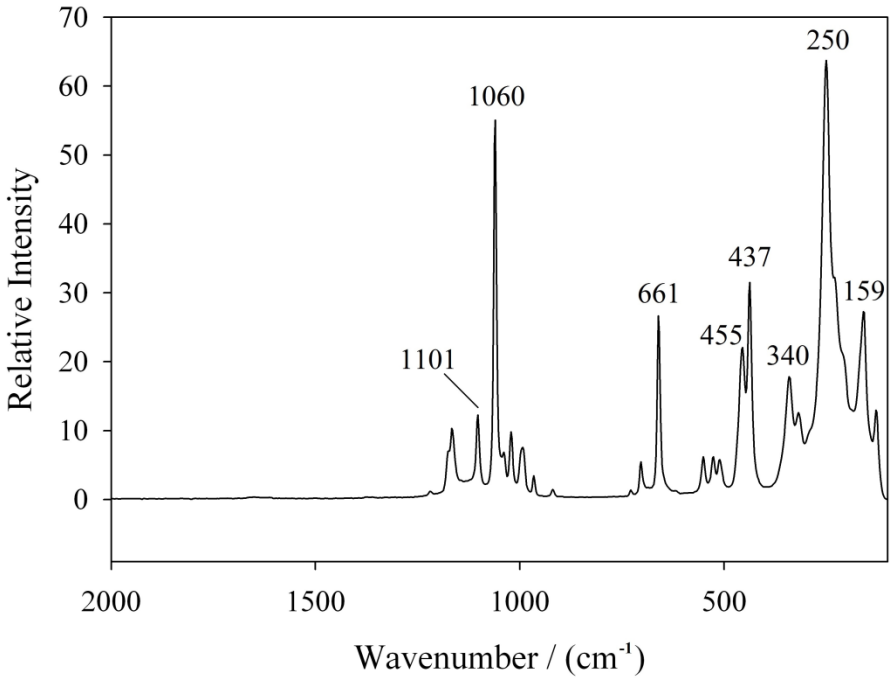

Figure B33. Raman spectrum of solid Sample 5.

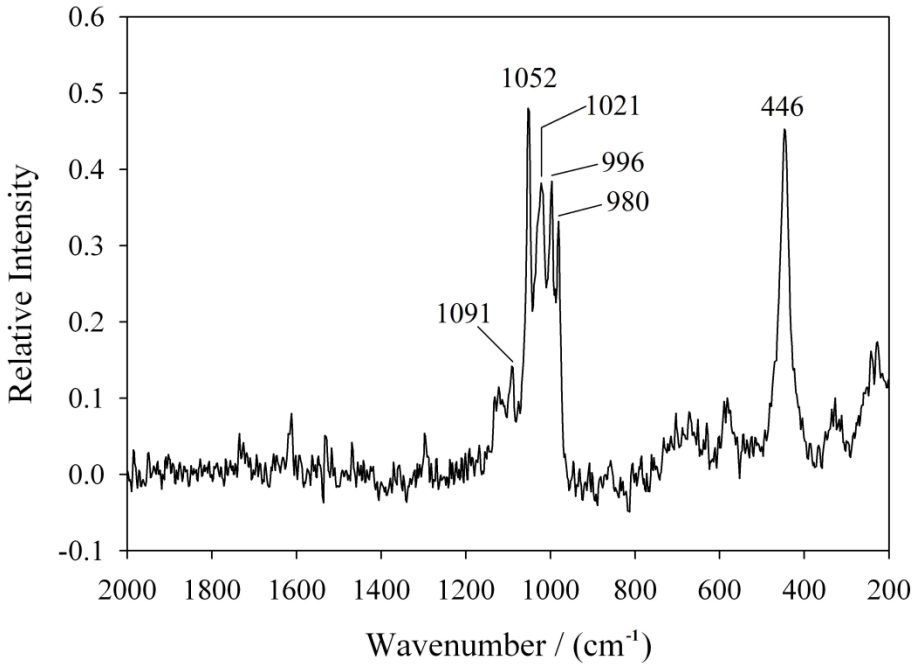

Figure B34. Raman spectrum of Sample 5 in solution.

Sample 6 – Produced February 1985, Fischer Scientific

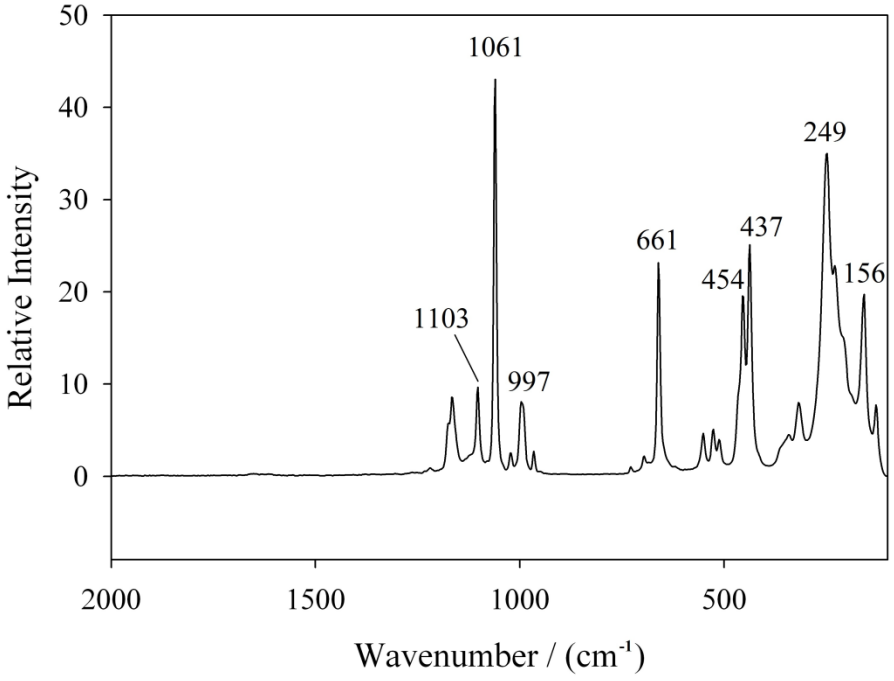

Figure B35. Raman spectrum of solid Sample 6.

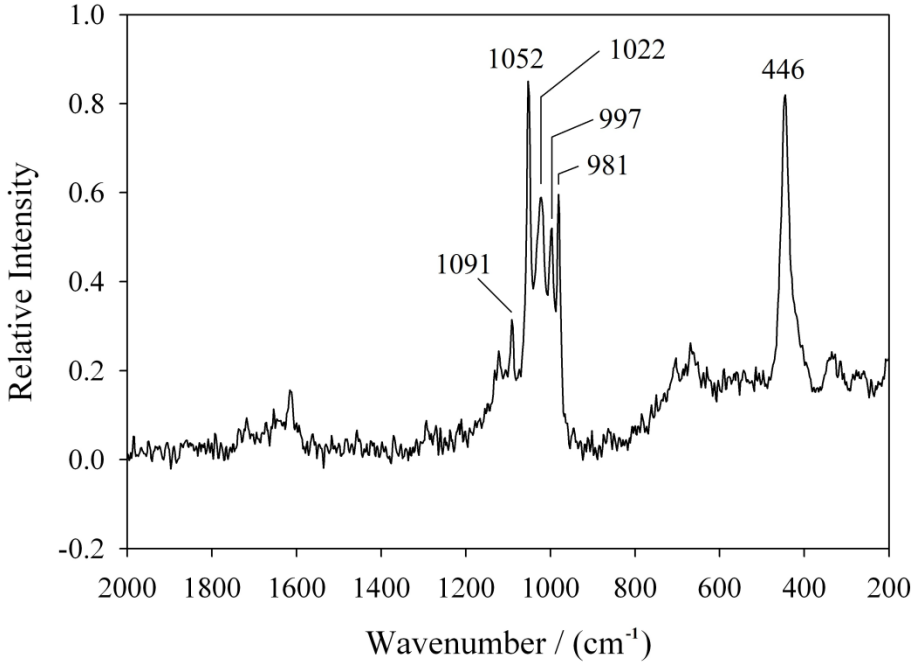

Figure B36. Raman spectrum of Sample 6 in solution.

Sample 7 – Produced February 1985, Fischer Scientific

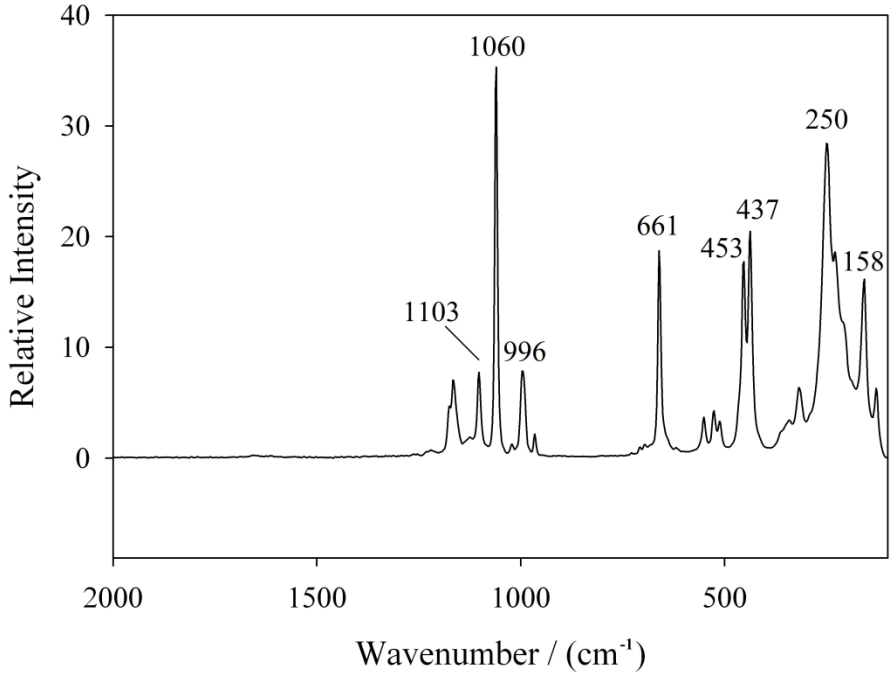

Figure B37. Raman spectrum of solid Sample 7.

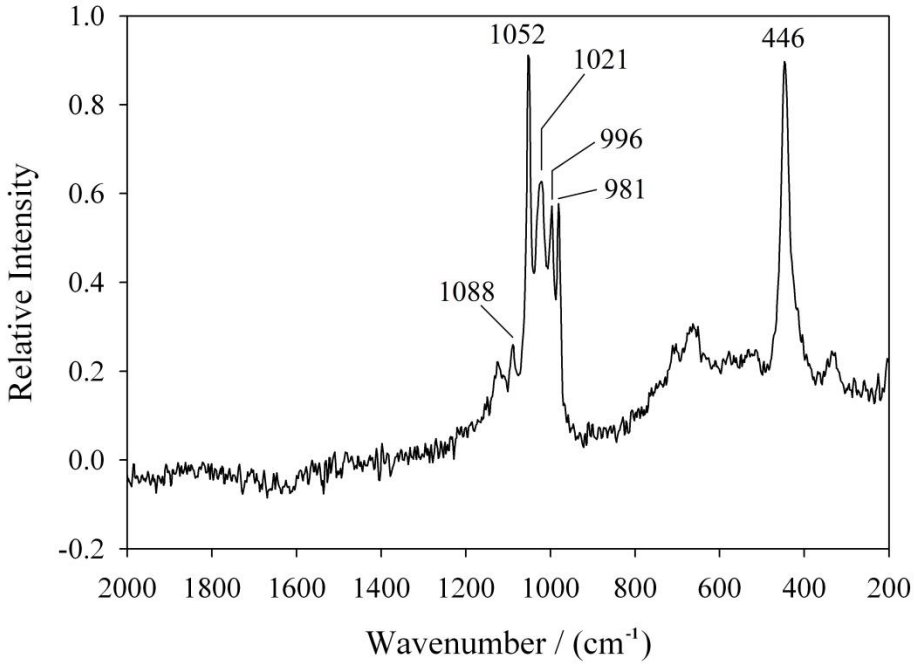

Figure B38. Raman spectrum of Sample 7 in solution.

Sample 8 – Produced September 1978, J. T. Baker

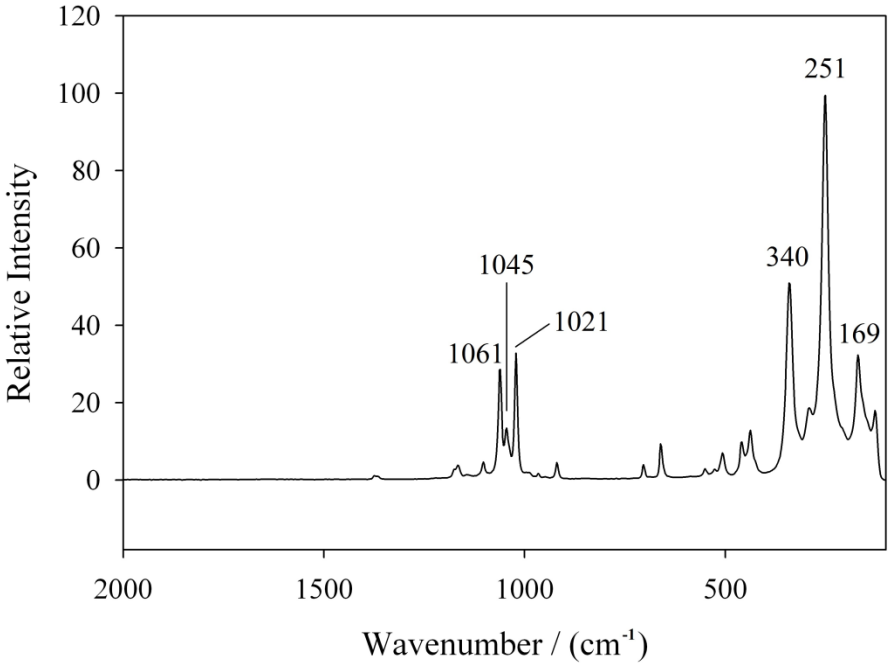

Figure B39. Raman spectrum of solid Sample 8.

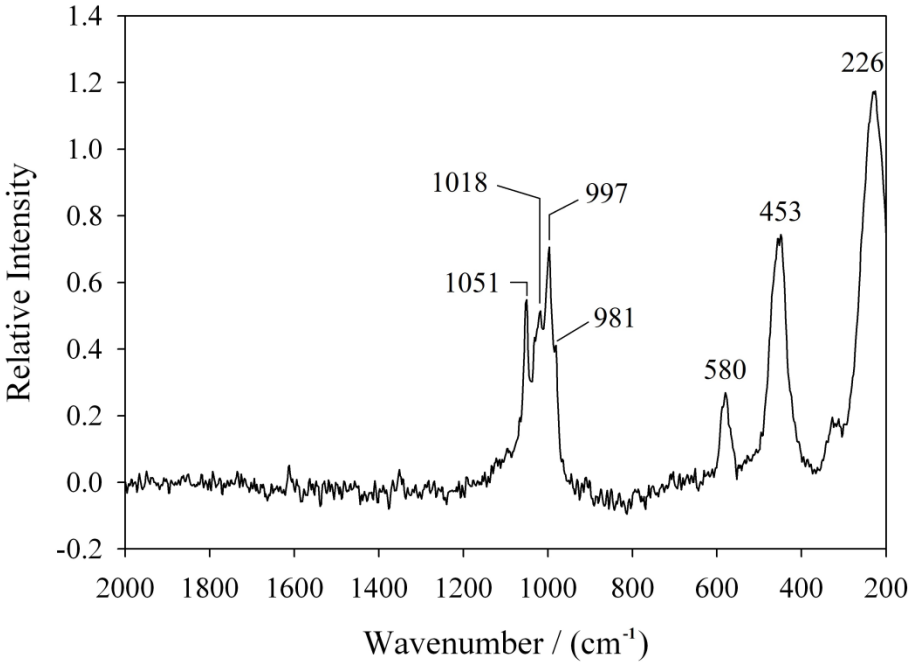

Figure B40. Raman spectrum of Sample 8 in solution.

Sample 9 – Produced August 1978, J. T. Baker

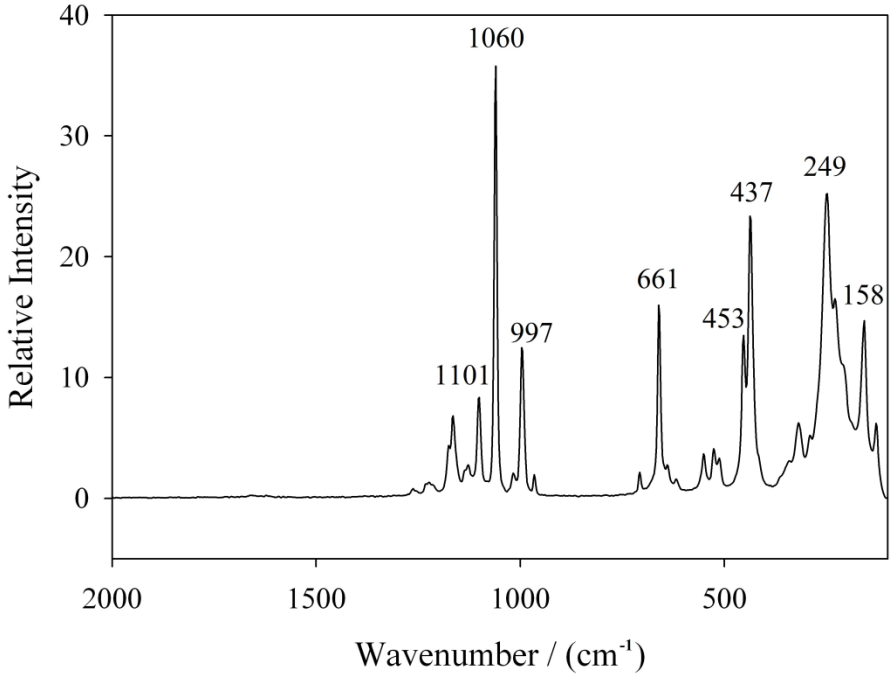

Figure B41. Raman spectrum of solid Sample 9.

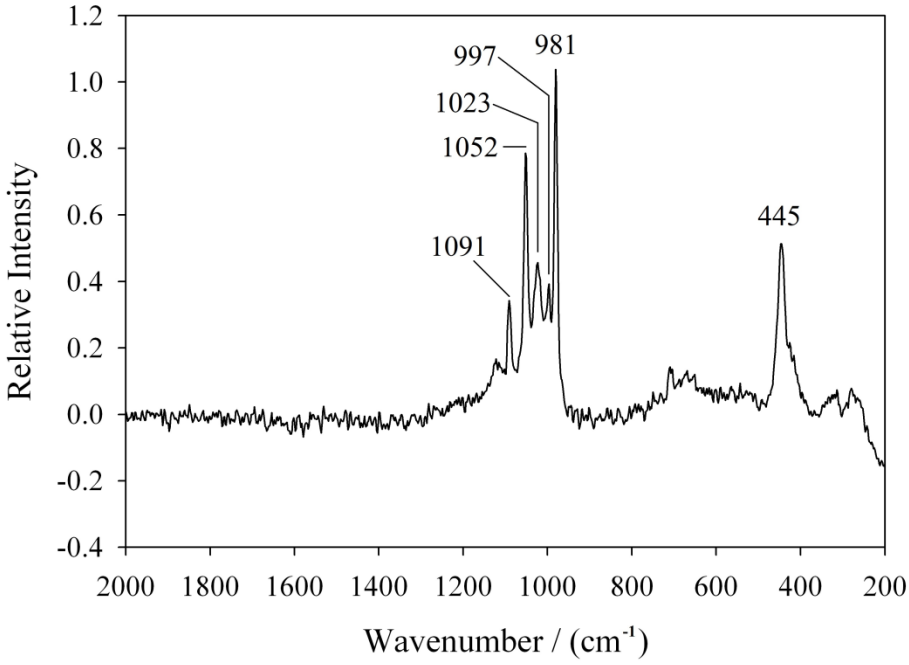

Figure B42. Raman spectrum of Sample 9 in solution.

Sample 10 – Produced September 1963, J. T. Baker

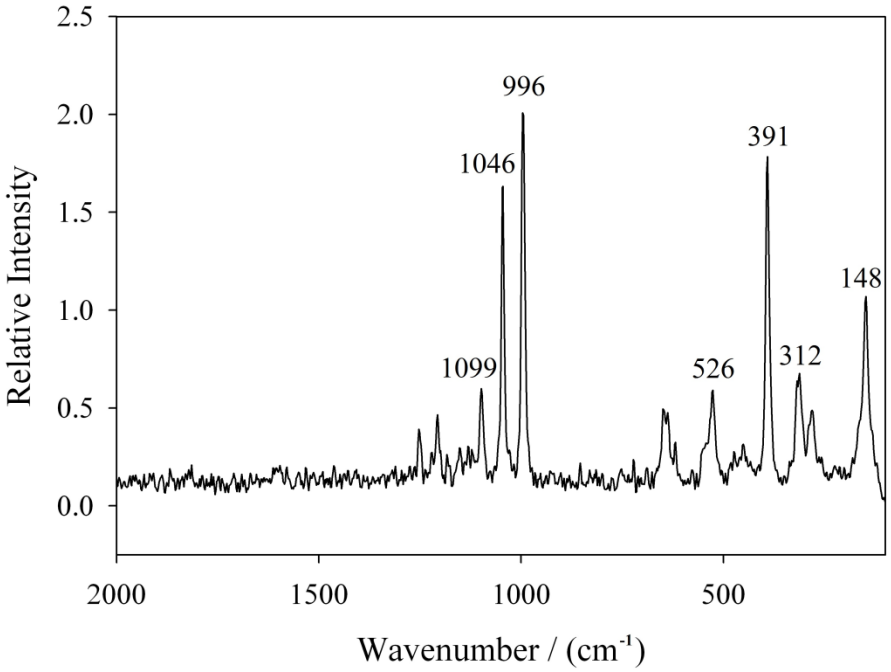

Figure B43. Raman spectrum of solid Sample 10.

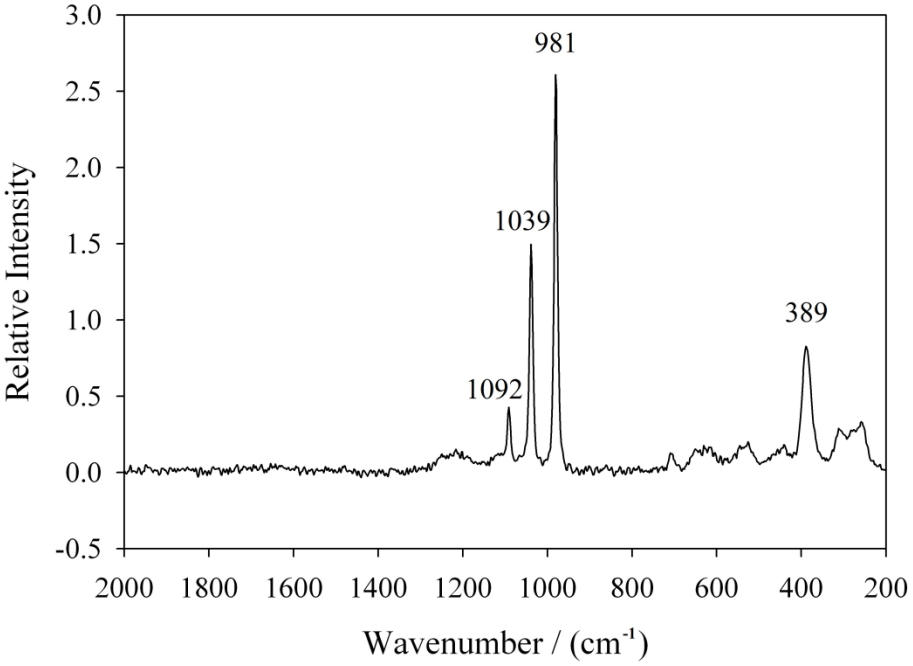

Figure B44. Raman spectrum of Sample 10 in solution.

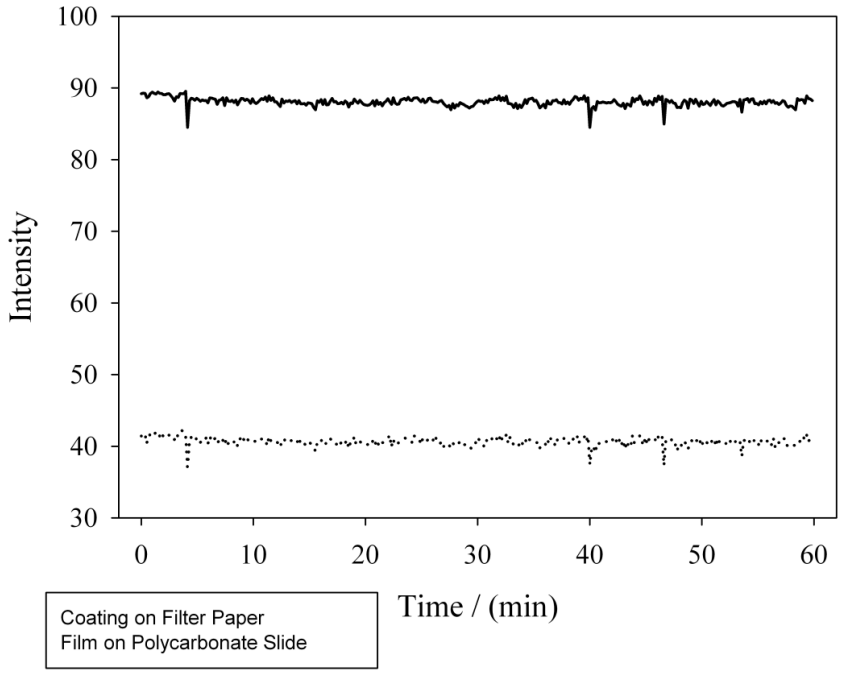

Figure C1. Reflected intensity of a 50 mass percent titania coating on filter paper (solid line) and film on polycarbonate (dotted line) when illuminated for one hour.

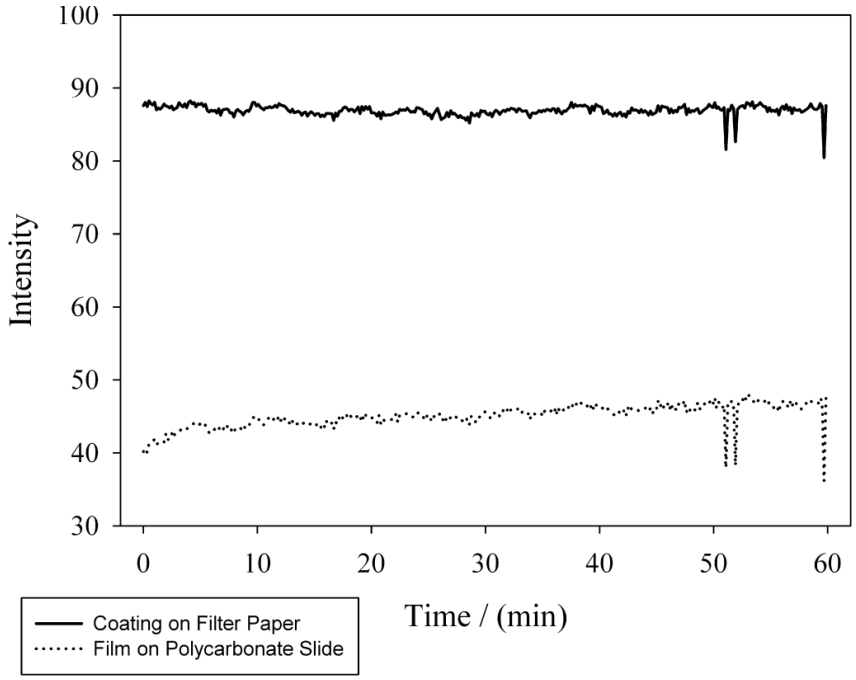

Figure C2. Reflected intensity of a 50 mass percent titania coating on filter paper (solid line) and film on polycarbonate (dotted line) when illuminated and exposed to a steady flow of water vapor for one hour.

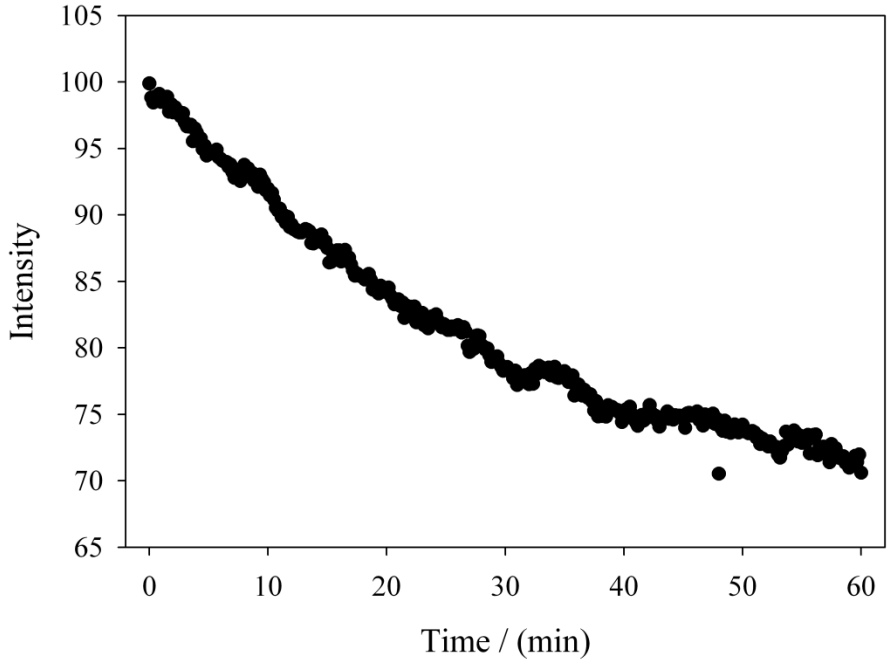

Figure C3. Reflected intensity of a 50 mass percent titania film on polycarbonate when exposed to 6.5 ppm hydrogen peroxide for one hour.

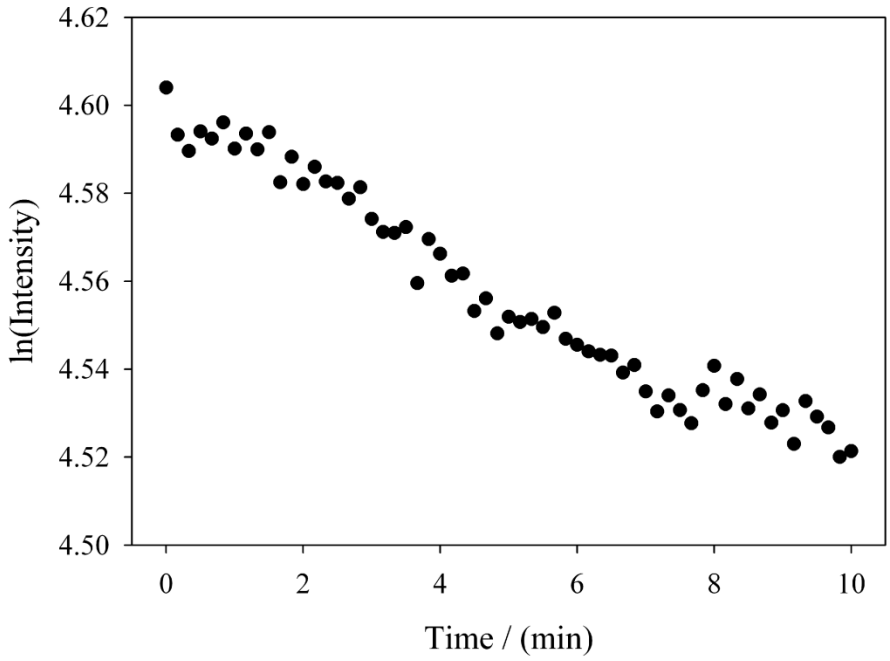

Figure C4. First-order approximation (natural log intensity vs. time) for the first ten minutes of exposure of a 50 mass percent titania film to 6.5 ppm hydrogen peroxide. This approximation showed increased noise but remained moderately linear ($y = -0.0081x + 4.60$, $R^2 = 0.96$).

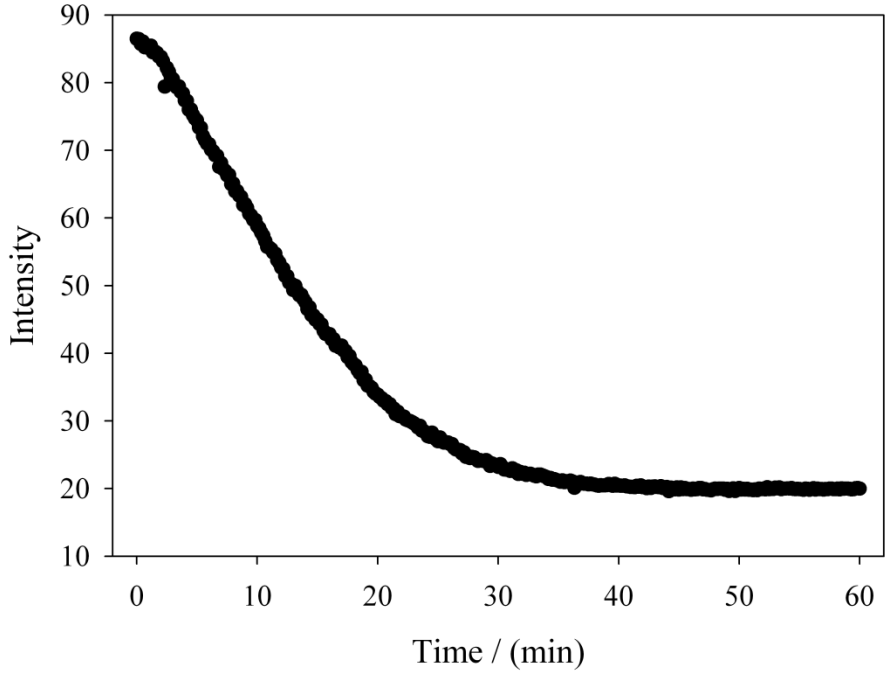

Figure C5. Reflected intensity of a 50 mass percent titania film on polycarbonate when exposed to 42 ppm hydrogen peroxide for one hour.

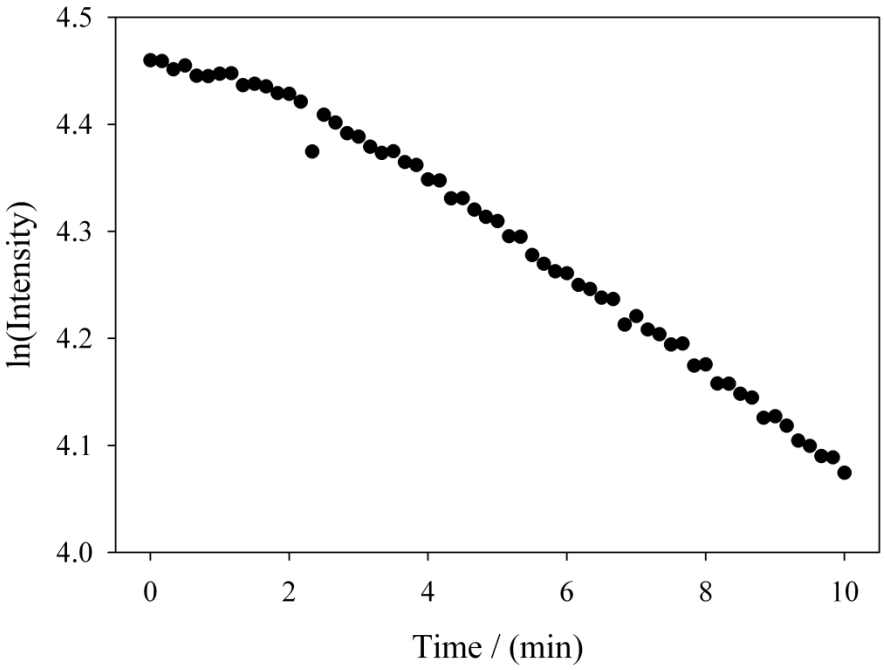

Figure C6. First-order approximation (natural log intensity vs. time) for the first ten minutes of exposure of a 50 mass percent titania film to 42 ppm hydrogen peroxide. This approximation showed good linearity ($y = -0.0447x + 4.56$, $R^2 = 0.99$).

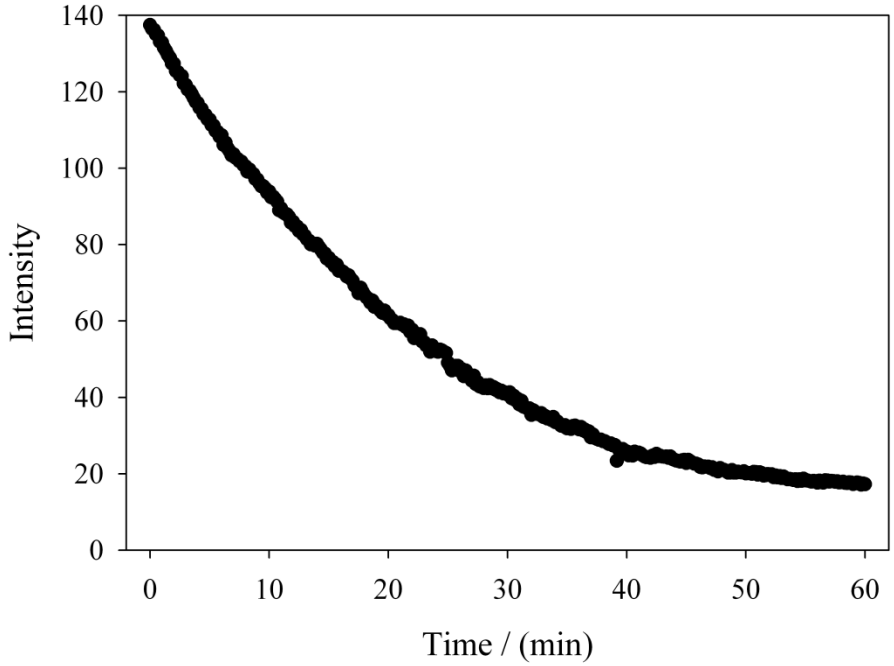

Figure C7. Reflected intensity of a 50 mass percent titania coating on filter paper when exposed to 12.6 ppm hydrogen peroxide for one hour.

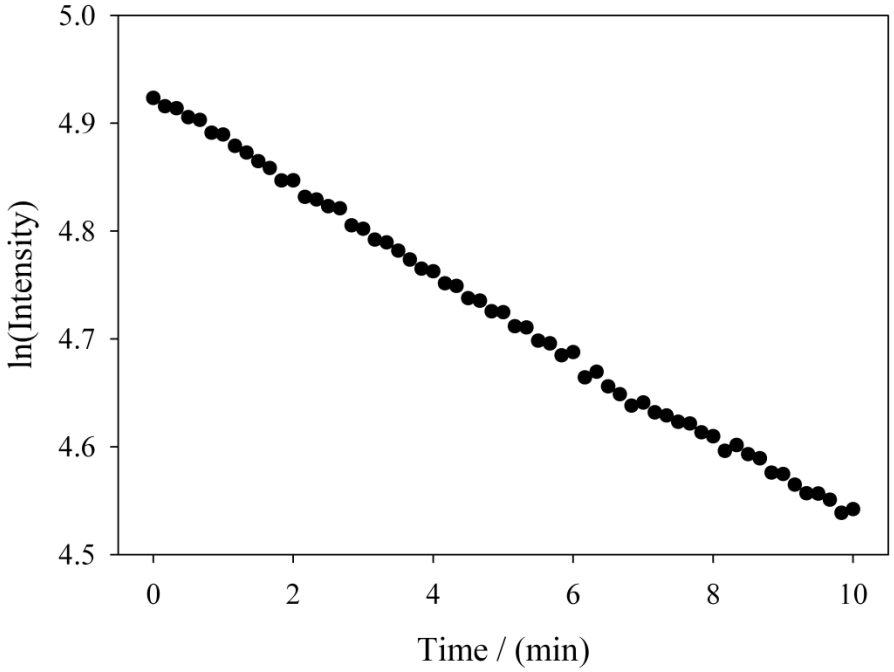

Figure C8. First-order approximation (natural log intensity vs. time) for the first ten minutes of exposure of a 50 mass percent titania coating to 12.6 ppm hydrogen peroxide. This approximation showed excellent linearity ($y = -0.0398x + 4.96$, $R^2 = 1.00$).

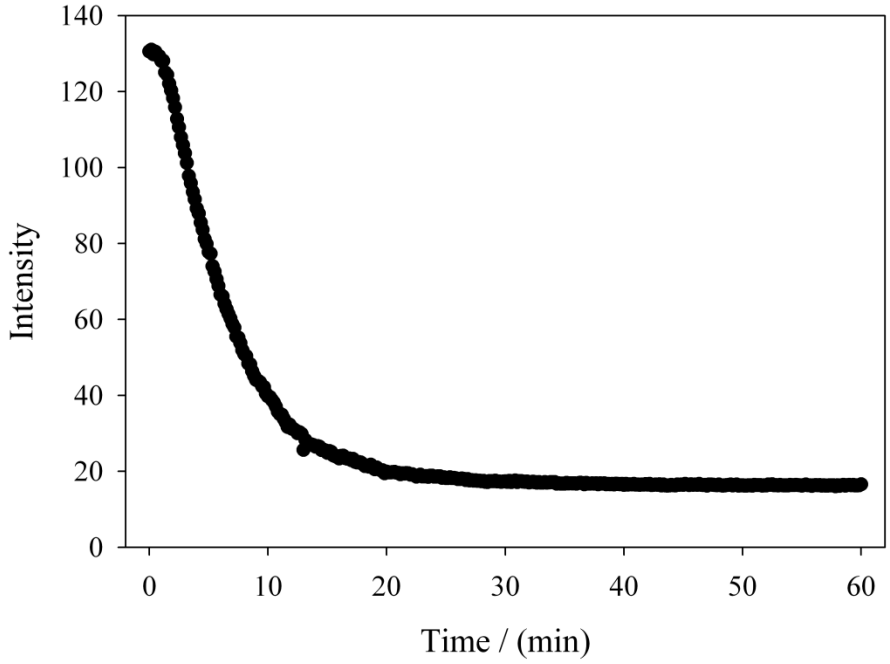

Figure C9. Reflected intensity of a 50 mass percent titania coating on filter paper when exposed to 38.5 ppm hydrogen peroxide for one hour.

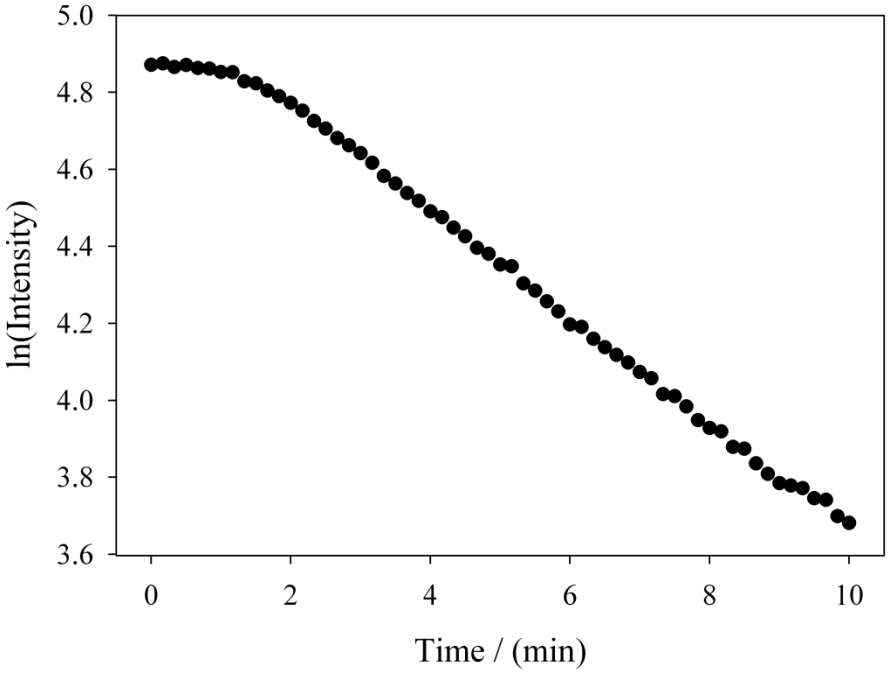

Figure C10. First-order approximation (natural log intensity vs. time) for the first ten minutes of exposure of a 50 mass percent titania coating to 38.5 ppm hydrogen peroxide. This approximation showed good linearity ($y = -0.131x + 5.12$, $R^2 = 0.99$).

VITA

Travis Houston James

Candidate for the Degree of

Doctor of Philosophy

Title: THE ELUCIDATION AND QUANTIFICATION OF THE DECOMPOSITION PRODUCTS OF SODIUM DITHIONITE AND THE DETECTION OF PEROXIDE VAPORS WITH THIN FILMS

Major Field: Chemistry

Biographical:

Personal Data:

Born in Aix En Provence, France, on April 3, 1986, the son of Randal and Cheryl James.

Education:

Completed the requirements for the Doctor of Philosophy in Chemistry in Chemistry at Oklahoma State University, Stillwater, Oklahoma in July, 2014.

Completed the requirements for Bachelors of Science in Chemistry at Hillsdale College, Hillsdale, MI, in May 2009.

Experience:

Employed by Hillsdale College as an undergraduate teaching assistant, 2008-2009; employed by Oklahoma State University as a graduate teaching and research assistant, 2009 to present.

Professional Memberships:

American Chemical Society, Phi Lambda Upsilon Chemical Honorary Society